Human myeloid enhanced model systems: Tools for advanced evaluation of short-term CAR T cells and *in vivo* CAR T cell generation

Vom Fachbereich Biologie der Technischen Universität Darmstadt

Zur Erlangung des akademischen Grades

Doctor rerum naturalium

Dissertation von

Naphang Ho, M. Sc.

Aus Frankfurt am Main

Referent: Prof. Dr. Alexander Löwer

Referent: Prof. Dr. Christian J. Buchholz

Darmstadt, 2022

Ho, Naphang: Human myeloid enhanced model systems: Tools for advanced evaluation of short-term CAR T cells and *in vivo* CAR T cell generation

Darmstadt, Technische Universität Darmstadt

Jahr der Veröffentlichung der Dissertation auf TUprints: 2023

URN: urn:nbn:de:tuda-tuprints-230093

Tag der mündlichen Prüfung: 15.12.2022

Summary

Immunotherapies have emerged as a viable treatment option in cancer, by harnessing the natural ability of the immune system to eliminate tumor cells. Additional modification of the effector cells paved the way for novel strategies, such as equipping T cells with a chimeric antigen receptor (CAR) for efficient and target-specific tumor cell lysis. In particular, CD19CAR T cells showed tremendous results against B cell malignancies with currently four CD19CAR T cell products on the market. Despite the great successes CAR T cell manufacturing requires long *ex vivo* generation and cultivation time up to several weeks and therefore limits the application. Current efforts to reduce and avoid this limitation involves *ex vivo* manufacturing within few days and CAR T cell generation *in vivo*. This thesis evaluates these novel CAR T cell generation approaches in myeloid enhanced model systems to get a better understanding of potential safety risks and obstacles.

Proof of concept for *in vivo* CAR T cell generation has been shown before with CD8 and CD4 receptor-targeted lentiviral vectors (CD8-LV and CD4-LV) in preclinical humanized mouse models. However, these studies were limited to humanized model systems that do not reflect the physiological myeloid cell composition in human accurately. That is why this thesis used the CD34+ stem cell humanized NSG-SGM3 (huSGM3) mouse model, which develops pronounced human innate immune cells including monocytes and macrophages, to evaluate *in vivo* CAR T cell generation. Intravenous (*i.v.*) injection of CD4-LV, CD8-LV or mixture of both vector types resulted in successful CD19CAR T cell generation in the blood of some mice. Importantly, CAR expression was restricted to the respective targeted CD4+ or CD8+ T cell subset without detectable off-target transduction. CD19+ target cell reduction in the system further underlined the presence of functional CD19CAR T cells in the periphery as well in various lymphocyte-residing and biodistribution-relevant organs. In addition, expansion of CAR T cells in the presence of tumor antigen confirmed presence and long persistence of CAR T cells in the spleen and transgene integration could be verified by qPCR analysis. Overall, *in vivo* CAR T cell generation was less efficient in huSGM3 compared to previous described CD34+ humanized NSG mice. Intriguingly, CD4-LV injected mice showed the least pronounced *in vivo* CAR T cell generation efficiency and correlated with a distinct plasma cytokine pattern associated with activated human myeloid cells. Reduced *in vitro* transduction of T cells with CD4-LV

and CD8-LV in the presence of monocytes or macrophages identified these cells as potential barrier for *in vivo* CAR T cell generation. Strikingly, shielding CD4-LV and CD8-LV from phagocytosis, by using ß2M$^{-/-}$, CD47^{high} HEK-293T packaging cells for vector particle production, substantially improved CAR T cell generation in the co-culture. Furthermore, these modifications also improved *in vivo* CAR T cell generation in huSGM3 mice compared to conventional CD4-LV and CD8-LV. This was shown by higher vector copy numbers, more pronounced CD19+ cell reduction in the spleen and bone marrow for both shielded vector types and in addition by higher CAR T cell numbers in the blood for shielded CD4-LV.

Reducing *ex vivo* CAR T cell generation time is another attractive approach to refine manufacturing. In this thesis CD19CAR T cells generated within 3 days (short-term CAR T cells) using lentiviral vector incubation were evaluated for cellular composition and potential to induce cytokine release syndrome (CRS), a common side effect in CAR T cell therapy. Characterization of short-term CAR T cells after production revealed that most of the cells were vector particle-bound and only a minority was CAR positive. A designed co-culture model with tumor cells and monocytes demonstrated tumor cell specific cytotoxicity for short-term CAR T cells, which showed substantial CAR expression after 24h of co-culture. Moreover, the co-culture model revealed high release of CRS-relevant cytokines including IL-6, IFN-γ, TNF-α, GM-CSF, IL-2 and IL-10 during the killing assay. Using NSG-SGM3 mice with high tumor burden, *i.v.* administration of high numbers of short-term CAR T cells showed severe acute events within 24h. This included body signs of ill-being, temperature and weight drop and systemic cytokine elevation of human IFN-γ, TNF-α, IL-2 and IL-10 by short-term CAR T cells and murine MCP-1, IL-6 and G-CSF by the mouse system.

Taken together, this thesis highlights the potential of sophisticated model systems to evaluate possible roadblocks and safety risks of novel CAR T cell therapy manufacturing approaches. They allowed the identification of human monocytes and macrophages as potential barrier for *in vivo* CAR T cell generation and highly supports the implementation of phagocytosis shielding in targeted LVs to reduce innate immune response for this approach. Moreover, such model systems revealed the potential of short-term CAR T cells to induce severe acute CRS and emphasize a careful approach in the clinic and further assessment on these model platforms.

Zusammenfassung

Immuntherapien haben sich als erfolgreiche Behandlungsmethode im Kampf gegen Krebs herausgestellt, indem die natürliche Fähigkeit des Immunsystems genutzt wird Tumorzellen zu bekämpfen. Zusätzliche Modifikationen an den Effektorzellen haben ein neues Feld eröffnet. Zum Beispiel die Ausstattung der T-Zellen mit einem chimären Antigen-Rezeptor (CAR), um spezifisch und effizient Tumorzellen zu eliminieren. Vor allem CD19-CAR-T-Zellen haben erstaunliche klinische Erfolge in B-Zell Krebserkrankungen gezeigt und spiegelt sich in der Marktzulassung von aktuell vier CD19-CAR-T-Zellprodukten wider. Trotz der großen Erfolge von CAR-T-Zellen ist die Anwendung dieser Therapie durch die lange *ex vivo* Produktionszeit limitiert, die mehrere Wochen andauern kann. Derzeitige Bemühungen die Produktionszeit zu verkürzen oder zu vermeiden, beinhalten die *ex vivo* Herstellung von CAR-T-Zellen innerhalb weniger Tage oder die Erzeugung von CAR-T-Zellen *in vivo* im Körper. Die vorliegende Arbeit untersucht diese neuen Herstellungsansätze näher in Modelsystemen mit besonderem Fokus auf myeloiden Zellen, um ein besseres Verständnis über potenzielle Sicherheitsrisiken und Hürden in der klinischen Umsetzung zu bekommen.

Die Umsetzbarkeit von *in vivo* CAR-T-Zellgenerierung konnte bereits mit CD8 und CD4 Rezeptor-targetierten lentiviralen Vektoren (CD8-LV und CD4-LV) in präklinischen humanisierten Mausmodellen in früheren Studien der Arbeitsgruppe gezeigt werden. Allerdings haben sich diese Studien nur auf humanisierte Mausmodelle beschränkt, die nur bedingt den physiologischen Anteil von myeloiden Zellen im Menschen darstellen. Deswegen wurde in dieser Arbeit das CD34+ Stammzell-humanisierte NSG-SGM3 (huSGM3) Mausmodell verwendet, das einen bedeutenden Anteil an humanen angeborenen Immunzellen, vor allem Monozyten und Makrophagen, im System entwickelt, um in vivo CAR-T-Zellgenerierung zu untersuchen. Intravenöse (*i.v.*) Injektion von CD4-LV, CD8-LV oder eine Mischung von beiden Vektorarten führte zur erfolgreichen Generierung von CD19-CAR-T-Zellen im Blut von einigen Mäusen. Bedeutenswert war hierbei die spezifische CAR Expression in den jeweilig targetierten CD4 oder CD8 T-Zellsubtyp, ohne bemerkbare unspezifische Transduktion anderer Zelltypen. Die Reduktion von CD19+ Zielzellen im Körper unterstrich die Präsenz von funktionalen CD19-CAR-T-Zellen im peripheren System aber auch in verschiedenen lymphozytenreichen und biodistributionsrelevanten Organen. Weiterhin zeigte die

Expansion von CAR-T-Zellen in der Zellkultur in der Gegenwart von Tumorantigen die Präsenz und lange Persistenz von *in vivo* generierten CART-Zellen in der Milz von einigen Mäusen. Außerdem konnte eine erfolgreiche Transgenintegration mittels qPCR-Analyse bestätigt werden. Im Allgemeinen war die Effizienz für *in vivo* CAR-T-Zellgenerierung in huSGM3 Mäusen jedoch geringer verglichen zu vorhanden Daten in CD34+ Stammzell-humanisierten NSG Mäusen. Überraschend war insbesondere die geringe *in vivo* CAR-T-Zellgenerierungseffizienz in CD4-LV injizierten Mäusen. Dies korrelierte zudem mit einem typischen Zytokinmuster für aktivierte humane myeloide Zellen im Plasma dieser Tiere. Eine reduzierte *in vitro* Transduktion von T-Zellen mit CD4-LV und CD8-LV in der Präsenz von Monozyten oder Makrophagen identifizierte diese Zellen als potenzielles Hindernis für *in vivo* CAR-T-Zellgenerierung. Bemerkenswert war, dass die Abschirmung der CD4-LV und CD8-LV vor Phagozytose, durch die Nutzung von ß2M$^{-/-}$, CD47^{high} HEK-293T Verpackungszellen für die Vektorpartikelproduktion, die CAR-T-Zellgenerierung in der Ko-kultur wesentlich verbesserte. Des Weiteren konnten diese Modifikationen die *in vivo* CAR-T-Zellgenerierung in huSGM3 Mäusen im Vergleich zu den konventionellen CD4-LV und CD8-LV verbessern. Das zeigte sich in höheren Vektorintegrationszahlen und ausgeprägteren CD19+ Zellreduktionen in der Milz und Knochenmark für beide abgeschirmte Vektorarten und zusätzlich auch in höheren CAR-T-Zellzahlen im Blut für abgeschirmte CD4-LV.

Die Reduzierung der *ex vivo* Produktionszeit von CAR-T-Zellen ist ein anderer Weg, um das Herstellungsverfahren zu verbessern. In dieser Arbeit wurden CD19-CAR-T-Zellen, die innerhalb von 3 Tagen mittels lentiviraler Vektorinkubation hergestellt wurden (Kurzzeit-CAR-T-Zellen), auf ihre Zellkomposition untersucht und deren Potential das Zytokin-Freisetzungssyndrom (CRS) auszulösen, welches eine häufig auftretende Nebenwirkung in der CAR-T-Zelltherapie ist. Die Charakterisierung der Kurzzeit-CAR-T-Zellen nach der Produktion zeigte, dass die meisten Zellen Vektorpartikel gebunden haben, jedoch nur ein geringer Anteil der Zellen positiv für das CAR war. In einem eigens konzipierten Ko-kultur-Model mit Tumorzellen und Monozyten konnte die anti-tumorale Aktivität von den Kurzzeit-CAR-T-Zellen nachgewiesen werden, die bereits nach 24h der Ko-kultur erhebliche CAR Expression zeigten. Des Weiteren wurde eine hohe Ausschüttung von CRS-relevanten Zytokinen mitunter IL-6, IFN-γ, TNF-α, GM-CSF, IL-2 und IL-10 während der Ko-Kultivierung gemessen. Abschließende Evaluierung der Kurzzeit-CAR-T-Zellen in NSG-SGM3

Mäusen mit hoher Tumorlast zeigte nach *i.v.* Verabreichung einer hohen Zelldosis schwerwiegende akute Nebenwirkungen innerhalb der ersten 24 Stunden. Dazu zählten körperliche Krankheitszeichen, Temperatur- und Gewichtsverlust, sowie systemisch erhöhte Zytokine für humanes IFN-γ, TNF-α, IL-2 and IL-10 durch die Kurzzeit-CAR-T-Zellen und murines MCP-1, IL-6 and G-CSF durch das Maussystem.

Zusammenfassend zeigt diese Arbeit das Potential von komplexen Modelsystemen mögliche Hürden und Sicherheitsrisiken von neuartigen Herstellungsansätzen von CAR-T-Zelltherapie zu erforschen. Sie ermöglichten die Identifizierung von humanen Monozyten und Makrophagen als potentielle Barriere für *in vivo* CAR-T-Zellgenerierung und legen die Implementierung von Phagozytoseabschirmung in targetierten LVs nah, um die angeborene Immunantworten in einem solchen Ansatz zu reduzieren. Des Weiteren zeigten diese Modelsysteme das mögliche Risiko auf, dass Kurzzeit-CAR-T-Zellen schwerwiegendes akutes CRS auslösen können und halten zu einem vorsichtigen Angehen in der Klinik an und weiteren Untersuchungen mit diesen Modellplattformen.

Table of Content

1 Introduction 11

1.1 Human immune system 11

1.1.1 Innate immunity 11

1.1.2 Adaptive immunity 12

1.1.3 Cytokines 14

1.1.4 Cancer immunotherapies 15

1.2 CAR T cell therapy 16

1.2.1 CAR structure 16

1.2.2 Manufacturing 18

1.2.3 Safety and toxicity 19

1.2.4 Limitations and ongoing research 21

1.3 Lentiviral vectors 22

1.3.1 Basics 22

1.3.2 T cell targeted lentiviral vector 24

1.4 Humanized mouse models 26

1.5 Objective 29

2 Results 30

2.1 Characterization of the humanized NSG-SGM3 mouse model 30

2.1.1 Humanization level in blood of huSGM3 mice 30

2.1.2 Murine immune cells in huSGM3 mice 31

2.2 *In vivo* CAR T cell generation in humanized NSG-SGM3 mice 33

2.2.1 Experimental set up 34

2.2.1.1 CAR T cells in the peripheral system 35

2.2.1.2 Presence of CAR T cells in organs verified by FACS 37

2.2.1.3 Gene delivery verification on genomic level 40

2.2.2 Distinct cytokine pattern for CD4-LV treated mice 41

2.3 *In vitro* T cell transduction in the presence of myeloid cells 42

2.3.1 Reduced T cell transduction in the presence of monocytes and macrophages 43

2.3.2 Phagocytosis shielding of CD4-LV and CD8-LV 45

2.3.3 Phagocytosis shielding of CD4-LV and CD8-LV improves T cell transduction in presence of macrophages 47

2.4 *In vivo* CAR T cell generation with phagocytosis shielded CD4-LV and CD8-LV 48

2.4.1 Improved *in vivo* gene delivery with CD4-LV^{sh} and CD8-LV^{sh} 49

2.4.2 Pronounced B cell reduction with shielded LVs 54

2.4.3 No pathological cytokine release in plasma 56

2.5 Modeling of CAR T cell induced acute cytokine release syndrome 60

2.5.1 Impact of CAR co-stimulatory domain on CAR T cell cytotoxicity in continuous killing assay 60

2.5.2 Short-term generation protocol yields substantial CAR T cells 63

2.5.3 *In vitro* CRS model with monocyte supplementation 66

2.5.3.1 Presence of monocytes does not influence CAR T cell cytotoxicity, but induces clinically relevant cytokine release 66

2.5.4 CRS tumor model in NSG-SGM3 mice with short-term CAR T cells..... 68

2.5.4.1 Distribution of short-term CAR T cells in blood and bone marrow .. 70

2.5.4.2 Short-Term CAR T cell induced acute side effects 72

2.5.4.3 Acute human cytokine release after CAR T cell application 75

2.5.4.4 Involvement of murine immune system during cytokine release after CAR T cell application 76

2.5.4.5 No indication of tumor lysis syndrome 78

3 Discussion 79

3.1 Advances in model systems for CAR T cell therapy 79

3.2 Potential risks for short-term CAR T cells 81

3.3 Roadblocks for *in vivo* CAR T cell generation 86

4 Material and Methods 92
4.1 Materials 92
4.1.1 Chemical and Reagents 92
4.1.2 Kits 93
4.1.3 Cytokine panels 94
4.1.4 Buffer and solution 94
4.1.5 Cell culture media 94
4.1.6 Consumables 95
4.1.7 Antibodies 95
4.1.8 Plasmids 96
4.1.9 Oligonucleotide primers 97
4.1.10 Enzymes and growth factors 98
4.1.11 Cell lines and bacteria 98
4.1.12 Instruments 99
4.1.13 Software 100
4.2 Molecular biology methods 100
4.2.1 Transformation of chemically competent bacteria 100
4.2.2 Plasmid DNA preparation 100
4.2.3 Restriction digest of DNA 101
4.2.4 Agarose gel electrophoresis 101
4.2.5 DNA isolation from agarose gel 101
4.2.6 DNA dephosphorylation and ligation 102
4.2.7 DNA sequencing 102
4.2.8 Isolation of genomic DNA 102
4.2.9 Polymerase chain reaction 103
4.2.10 Quantitative polymerase chain reaction 103
4.3 Cell culture work 104
4.3.1 Freezing and thawing of cells 104

4.3.2 Cell lines 105
4.3.3 Lentiviral vector production 105
4.3.4 PBMC isolation 106
4.3.5 PAN T cell isolation 106
4.3.6 Monocyte isolation 106
4.3.7 *In vitro* Macrophage polarization 107
4.3.8 Primary cells 107
4.3.9 T cell activation 107
4.3.10 Cell line transduction 107
4.3.11 T cell transduction 107
4.3.12 Short-term CAR T cell generation 108
4.3.13 Gene transfer activity assessment of lentiviral vector stocks 108
4.3.14 T cell transduction in presence of human myeloid cells 108
4.3.15 Continuous Killing Assay 108
4.3.16 Monocyte supplemented cytotoxicity assay 109
4.3.17 Cytokine assay 109
4.3.18 Flow cytometry staining 110
4.3.19 Multi-dimensional reduction analysis 110
4.3.20 Nanoparticle tracking analysis 111
4.4 Animal work 111
4.4.1 *In vivo* CAR T cell generation 111
4.4.1.1 Cytokine administration 111
4.4.1.2 Vector particle administration 111
4.4.2 CRS model 112
4.4.2.1 Tumor cell engraftment 112
4.4.2.2 *In vivo* Bioluminescence imaging 112
4.4.2.3 Short-term CAR T cell administration 112
4.4.2.4 General health condition scoring 113

4.4.2.5 Temperature monitoring 113
4.4.3 Blood sampling and cell processing 113
4.4.4 Harvest of bone marrow cells 113
4.4.5 Harvest of splenocytes 114
4.4.6 Harvest of liver cells 114
4.4.7 Harvest of lung cells 114
4.4.8 Expansion Assay 115
4.5 Statistical analysis 115
5 References 116
6 Abbreviations 135
7 List of Publications 138
7.1 Original research 138
7.2 Review articles 138
7.3 Conference presentations 138
7.4 Conference poster presentations 139
8 *Curriculum Vitae* 140
9 Acknowledgement 141
10 Ehrenwörtliche Erklärung 142

1 Introduction

1.1 Human immune system

To withstand natural infection by viruses, bacteria and fungi, the human immune system has evolved as a complex protection system. Key feature for the success is splitting the immune system into the innate and adaptive immune system, which allows a fast, yet long-lasting, and antigen-specific response towards different kind of infectious diseases.

1.1.1 Innate immunity

As the so called “first-line defense”, the innate immune system generates the first response towards an infection within hours. Commonly, phagocytes, including neutrophils, monocytes, macrophages and dendritic cells (DCs) are the first cells to arrive on the infection site (1). These cells are expressing pattern recognition receptors (PRR), such as toll-like receptor (TLR), mannose receptors and scavenger receptors, which can recognize and bind common pathogen associated molecule pattern (1). This allows the phagocytes to be activated and further recruit other immune cells towards the infection site by cytokine and chemokine secretion (1). Moreover, pathogenic particles can be engulfed and lysed inside the phagosomal compartment of these cells and thereby directly eliminated (1). Therefore, a fast and direct immune response upon infection can be established. In addition, natural killer (NK) cells are playing an important part and are able to recognize infected and damaged cells. The interplay of inhibitory receptors (killer cell immunoglobulin-like receptors, cluster of differentiation (CD)94 and NK group 2A receptor) and activation receptors (Nkp30, Nkp44 and Nkp46), allows them to recognize differential expression of major histocompatibility complex (MHC) I molecule on infected cells compared to healthy cells (2, 3). Activated NK cells can then directly lyse the infected cells by perforin and granzyme release or through death receptor mediated FasL and tumor necrosis factor-related apoptosis-inducing ligand apoptosis (4). Mast cells, basophils and eosinophils are further innate immune cells, which are highly involved in promoting local inflammation. They contain big granules with inflammatory mediators and are released upon activation (1).

Another important function of the innate immune system is the activation and induction of the adaptive immune response. This is mediated mainly by DCs, but also macrophages, which are functioning as antigen-presenting cells. Through receptor mediated endocytosis, phagocytosis and macropinocytosis, pathogens are taken up,

lysed and processed pathogen derived antigens are presented on the MHC II complexes, where they can interact with the receptors of the adaptive immune cells and induce antigen-specific response (5). In addition to MHC II antigen presentation, which is restricted to antigen-presenting cells only and contain lysosomal derived antigens, MHC I is expressed on all nucleated cells and allows presentation of peptides derived from cytosolic protein-synthesis (6). This is important for developing a response towards infected or tumor cells, which can have altered protein expression.

1.1.2 Adaptive immunity

In the adaptive immune system, T-lymphocytes (T cells) and B-lymphocytes (B cells) are the central key players. They provide an antigen-specific protection towards pathogens and cancer cells through adapted cellular and humoral immune responses. However, this response requires several days to unfold (1). B cells are covering the humoral response and develop inside the bone marrow, where they mature and undergo immunoglobulin gene rearrangement resulting in the expression of highly antigen-specific B cell receptor (7). Upon antigen specific activation, naive B cells can further develop to memory B cells and plasma cells with antibody secreting function and long-term persistence (8).

T cells are in many ways similar but complementary to B cells. They mediate cellular response and can facilitate direct cytotoxicity towards infected cells and tumor cells after respective activation. In contrast to B cell, T cells are developing in the thymus where they undergo a maturation step called thymopoiesis. This is an essential maturation step for T cells, where each T cell undergoes random T cell receptor (TCR) rearrangement that results in a unique TCR expression and allows the recognition of a specific epitope structure. Importantly, in this process the T cells are “educated” to self-antigens and thereby autoreactive T cells are eliminated (9). Afterwards, mature T cells migrate to secondary lymphoid organs, where they remain until they encounter their specific antigen activation. The TCR consist of the TCR-α and TCR-β linked to a αβ-heterodimer that dictates the antigen-specificity of the T cell (1). Upon binding to the specific antigen presented by MHC complexes it facilitates activation through the TCR associated CD3 receptor complex. The CD3 complex consist of a CD3εδ and a CD3εγ heterodimer and a CD3ζ homodimer that contain multiple immunoreceptor tyrosine-based activation motifs, which are phosphorylated by Src tyrosine kinases upon TCR activation and results in further downstream signaling and finally activation

of T cell activating genes (10). However, TCR activation is not sufficient for functional T cell activation (11, 12). A second stimulus by a co-stimulating receptor, such as CD28 and 4-1BB (CD137) is required, which interacts with the B7 receptor and the 4-1BB ligand on antigen-presenting cells and a third activating stimulus by cytokine stimulation by IL-2 or a similar T cell activating cytokine. Only in this combination T cell will be activated and can exert their proper function, while in absence of sufficient activation stimuli T cells will go into anergy, a state of unresponsiveness and dysfunction (13–15).

Within the T cells, two different subsets can be differentiated: CD8 and CD4 T cells. In the classical concept, CD8 T cells are exerting the cytotoxic function and induce lysis of infected and abnormal cells, whereas CD4 T cells are attributed to helper and regulatory function, such as activation of B cells for antigen maturation and down modulating inflammatory responses by regulatory T cells (1). However, this paradigm has changed in the recent years showing more evidence that CD4 T cells can also mediate cytotoxic function (16, 17). Cytotoxicity of T cells can be mediated by different ways. Release of perforin and granzymes as a complex with the proteoglycan serglycin from cytosolic granules of the T cells into the intercellular surrounding is one mechanism for target cell destruction (18). Another is the FAS-dependent pathway, which induces apoptosis in the respective target cell. But also via cytokine secretion of interferon γ (IFN-γ) or Tumor necrosis factor α (TNF-α) T cells can mediate indirect cell killing through further immune cell activation (18).

In this regard, phenotype and exhaustion states are tightly connected to T cell cytotoxicity and functionality. The phenotype characterizes the differentiation stage of T cells after thymopoiesis, where T cells are initially naïve and have high proliferative and long persistent qualities but are associated with less effector function (19). Upon antigen-encounter and T cell stimulation the phenotype shifts and T cells differentiate towards a stem cell memory, central memory, effector memory and then effector cell state with increasing effector but decreasing proliferative function (19). Depending on the context, different phenotypes can be beneficial, although generally in T cell-based therapies a less differentiated naïve phenotype is preferred.

1.1.3 Cytokines

In the immune system, cytokines are playing a crucial role for the communication between immune cells and are main mediators of the innate and adaptive immune response. In general, cytokine functions can be divided into three categories: **1)** pro-inflammation, which is important during infection to attract immune cells and promote pathogen clearance by the immune system, **2)** anti-inflammation, which acts often counteractive towards pro-inflammation to restore homeostasis after successful clearance of the pathogens, and **3)** cell type differentiation of progenitor cells into the different immune cell types.

In particular, macrophages and monocytes are playing a major role in secreting initial inflammatory cytokines during an infection (1). Acute-phase cytokines, such as IL-1β and IL-6 are pyrogens and highly released by these cells, which induces fever and promotes activation of further immune cells (20). TNF-α is another highly relevant cytokine, which is secreted by phagocytes, but also T cells upon activation and helps containing a local infection in the tissue (21, 22). Although, TNF-α is highly important and beneficial for infection control in tissue, systemic release of high TNF-α level can be destructive. It acts systemically on the vascular system and results in vascular dilation and extreme hypotension with possible multi-organ failure (23, 24). This shows that the effect of cytokines highly depends on the location, the interacting cell types and especially the concentration. Moreover, cytokines can also be secreted towards specific infection types, such as viruses. Innate PPRs, such as TLR3, 7, 8, 9, can sense viral-associated molecules and induce the release of anti-viral cytokines, like IFN-α and IFN-β, that helps to resolve ongoing viral infection (25). In contrast, anti-inflammatory cytokines are there to control and resolve an inflammation after or during elimination of the infection. IL-10 has been shown to have potent anti-inflammatory properties and can repress inflammatory cytokine expression (26). But cytokines can also act on other parts of the immune system and be involved in cell differentiation. For example, tissue entering activated monocytes have the capability to differentiate into different types of macrophages (M1 or M2) or into DCs (27, 28). Which path they will go is mainly driven by the cytokines in tissue environment. In cell culture for instance, monocytes can be polarized towards M1 macrophages with granulocyte-macrophage colony-stimulating factor (GM-CSF) (29), whereas M-CSF stimulation results in M2 type macrophages (29), and IL-4 and GM-CSF in DCs (30). Also, maintenance of the

hematopoietic stem cells in the bone marrow and further cell type differentiation are dictated by the interplay of various growth factors and cytokines (31).

1.1.4 Cancer immunotherapies

Immunotherapies have emerged as a powerful therapy platform besides radio- and chemotherapy in the fight against cancer. By harnessing the power of the immune system, it allows a more specific approach to eliminate cancer and tumor cells. Especially the use of T cells as the effector cells holds great potential due to their natural repertoire of diverse TCRs recognizing various antigens, including tumor associated ones. Further, they are naturally cytotoxic, expand to high numbers after activation, persist in the system for a long time and can differentiate to subsets with memory function. One approach is using immune-checkpoint blockade to boost tumor antigen specific T cells in the body by blocking immune checkpoint receptors that inhibit and downregulate T cell activity in the tumor microenvironment (32). Using checkpoint inhibitor against programmed cell death (PD-1) or cytotoxic T cell antigen 4 impressive tumor control in melanoma patients have been shown with multiple drugs approved for the clinics (33, 34).

Adoptive T cell therapy is another strategy to utilize T cells directly for cancer treatments. Initial approaches were focusing to activate, enrich and expand tumor infiltrating T cells from biopsies in cell culture and apply them back in a higher amount to the patients to facilitate ongoing T cell mediated anti-tumor response (35, 36). However, this relies on tumor antigen specific T cells present in the tumor tissue, which can be limited in certain cancer types and are often highly exhausted or dysfunctional (37, 38). Therefore, other approaches in adoptive T cell therapies are using engineered TCR or chimeric antigen receptor (CAR), which are genetically introduced into T cells. Thereby, the tumor target antigen can be selectively chosen and designed for the respective tumor type. A big difference between these two receptor forms are the targetable types of antigens and the mechanism of activation. Since engineered TCR T cells rely on the mechanistic feature for natural T cell activation, they require the presentation of the processed targeted antigen by MHC molecules and additional activation stimulation via co-receptor to exert proper function. However, this enables the possibility to target surface as well intracellular antigenic peptides with successes in melanoma and synovial sarcoma (39). On the other hand, CAR target antigens are restricted to surface structures only but are they recognized in their native form and

importantly, MHC-independently (40). Further, they do not require additional exogenic activation stimulus and emerged as highly successful platform with promising results in hematological cancer.

1.2 CAR T cell therapy

In the past years, CAR T cells widely changed the field for cancer treatment. Tremendous successes could be achieved for CAR T cells targeting CD19 as tumor antigen in patients with refractory or relapse B cell acute lymphoblastic leukemia (B-ALL) and diffuse large B cell lymphoma. Later, also complemented with promising results in follicular lymphoma, and mantle-cell lymphoma, which paved the way for the approval of four CD19-CAR T cell products so far by the Food and Drug Administration (FDA) and European Medicines Agency (EMA). The first milestone was set by the approval for the CD19-CAR T cell products tisagenlecleucel (Kymriah) and axicabtagene ciloleucel (Yescarta) through the FDA in 2017 and EMA in 2018. Shortly after market authorization was also given for brexucabtagene autoleucel (Tecartus) 2020 and lisocabtagene maraleucel (Breyanzi) 2021, which included some additional pre-selection steps for T cells in the manufacturing process. But besides using CD19 as tumor marker, efforts have been made for evaluating further markers for CAR T cell therapy. Therefore, a second milestone was marked by idecabtagene vicleucel (Abecma) reaching market authorization in 2021, which is using B cell maturation antigen (BCMA) targeted CAR T cells to treat multiple myeloma. Moreover, there are currently many more tumor markers under clinical investigation for CAR T cell therapy, including CD20 and CD22 for B cell malignancies (41, 42), CD33 for acute myeloid leukemia (43) or signaling lymphocytic activation molecule F7 for multiple myeloma (44), which might open new treatment options for cancer patients.

1.2.1 CAR structure

To enable tumor cell killing of CAR T cells, the CAR combines specific binding to the tumor antigen and activation of the CAR T cells to induce its cytotoxic activity. An important part of the CAR structure is the antigen binding domain on the extracellular site, which mediates MHC independent recognition and binding to the native tumor antigen of choice. Commonly, this is achieved by single chain variable fragment (scFv), which can be easily derived from an existing antibody, such as the CD19 specific mouse FMC63 antibody clone used in the current approved CD19-CAR T cell products. Alternatively, designed ankyrin repeat protein (DARPin) or nanobodies have been

reported for use, which would provide a smaller, more stable and less immunogenic high affinity ligand for targeting (45–47). The hinge region and the transmembrane domain (TMD) of the CAR are linking the extracellular binding part with the intracellular signaling domain and critically influence the overall performance of the CAR (40). Whereas the hinge region acts predominantly as spacer and impacts flexibility and binding (48–50), recent studies showed that the TMD can significantly influence activation strength and cytokine release intensity of CAR T cells (51, 52). Cytotoxic activity of the CAR T cell upon target binding is facilitated by intracellular signaling domains. Depending on the number of signaling domains included in the CAR constructs they are categorized into different generations (Figure 1).

By combining an antigen-binding domain via a hinge and TMD to the intracellular CD3ζ activation domain the first CAR was generated and introduced into T cells by Zelig Eshhar and colleagues in 1989 (53, 54). This first generation of CAR T cells demonstrated the feasibility to redirect T cells via a scFv to target 2,4,6-trinitrophenyl or MOV18 and induce target cell killing, but lacked sufficient *in vivo* persistence (55). It was recognized later that inclusion of further co-stimulatory molecules was necessary to increase survival and persistence of CAR T cells after activation (56) and prevent T cell anergy, a state of T cell dysfunction induced through solely CD3 activation (13–15). This paved the way for the 2nd generation of CAR constructs using for example CD28 or 4-1BB intracellular activation domain as costimulation (Figure 1) (57, 58). Further, 3rd generation CARs were combining multiple co-stimulation together (Figure 1). Although, preclinical data show tendentially a benefit of such combination (59, 60), clinical data did not confirm clear superiority over 2nd generation CAR T cells so far (61–63).

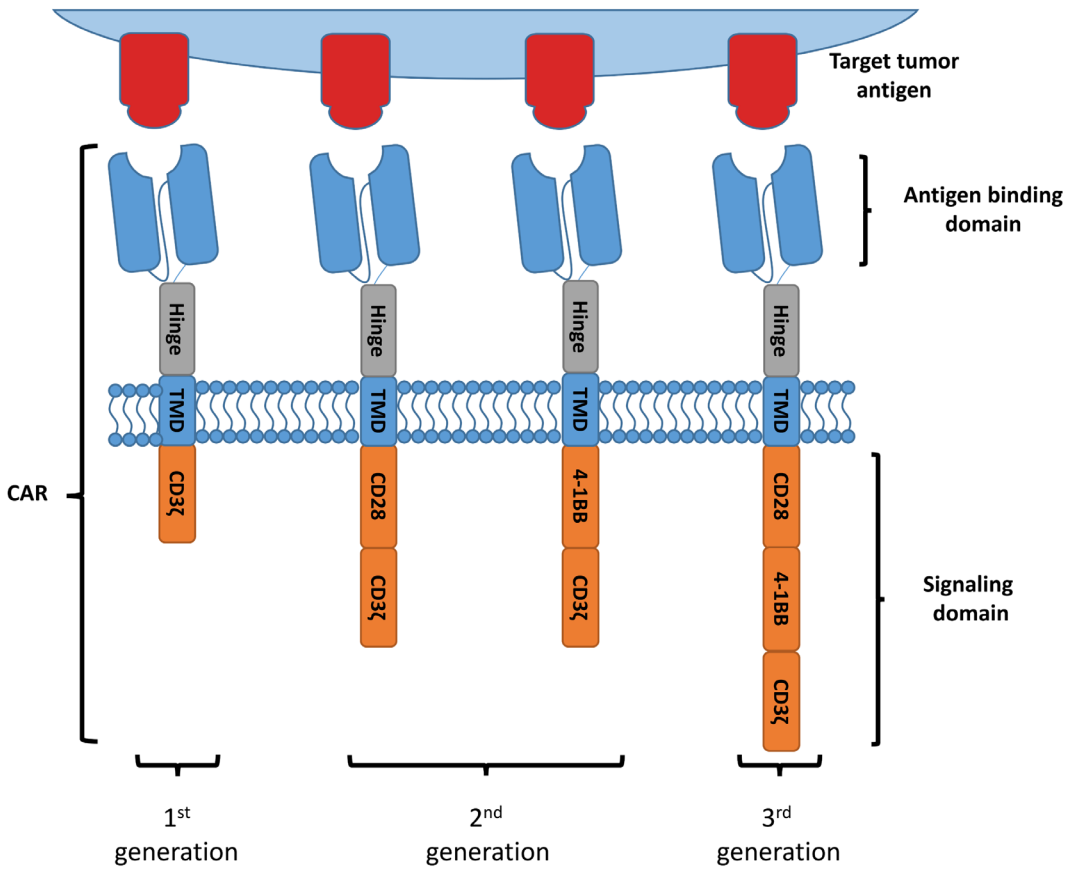

Figure 1: Schematic CAR structure.
The CAR consists of an antigen binding domain, which enables tumor antigen binding via a scFv. Through a hinge domain the high-affinity ligand is linked to the transmembrane domain (TMD) and the intracellular signaling domains. First generation CAR constructs only contain a CD3ζ domain, whereas second generation CARs enclose an additional intracellular co-stimulation domain from the CD28 or 4-1BB receptor or similar. Third generation of CAR further include a second co-stimulatory domain.

1.2.2 Manufacturing

The conventional process for CAR T cell manufacturing is similar in all current approved CAR T cell products and can be divided in five different steps: **1)** T cell isolation, **2)** CAR modification, **3)** expansion, **4)** quality control and **5)** reinfusion (Figure 2) (64–67). First, peripheral blood mononuclear cells (PBMC) are isolated from patient's blood by leukapheresis in the clinic and transported to a GMP manufacturing facility. During this step different positive or negative selection processes can be applied to enrich for CD4+ and CD8+ T cell subsets to generate a more defined composition (68–70). Afterwards, T cells are activated with αCD3 and αCD28 activating antibodies in the presence of T cell stimulating cytokines, such as IL-2 or IL-7 and IL-15 (64, 65). This is important to stimulate T cells for subsequent proliferation and to make the T cells more permissive for viral transduction (71–73). The CAR gene is then delivered into T cells with γ-retroviral or lentiviral vectors, which achieve high

transduction efficiencies and stable genome integration (64, 66). The resulting CAR T cells are further expanded *ex vivo* to increase total yield of therapeutic cells for the patients, including multiple medium changes to remove remaining viral vector particles in the product (65, 66). Afterwards, successfully expanded CAR T cells are frozen and stored while the quality control is performed. Sterility, vector copy number (VCN) and absence of replication competent viruses from production are critical parameters, which need to be assessed and confirmed before the CAR T cell product is released for the use in the patient (65, 67, 74). After all criteria are fulfilled, the frozen therapeutic cells are shipped back to the clinic, where they are administered into the patient. To increase engraftment and therapeutic activity of the CAR T cells, lymphodepletion is usually performed prior CAR T cell infusion (64, 75). In total the complete process usually takes two to six weeks between leukapheresis and administration of the final CAR T cell product (76, 64, 66, 67, 74).

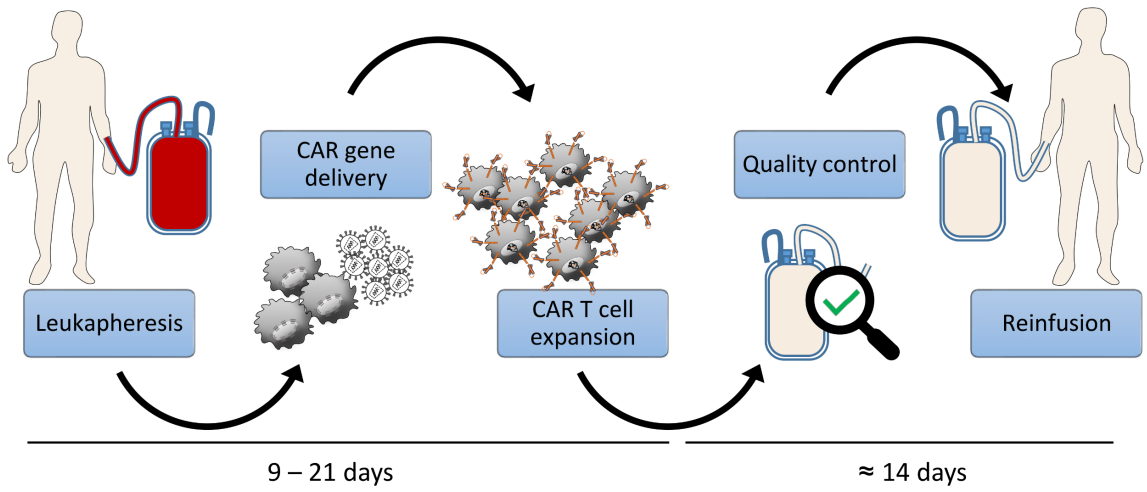

Figure 2: Conventional CAR T cell manufacturing process.
Timeline for conventional CAR T cell manufacturing. First, patient's T cells are isolated via leukapheresis and then modified by viral vector transduction to express the CAR. The resulting CAR T cells are then further expanded for several days to weeks before quality control is performed. Afterwards, the final CAR T cell product is reinfused into the patient.

1.2.3 Safety and toxicity

Besides the great efficacies of CD19CAR T cells in the clinics for hematologic cancer, unique adverse effects have been reported, which are associated with immune effector activation (77–80). Cytokine release syndrome (CRS) and immune effector cell-associated neurotoxicity syndrome (ICANS) are the most prominent side effects observed after CAR T cell treatment. They are a result of an excessive on-target activity by the CAR T cells, which can reach life-threatening grade in patients. By

definition of the ASTCT consensus grading system for CAR T cell therapy, described by Lee and colleagues (81), CRS is a “supraphysiologic response following (…) immune therapy that results in the activation or engagement of (…) immune effector cells (. …) [, which] can be progressive, must include fever at the onset, and may include hypotension, capillary leak (hypoxia) and end organ dysfunction.” ((81), p. 4).

Usually, CRS onset appears few days after CAR T cell infusion and reaches its peak within a week. During that time high CAR T cell expansion is observed within the system, which is accompanied by tremendous elevation of various inflammatory cytokines in the serum, including IL-6, IL-10, IL-8, IFN-γ and TNF-α (77–80). However, current standard of care management includes treatment with anti-IL-6 or anti-IL-1 receptor blocker (tocilizumab, anakinra) that can effectively control CRS (82, 83). In severe cases treatment with corticosteroids is necessary, which however may limit CAR T cell activity (84). Pre-clinical studies in mouse models showed that CRS is a complex interplay of activated CAR T cells encountering tumor antigens and further immune cells (85, 86). In particular monocytes and macrophages have been identified as a major source for IL-6 and IL-1 and therefore key driver for progression and induction of CRS (87, 88, 85, 86, 89). A recent study further revealed that the activation of the inflammasome pathway in monocytes might play an important role in CRS (90).

ICANS often follows timely after onset of CRS but it has also been reported to appear independently (91). Therefore, in the clinic ICANS is assessed separately from CRS including its own grading system (81). Common manifestations are lethargy, headache and delirium, but can reach over to severe symptoms such as seizures, encephalopathy and cerebral edema (92, 93). So far, the mechanism behind ICANS is still not fully understood, but endothelial cell activation resulting in disruption of the blood-brain-barrier (BBB) and influx of immune cells and systemic cytokines have been linked with ICANS induction (92). Recent findings revealed the presence of low CD19 expression in mural cells in prenatal brain samples by single cell RNA sequencing (94). The mural cells are relevant for the BBB integrity and the study suggests an on-target off-tumor activity of CAR T cell being responsible for ICANS development in CD19CAR T cell therapy and is in line with the higher ICANS incidence in patients with CD19 targeted CAR therapy (95). In general, on-target, but off-tumor CAR T cell activity is a common side effect of CAR therapy since most tumor-associated antigens are also expressed to some extend in healthy tissues. For CD19-targeted CAR therapy natural

B cells are quickly eliminated in the system after CAR T cell infusion, which is referred to as B cell aplasia (96). Although, this is an indication for ongoing CD19CAR T cell activity, it results in higher susceptibility to natural infection due to the loss of B cell function in patients (75). However, patients can be treated with immunoglobulin injection to partially compensate for the missing B cells, therefore B cell aplasia is considered as an acceptable side effect (96, 75).

1.2.4 Limitations and ongoing research

A major drawback with current CAR T cell products is the long manufacturing time, which can take weeks until the patient receives the therapeutic cell product (76, 64, 66, 67, 74). Therefore, shortening manufacturing time would especially benefit patients, which cannot wait long for treatment due to progressive disease. Moreover, labor and cost intensity need to be reduced to make the therapy more viable. Besides the long manufacturing time, also persistence of infused CAR T cells is crucial for therapy outcome. Exhausted and more differentiated phenotype of infused CAR T cell products are known parameter correlating with reduced *in vivo* persistence and therapy response in patients (97, 98). In this regard, a more naïve and stem cell memory associated phenotype has been reported to be most beneficial for therapy outcome in preclinical models (97, 99). Therefore, an approach, which is currently in focus of CAR T cell therapy research, is the generation of CAR T cells within a few days. The benefits of such CAR T cells would not only be a faster application to the patient, but would also result in a more beneficial cell composition of the CAR T cells. For instance, CAR T cells generated within three days showed a more naïve-like phenotype and exhibited a superior proliferation and effector function capacity post adoptive cell transfer into tumor engrafted mice than nine days cultivated CAR T cells (100).

Interestingly, there are also attempts in the field to move the therapy from a personalized medicine towards an off-the-shelf product that can be used in multiple patients. For instance, allogeneic CAR T cells use T cells from healthy donors, which are having a better cellular fitness and can be manufactured ahead of time prior patients need. A crucial step in there is the removal of endogenous TCR and HLA expression to reduce allogenic reaction within the recipient. This is usually combined with the insertion of the CAR gene directly into the TCR alpha constant (TRAC) locus with additional benefits towards phenotype and exhaustion for the CAR T cells (101, 102) and is already in ongoing clinical trials (103). A second strategy is the *in vivo*

generation of CAR T cells directly inside the body by systemic administration of T cell specific vectors that deliver the genetic material for the CAR specifically to T cells. This would completely avoid the necessity of *ex vivo* handling of the cells, which would highly reduce time and cost, while increasing availability of the therapy product. First studies already showed proof-of-concept for *in vivo* CAR T cell generation in preclinical mouse models (104). So far *in vivo* CAR T cell generation has been described for vector platforms using synthetic nanoparticles (105–107) and mainly lentiviral vectors (108, 109, 17, 73, 110) with T cell targeting motifs.

1.3 Lentiviral vectors

Viral vectors are an attractive tool in gene therapy because of their natural ability to deliver genetic material efficiently into cells. In particular lentiviral vectors (LVs) have become a widely used platform due to their capability to transduce quiescent and non-dividing cells (111) and exhibit lower genotoxicity compared to retroviral vectors (112–114). Furthermore, transduction results in stable integration of the transgene into the genome, which allows long-time expression of the gene and makes them suitable for modifying highly proliferative cells, such as stem cells or T cells (111).

1.3.1 Basics

LVs are commonly derived from the human immunodeficiency virus-1 (HIV-1), which is a single stranded ribonucleic acid (ssRNA) virus from the *Retroviridae* family. It consist of two copies of ssRNA with a packaging capacity for up to 10kb genetic material packaged inside a conic capsid structure and surrounded by an envelope membrane (115). A necessary step to enable safe usage of such virus derived LVs for gene therapy was the removal of self-replicative elements from the viral genome rendering the vector particle replication incompetent (116, 115). This is achieved by splitting the viral genome onto three different plasmids (Figure 3A): **1)** The packaging plasmid includes the *gag* and *pol* elements, which are essential for structural and genome integrating proteins, together with regulatory *tat* and *rev* elements needed for viral transcriptional activation. The accessory genes *vpr*, *vif*, *vpu* and *nef*, which are non-essential virulence factors, have been removed. **2)** The transfer plasmid only contains the therapeutic gene, driven by an internal promotor, and is flanked by 5’ and 3’ long terminal repeat (LTR) sequences needed for genome integration. Further, the packaging signal ψ and the rev response element are included, which facilitate packaging of the transgene sequence as ssRNA into the vector particle. **3)** In the

envelope plasmid the genes for the envelope proteins, such as vesicular stomatitis virus glycoprotein (VSV-G), are encoded that are determining the tropism of the LV. In addition to these safety measures, the 3' LTR of the transgene can be designed to be self-inactivating (SIN) to further minimize the risk of generating replication competent vector particles.

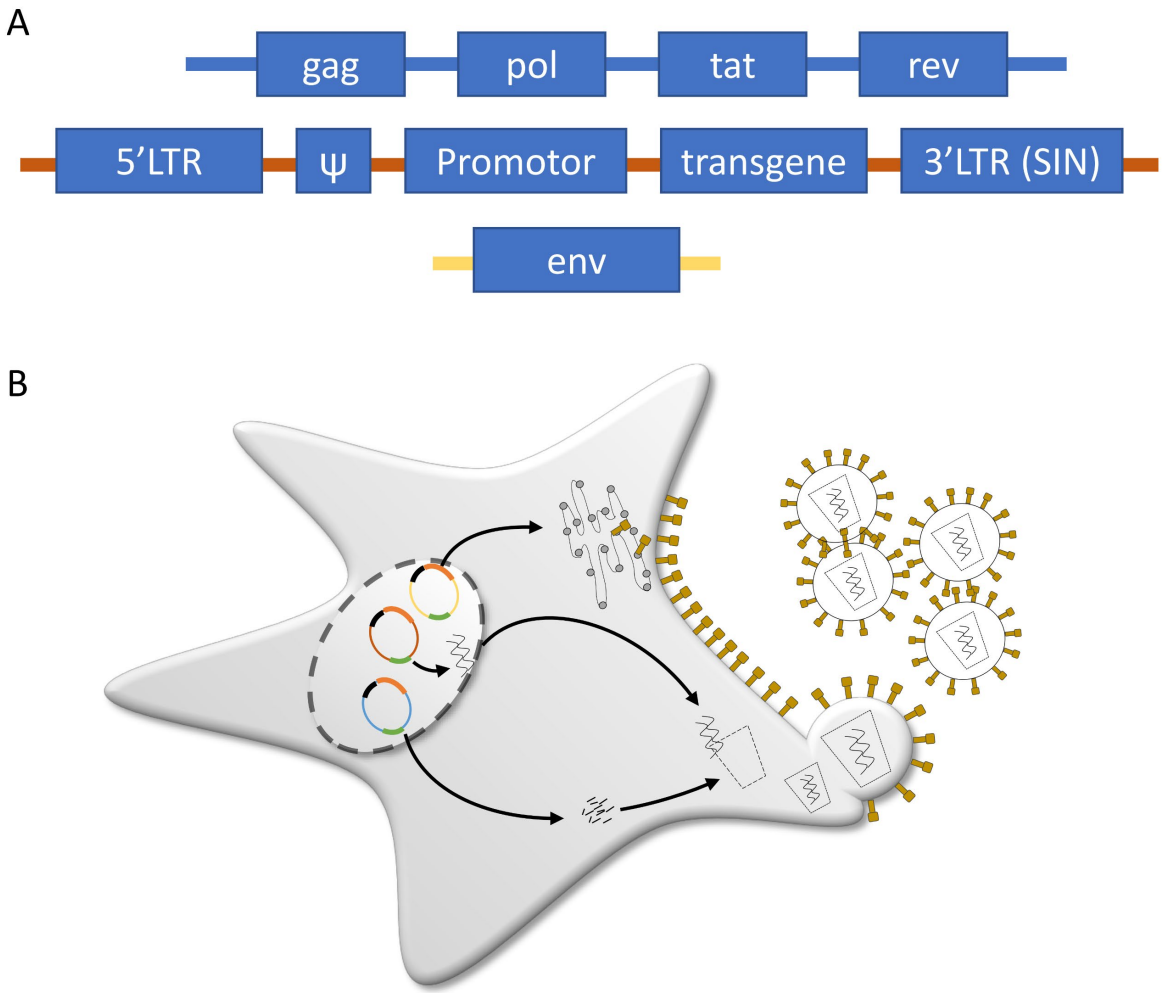

Figure 3: 2nd generation lentiviral vector production.
Genetic informations for 2nd generation lentiviral vectors are splitted onto three transfection plasmids. **A)** Packaging plasmid, transgene plasmid and envelope plasmid. **B)** For lentiviral vector generation, all three plasmids are transfected in HEK cells, where the transgene is transcribed into ssRNA and integrated into the viral capsid, which then buds from the production cell. Thereby the envelope glycoproteins, which are translated and trafficked via the rough endoplasmic reticulum to the cell membrane, are incorporated into the vector surface. Panel **(B)** is adapted from (115).

For LV production these vector plasmids are commonly transfected in human embryonic kidney (HEK) cells (Figure 3B). In there the viral capsid is assembled through the viral structural proteins encoded on the packaging plasmid and two copies of ssRNA transgene, which is transcribed from the transgene plasmid, is incorporated via the packaging signal into the viral capsid near the plasma membrane (115).

Meanwhile, the envelope protein is translated and trafficked through the endoplasmic reticulum to the cell surface membrane where the assembled viral capsid is budded from the HEK cell and enveloped with the cell membrane including the envelope proteins (115).

1.3.2 T cell targeted lentiviral vector

Conventionally, LVs pseudotyped with VSV-G envelope protein (VSV-LV) are widely used in gene therapy because of their broad tropism. VSV-LV binds to the low-density lipid receptor and uses this receptor for cell entry (117), which is widely expressed on many cell types including activated T cells (118). Therefore, VSV-LV is a common tool for conventional CAR T cell generation since it achieves high transduction efficiencies and can be concentrated to high titers (116, 119). However, recent report about transduction of a B cell leukemic cell with CD19CAR during *ex vivo* manufacturing using VSV-LV resulted in a CAR resistant leukemic clone that ultimately led to relapse in a patient during therapy (120). Although this has been a single case so far, it raises a demand for LVs with more restricted tropism. Therefore, CAR T cell therapy would highly benefit from LVs being able to transduce T cells selectively. Tools to achieve this have been described for LVs using a targeting system based on modified paramyxovirus derived glycoproteins in combination with high affinity ligands towards a receptor of choice (121, 122). But also modified sindbis virus derived glycoproteins have been reported as possible platform for receptor retargeting of LVs towards various cell types (123–125).

These retargeting strategies take advantage of the separated glycoproteins mediating fusion and binding, thus allowing alteration of the binding and targeting properties without impacting fusion capability (126). In the paramyxovirus-based platform, glycoproteins from Nipah and measles virus (NiV and MV) are used (Figure 4). In both cases a crucial step is the disruption of the natural binding site of the receptor, which can be achieved by mutation of residues in the glycoprotein sequence. Further, truncation of the cytoplasmic domain in the fusion and binding receptor can increase incorporation rate into vector particles due to possible steric hindrances (122). Finally, a high affinity ligand is attached to the binding glycoprotein to redirect the LV towards the receptor of choice. Incorporation of scFv and DARPins have been shown effectively for this purpose, although the latter ligand type is preferred due to its lower immunogenicity, higher stability and smaller size (127).

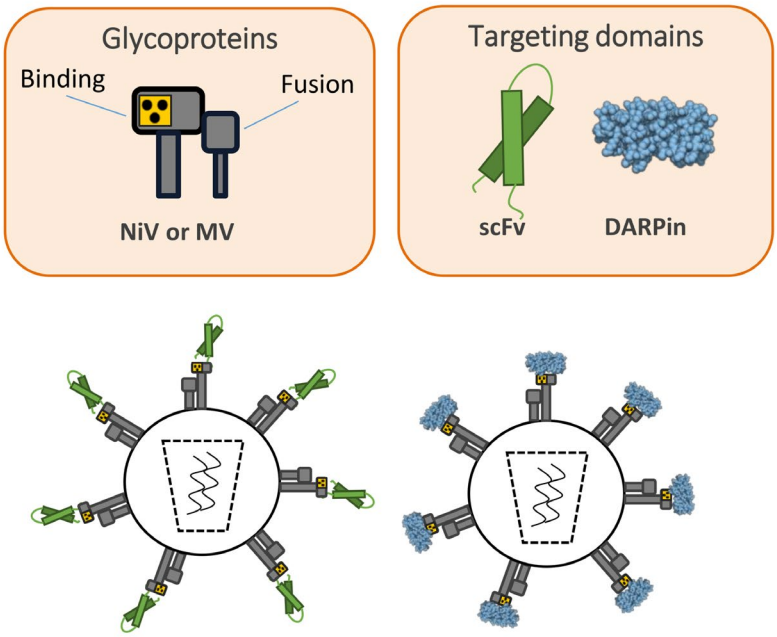

Figure 4: Schematic representation of receptor targeting strategy of LVs using paramyxovirus derived glycoproteins.
Receptor targeting of LVs can be achieved with modified glycoproteins derived from Nipah or measles virus (NiV, MV). Mutational blinding of the natural binding site of the binding mediating glycoprotein is required to allow specific retargeting through high-affinity ligands. scFv or DARPins can be used for this purpose to change the tropism of the engineered lentiviral vector to a target receptor of choice.

So far, many cell types have been targeted using this approach, including hematopoietic stem cells, endothelial cells, B cells and T cells (121, 128–130, 122, 73, 131). Using an anti-human CD8-scFv as targeting motif derived from the OKT8 hybridoma cell line in combination with modified MV glycoproteins, Zhou and colleagues (129) could generate a human CD8 receptor-targeted LV (CD8-LV). They could show highly specific gene transfer into CD8+ T cells when activated bulk PBMC were transduced *in vitro* and as well *in vivo* in PBMC-humanized mice (129). Later, Bender and colleagues (122) refined the CD8-LV and adapted it to the NiV-based targeting system, which further improved gene transfer activity and stability of the vector particle. Targeting the complementary human CD4 T cell subset was also achieved by a high affinity CD4 DARPIn on the MV platform and resulting in a human CD4 receptor-targeted LV (CD4-LV) (130). Interestingly, incorporation of a CD3 scFv as targeting ligand on LV could facilitate an overall T cell specific gene transfer into both T cell subsets and additional T cell activation through the agonistic binding of the CD3-LV (73). The high specificity of the receptor-targeted LVs as confirmed by low cytometry analysis in the initial studies (129, 130, 73) or by single cell transcriptomic analysis for CD8-LV (132), enabled the use of these LVs for *in vivo* gene transfer. First

application to generate human CAR T cell *in vivo* was shown with CD8-LV and later also demonstrated for CD4-LV and CD3-LV by systemic administration into NSG mice humanized with CD34+ human stem cells or human PBMC (108, 17, 73).

1.4 Humanized mouse models

Humanized mouse models evolved as a powerful platform to perform preclinical studies and testing of novel immunotherapies. They allow the assessment of therapeutic drugs in the presence of human immune cells *in vivo* and often provide a more accurate prediction than cell culture and syngeneic mouse models. A requirement for the reconstitution of human immune cells inside a mouse system is the use of immunodeficient mice. Ablation of murine T cells, B cells and NK cells are essential to avoid host versus graft rejection of the human cells. Current mouse strains, which have been optimized for such humanization procedure are for instance NOD.Cg-Prkdc^{scid}Il2rg^{tm1Wjl} (NSG) (133), NODShi.Cg-Prkdc^{scid}Il2rg^{tm1Sug} (NOG) (134) or NOD.Cg-Rag1^{tm1Mom}IL2rg^{tm1Wjl} (NRG) (135) mice. Furthermore, the choice of the human source material used for humanization determines which human immune cells will be able to reconstitute later in the system (Figure 5).

The most frequent used humanization model is the PBMC reconstitution. In there, human PBMC are injected intravenously or intraperitoneally into adult mice. Although, this is a simple, fast and cost-effective way to generate humanized mice, the human system will be dominated by T cells due to missing human cytokine support and short half-life of other immune cells (136). Another drawback of this humanization platform is the development of graft-versus host disease (GvHD) due to xenogeneic reactivity of the human T cells against the foreign mouse antigens. This ultimately limits study time of the experiments to approximately three to six weeks after PBMC humanization (137–139). However, novel NSG-based strains were developed, where the mouse MHC I and MHC II expression is removed on the mouse tissue and successfully delayed the onset of GvHD to two to three months (139).

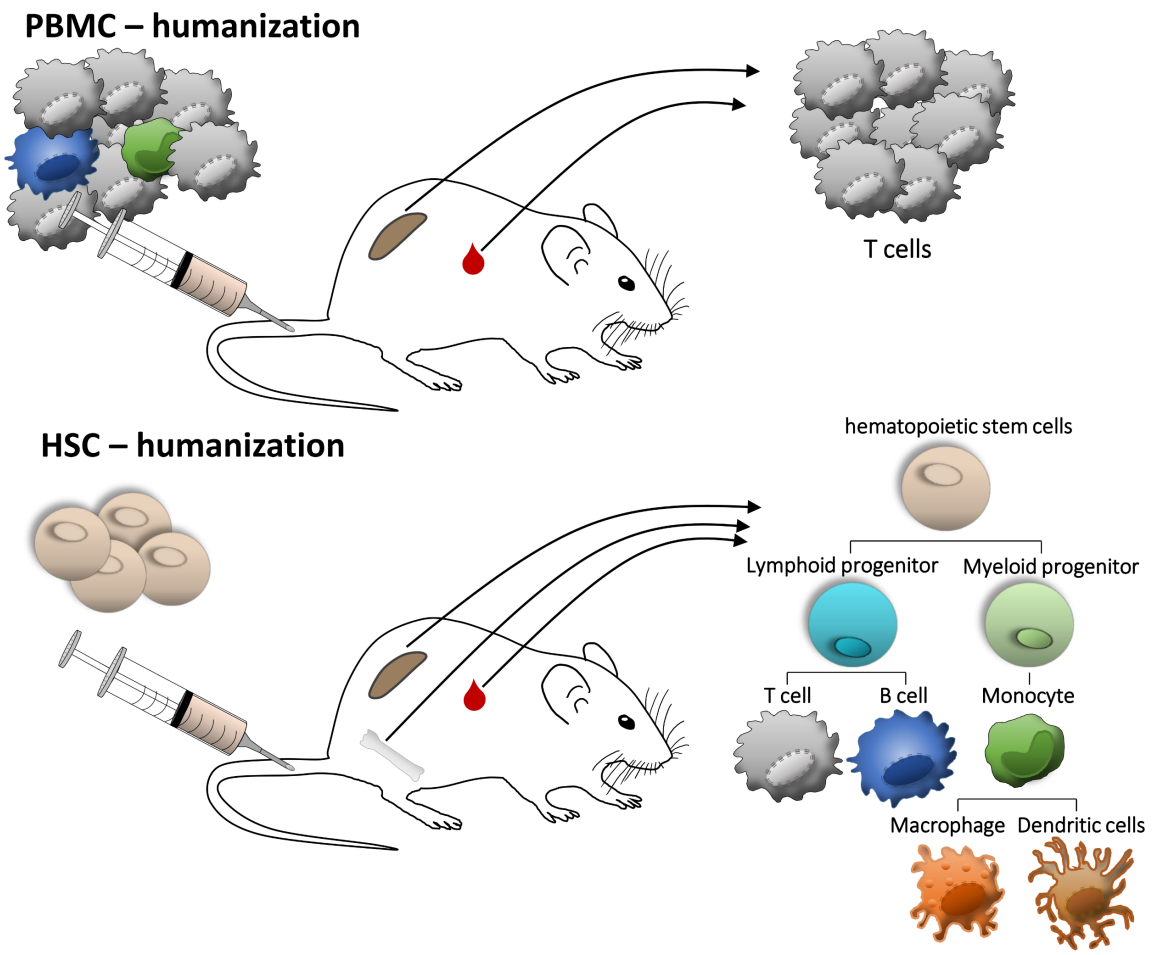

Figure 5: Platforms for humanization of immunodeficient mice.
Humanization of immunodeficient mice can be achieved by human PBMC engraftment or using purified human CD34+ stem cells. Intravenous delivery into mice results in different human immune cell type reconstitution. PBMC engraftment results mainly in human T cells residing in the periphery and spleen. Humanization of hematopoietic stem cells (HSC) leads to cell engraftment in the bone marrow niche and gives rise of lymphoid and as well myeloid progenitor cells, which differentiate into lymphoid and myeloid cells in the system (spleen and blood). Depending on the mouse model, immune cell composition can vary in respect to monocyte derived lineages.

The second strategy for humanization uses human stem cells, which engraft into the bone marrow niche and can give rise of the human immune progenitor cells. As most promising cell source, CD34+ enriched hematopoietic stem cells from umbilical cord blood has proven to give best results for humanization level after engraftment into female newborn mice (140). This results in development of human T cells, B cells and to some degree cells of the myeloid lineage several weeks after engraftment in the conventional NSG and NRG models (140). An important difference to the PBMC humanized platform is the absence of xenoreactivity, since the developing human T cells undergo thymopoiesis in the mouse thymus and are therefore educated to mouse antigens. Consequently, the developing human immune system in these mice will be

in a resting and quiescent state. Yet, there are still certain limitation for this platform. Human myeloidpoiesis is limited in the system due to restricted crossreactivity of mouse cytokines to human cells and results in relatively low levels of monocytes and macrophages and no human NK cell development in the system. Therefore, efforts have been made towards next generation models, which support a more complete engraftment of the human immune system upon stem cell humanization. In particular, expression of human GM-CSF and IL-3 have shown to be important for the differentiation of human hematopoietic stem cells (HSCs) into myeloid progenitor cells (141), while stem cell factor (SCF) is a critical cytokine for maintenance of HSCs (142). Mouse models, such as NOG-EXL, MISTRG and NSG-SGM3 have been designed to constitutively express these or additional cytokines and showed to significantly improve human HSC engraftment and further development of human cells of the monocyte lineage (143–146). Studies using CD34+ stem cell humanized NSG-SGM3 (huSGM3) mice, which are transgenically expressing SCF, GM-CSF and IL-3, showed that the pronounced engraftment of human monocytes in the system allowed the recapitulation of clinically relevant CAR T cell induced CRS and ICANS in this model (86, 90).

1.5 Objective

Current efforts to refine CAR T cell generation include the direct *in vivo* generation of CAR T cells in the body using receptor targeted lentiviral vectors (LVs). However, preclinical studies have been limited so far to the humanized NSG model, which has some restrains regarding humanization and human myeloid cell engraftment. Therefore, deploying the CD34+ stem cell humanized NSG-SGM3 (huSGM3) mouse model allows the evaluation of *in vivo* CAR T cell generation in a humanized immune system with clinically relevant levels of human myeloid cells. The first part of the thesis aimed to evaluate if *in vivo* CD19CAR T cell generation using CD4 and CD8 targeted LVs is impacted in the presence of human myeloid cells in huSGM3 mice. To determine successful CAR T cell generation after intravenous injection of the LV, CAR T cell and B cell levels were monitored in the blood over time. Moreover, lymphocyte-residing organs (bone marrow and spleen) and as well, biodistribution relevant organs (lung and liver) were analyzed for CAR T cell presence and off-target CAR transfer. Performing vector copy number analysis and expansion assays with splenocytes samples further advanced detection of CAR T cells. In addition, analysis of human plasma cytokine gave insights into the activity of human lymphoid and myeloid immune cells. To confirm if human myeloid cells were negatively impacting T cell specific transduction, a co-culture assay with primary monocytes and macrophages was established. Finally, phagocytosis shielding of the targeted vectors from was evaluated for improved CAR T cell generation in the presence of human myeloid cells *in vitro* and *in vivo* in huSGM3 mice.

Another approach to refine CAR T cell manufacturing is the reduction of activation and transduction time *ex vivo*. Such “short-term” CAR T cells have shown to possess great anti-tumor activity *in vitro* and *in vivo*. However, the risk for adverse events, such as cytokine release syndrome CRS, has not been investigated. The second part of the thesis focuses on the evaluation of short-term CAR T cells to induce severe CRS. First, the short-term CAR T cells were characterized for bound vector particles and CAR expression after production. Next, the cytotoxic capability of short-term CAR T cells was analyzed in an *in vitro* killing assay that allowed simultaneous evaluation of cytokine release during tumor cell killing. Finally, systemic adverse events were investigated in tumor engrafted non-humanized NSG-SGM3 mice with weight and temperature change and systemic release of human and murine cytokines as readout.

2 Results

This thesis describes the usage of NSG-SGM3 mouse model for the evaluation and characterization of novel CAR T cell gene therapy approaches. In the first part, huSGM3 mice were used, which develop a sophisticated human immune system with physiologically relevant numbers of human myeloid cells. Intravenous injection of CD4- and or CD8-receptor targeted LV particles, produced in conventional HEK-293T cells, resulted in moderate *in vivo* CAR gene delivery in huSGM3 mice. This was accompanied for the CD4-LV group with an increase in myeloid associated human plasma cytokines. Further, primary macrophages were identified in a co-culture assay to interfere with the transduction of T cells. Phagocytosis shielding of the vector particles by production in β2M $^{-/-}$, CD47^{high} HEK-293T cells significantly improved T cell transduction in presence of macrophages. Finally, a direct comparison of shielded and non-shielded CD4-LV and CD8-LV was performed in huSGM3, which confirmed the improved *in vivo* CAR T cell generation in a sophisticated human immune system. In the second part, NSG-SGM3 mice were used to set up an *in vivo* model for the prediction of CD19-CAR T cell induced cytokine release syndrome. Pre-engraftment of mice with CD19+ tumor cells and subsequent administration of short-term CAR T cells resulted in severe adverse effects, including, weight loss, temperature drop and high cytokine release in the mice. Parts of the results in chapter 2.2, 2.3 and 2.4 are based on the publication Ho and colleagues, 2022 (147) and is indicated for the respective figures and tables.

2.1 Characterization of the humanized NSG-SGM3 mouse model

To have a general idea about the composition of the immune cells in huSGM3 mice human immune cells in blood were analyzed by flow cytometry analysis. In addition, presence of murine cell types in the spleen were compared to wildtype Balb/c mouse, which is frequently used as standard mouse model in translational oncology research.

2.1.1 Humanization level in blood of huSGM3 mice

To assess humanization levels, huSGM3 mice were bled retro-orbitally and total human CD45+ cells in blood were determined 15-26 weeks after human stem cell

reconstitution. huSGM3 mice showed on average 74% humanization in the periphery that resembled about 400 human cells per µL blood (Figure 6).

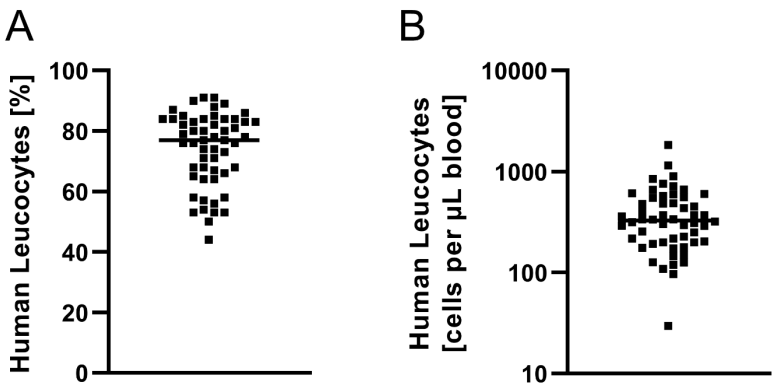

Figure 6: Humanization level in huSGM3 mice.
CD34+ cord blood humanized NSG-SGM3 mice were analyzed for human engraftment level in the blood. **A)** Frequency of humanization was determined by CD45+ cells of total viable cells measured by flow-cytometry. **B)** In addition, total cell number of human CD45+ cells per µL blood was determined. Mice were untreated before blood withdrawal and used in different experiments. Each data point represents one mouse with indicated mean value per group. n = 54.

Further phenotyping of the human immune cells in the blood revealed a pronounced T cell engraftment of about 76% (320 cells/µL blood) in huSGM3 mice followed by B cells at about 18% (65 cells/µL blood), monocytes below 1% (1,5 cells/µL blood) and over 3% unidentified cells (17 cells/µL blood) (Figure 7).

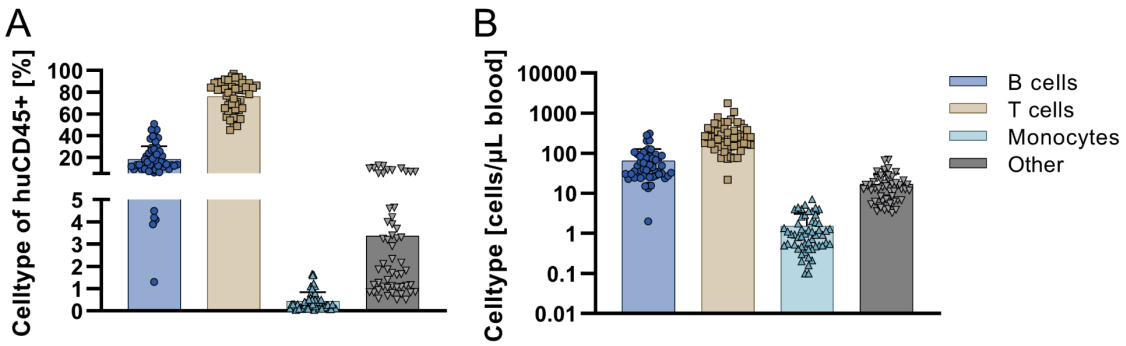

Figure 7: Human immune cell phenotyping in blood of huSGM3 and huNSG mice.
huSGM3 mice were analyzed for human cell type distribution in blood. **A)** Frequencies of B cells (dark blue), T cells (brown), monocytes (bright blue) and other cells (grey) were determined by human CD19, CD3 or CD14 marker expression or absence in CD45+ cells measured by flow-cytometry. **B)** Total cell number of human B cells, T cells and monocytes per µL blood was determined. Each data point represents one mouse with indicated mean value per group. n = 54.

2.1.2 Murine immune cells in huSGM3 mice

Since huSGM3 mice are based on the severe immunodeficient NSG strain, they lack major part of the murine innate and adaptive immune system. Identifying the remaining

murine immune cells in huSGM3 mice gives important information about potential interacting cells within the mouse system during an ongoing immune response due to partial cross-reactivity of human and murine cytokines. As the spleen is one of the major site for ongoing immune responses and a niche for various immune cells, splenocytes of one huSGM3 mouse were isolated and analyzed for immune cell composition. To compare to an immunocompetent mouse strain, splenocytes from a Balb/c mouse were included as a control. Flow cytometry data was reduced for its multi-dimensional parameter and visualized two-dimensionally by t-distributed Stochastic Neighbor Embedding (tSNE) data analysis. In there, cells with same combination of marker expression, and thus same cell types, were grouped into a cluster together (Figure 8). In the spleen of the Balb/c mouse a majority of the murine immune cells consisted of B cells located at bottom of the tSNE plot and T cells, which were located on the left side of the plot, with visible separation of the CD4 and CD8 subset. In addition, the innate immune cells, including monocytes, macrophages, lymphoid and myeloid DCs and neutrophils were identified in the Balb/c mouse sample and separated to the upper part of the tSNE figure. In contrast, murine T cells and B cells were completely absent in the huSGM3 mouse. Interestingly, innate immune cells of mouse origin, including monocytes, macrophages, lymphoid and myeloid DCs, and neutrophils, were detected in the huSGM3 spleen. Though, the majority of the cells residing in huSGM3 spleen were human leukocytes (Figure 8).

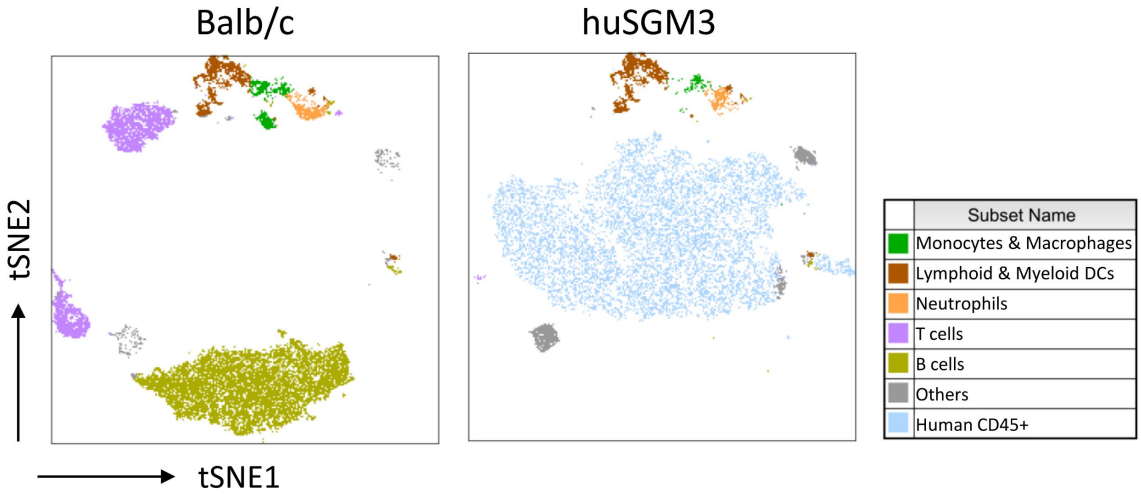

Figure 8: Murine immune cell phenotyping in spleen of huSGM3 and Balb/c mice. Untreated huSGM3 and Balb/c mice were analyzed for murine cell type distribution in the spleen by flow cytometry analysis and presented as multi-dimensional parameter reduced tSNE plot. Human cells (blue) and murine B cells (yellow), T cells (magenta), neutrophils (orange), DCs (brown), monocytes and macrophages (green) and non-identified cells (grey), identified by murine CD3, CD19, CD11b, CD11c, Ly-6G, Ly-6C and human CD45 surface marker expression, are depicted for the respective clusters for each mouse. Gating strategy as well multi-dimensional reduction data processing are described in the method section 4.3.19. Data are shown for one mouse each.

Taken together, immune phenotyping of the huSGM3 showed a pronounced human cell engraftment of T cells, B cells and to a lesser extend monocytes in the blood. In addition, analysis of murine immune cells in the spleen revealed a complete absence of T cells and B cells, however, with remaining DCs, monocytes, macrophages and neutrophils in the system.

2.2 *In vivo* CAR T cell generation in humanized NSG-SGM3 mice

In this chapter the generation of CAR T cells directly *in vivo* with targeted CD4-LV and CD8-LV is evaluated in the sophisticated humanized immune system of the huSGM3 mouse model. Kinetics of emerging CAR T cells and their respective target cells, the CD19+ human endogenous B cells, were assessed in the blood. Further, the presence of CAR T cells in lymphocyte residing organs was confirmed by direct detection of the CAR and indirectly by the reduction of B cell levels. To enhance detection sensitivity *in vivo* CAR gene delivery was confirmed on the genomic level by quantitative polymerase chain reaction (qPCR) analysis. Finally, human cytokine analysis in the plasma was performed to monitor ongoing immune cell activity.

2.2.1 Experimental set up

To generate CAR T cells directly *in vivo,* CD4-LV, CD8-LV, a mixture of both vector suspensions (MIX) or PBS as control were injected intravenously into huSGM3 mice (Figure 9). To have a comparable setting between the targeted LVs, similar transducing units were applied for the single vector groups (Table 1), whereas mice in MIX received approximately same transducing units for each of the receptor targeted LV. In addition, all mice were injected two times before and after vector application with human IL-7 (Figure 9) to improve *in vivo* T cell transduction as shown previously by Frank and colleagues (73). Mice were then monitored regularly for general health condition, bled weekly to assess CAR T cell and B cell presence and cytokine level in the blood. In total three mice from the same humanization cohort were excluded from the experiment, which had to be sacrificed within one week after vector or PBS injection due to weight loss below 20% of initial weight.

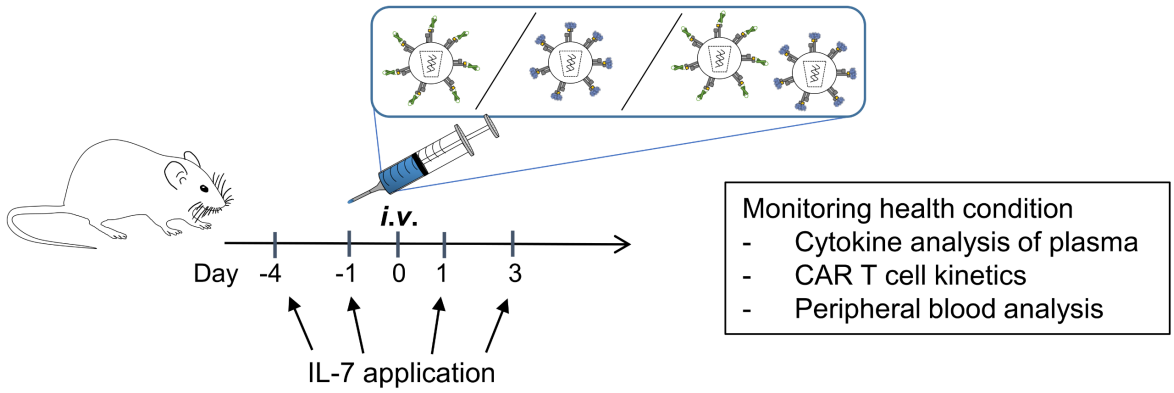

Figure 9: Experimental setup for *in vivo* CAR T cell generation.
huSGM3 were injected intravenously (*i.v.*) with CD4-LV, CD8-LV, a mix of both (MIX), or PBS (Control). Mice received human IL-7 by *i.v.* or subcutaneous (*s.c.*) injection 1 and 4 days before and 1 and 3 days after vector administration and monitored for general health condition and generation of CAR T cells. Figure modified from (147).

Table 1: Particle concentration and transducing units of injected LV stocks in Figure 10.

Vector	Particle/mL	[a]T.u./mL	Injected T.u / mouse
[b]CD4-LV	1.3×10^{12}	[d]1.4×10^{7}	2.58×10^{6}
[b]CD8-LV	1×10^{12}	[e]1.2×10^{7}	2.40×10^{6}
[c]CD4-LV	6×10^{11}	[d]3×10^{6}	1.20×10^{6}
[c]CD8-LV	5.7×10^{11}	[f]5.5×10^{6}	1.16×10^{6}

[a](T.u.) Transducing units.
[b]stock used in first experiment in Figure 10
[c]stock used in second experiment in Figure 10.
[d]t.u. determined on A301 cells.
[e]t.u. determined on J76S8ab cells.
[f]t.u. determined on PBMC.
Table modified from (147).

2.2.1.1 CAR T cells in the peripheral system

After vector administration CAR T cells emerged in the blood of some mice starting from day 17 in three out of four mice in the MIX group with a clear peak for two mice on day 25 reaching between 1 – 12% CAR+ T cells in the CD4 and CD8 T cell subtype (Figure 10). In the CD8-LV group two of nine mice showed rising CAR T cells reaching around 6 – 10% exclusively in the CD8 subset. However, about 2 – 3 weeks later than in the MIX group. In contrast, CD4-LV injected mice did not develop pronounced CAR signals in blood above the control background, except for one out of eight mice which showed early on day 10 transiently about 6% CD4+ CAR T cells (Figure 10).

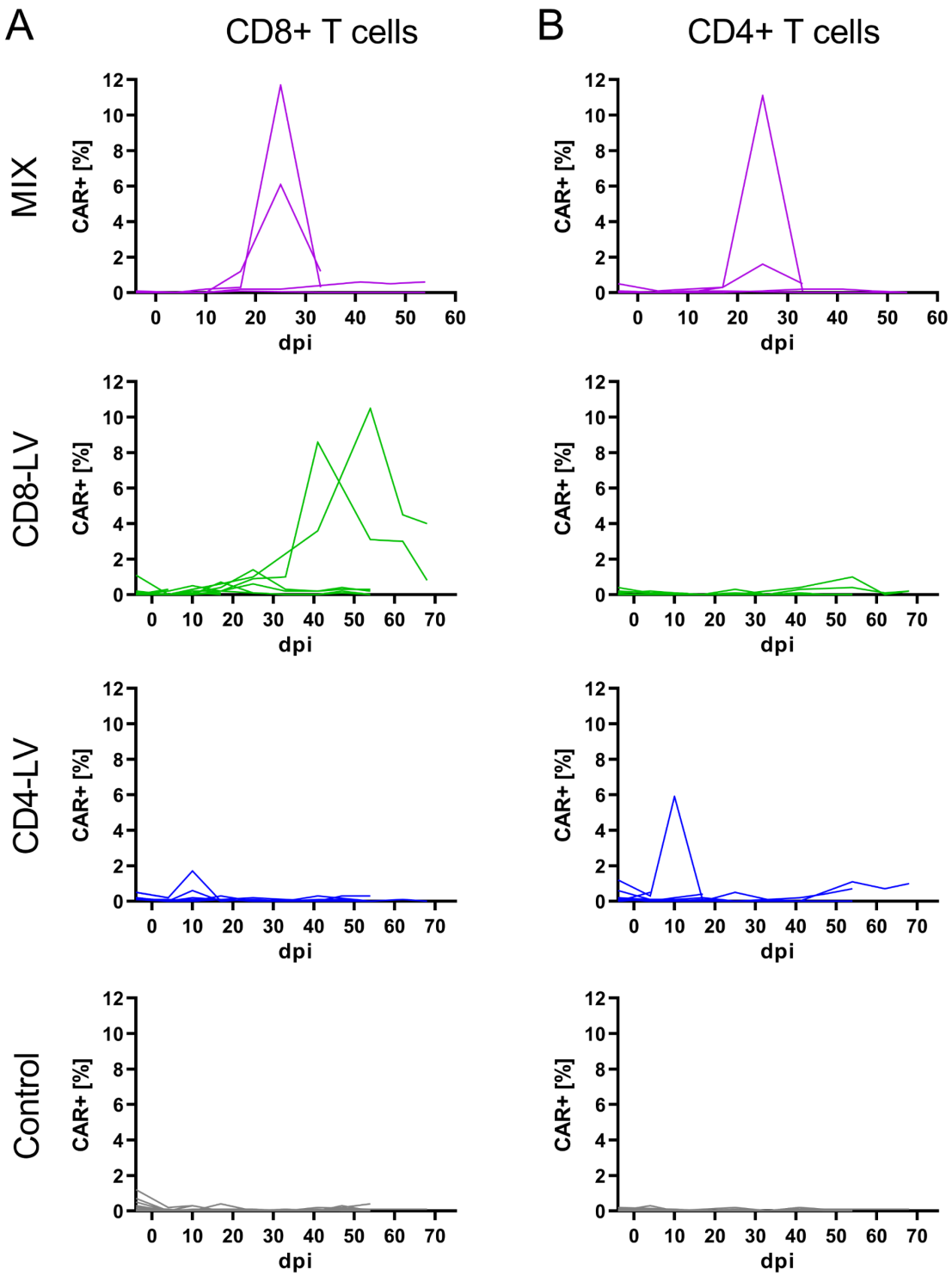

Figure 10: CAR T cell kinetic in blood of huSGM3 mice.
Kinetic of CAR+ T cells in blood of huSGM3 after vector administration were measured by flow-cytometry and shown as CAR positive signal of CD8+ T cells **(A)**, CD4+ T cells **(B)** for each mouse. n= 4 (MIX), 8 (CD4-LV), 9 (CD8-LV) and 12 (Control) in 2 independent experiments. dpi (days post vector injection). Figure modified from (147).

Activity and functionality of *in vivo* generated CAR T cells in the periphery was confirmed by the reduction of endogenous CD19+ human B cells that correlated with

the CAR T cell kinetic. All mice of the MIX group, four of nine mice in the CD8-LV group and three of eight mice in the CD4-LV group and none in the control displayed less than 50% of initial relative B cell levels (Figure 11). The eradication of CD19+ target cells was permanent for all respective mice except for one mouse in the MIX group with relapsing B cells in the blood within week three.

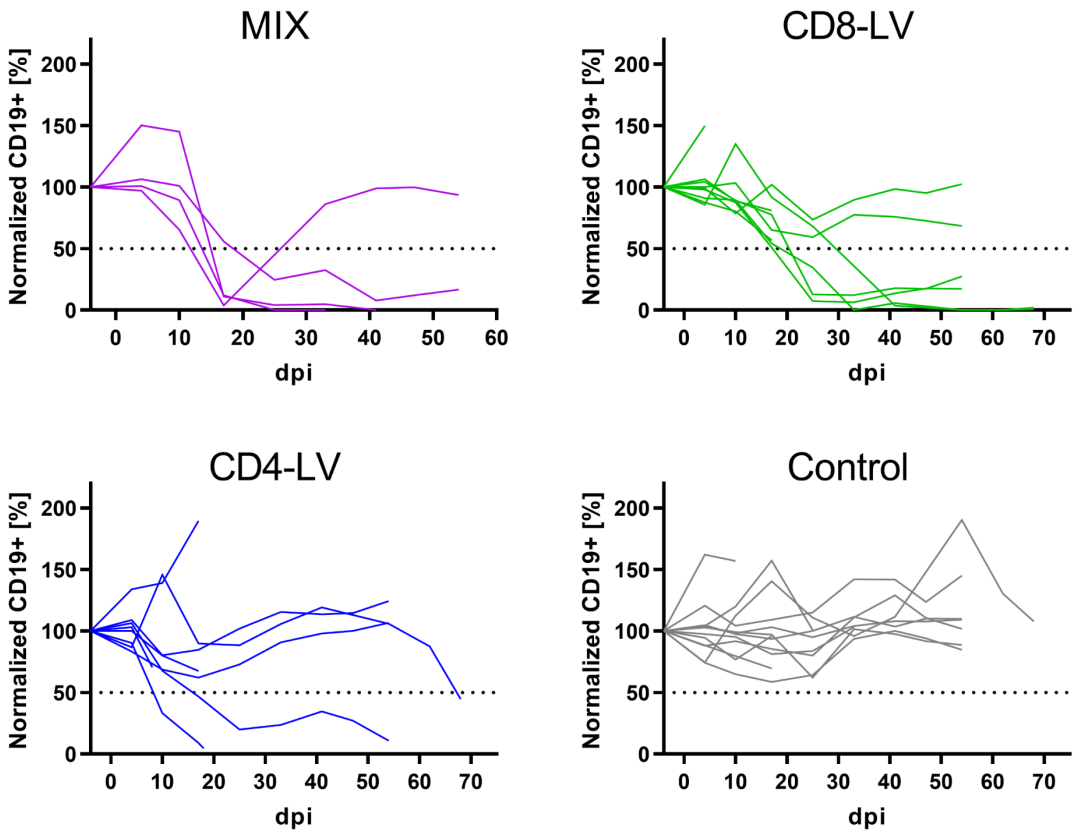

Figure 11: B cell kinetic in blood of huSGM3 mice after vector injection.
Kinetic of CD19+ target cells detected by flow cytometry in blood of huSGM3 after vector administration are shown as normalized B cell of CD3- cells for each mouse. Dotted line shows cut off for determining reduction of B cells in mice. n= 4 (MIX), 8 (CD4-LV), 9 (CD8-LV) and 12 (Control) in 2 independent experiments. dpi (days post vector injection). Figure modified from (147).

2.2.1.2 Presence of CAR T cells in organs verified by FACS

Further, the major lymphocyte residing organs, spleen and bone marrow, but as well the biodistribution relevant organs, lung and liver, were analyzed for the presence of CAR T cells on the final day. Flow cytometry analysis did not show pronounced CAR T cell signals over the control background in any vector-treated mice in the spleen and the liver (Figure 12). Only one CD4-LV mouse with over 6% CAR T cells in the bone marrow and one MIX mouse with 3% CAR T cells in the lung were positive (Figure 12).

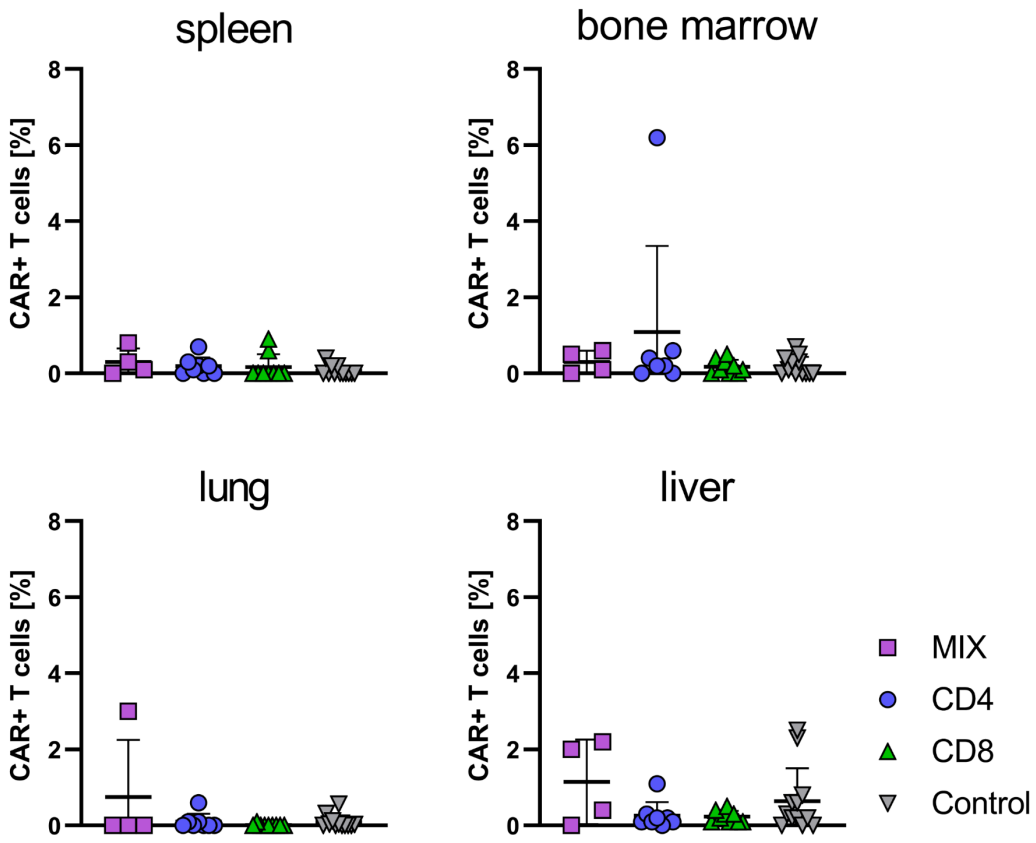

Figure 12: CAR T cells in organs.
Percentage of CAR T cells detected by flow cytometry in the spleen, bone marrow, lung, liver of huSGM3 mice after vector administration. Data are shown for each mouse with mean and standard deviation of the group. n= 4 (MIX), 8 (CD4-LV), 9 (CD8-LV) and 12 (Control) of two experiments. n= 4 (MIX), 6 (CD4-LV), 8 (CD8-LV) and 10 (Control) of two experiments. Statistics were determined by non-parametric Kruskal-Wallis (Dunn's multiple comparisons test). Figure modified from (147).

Although the detection of CAR T cells by flow cytometry was challenging in the organs, reduction of B cell frequencies could be confirmed at cellular level. Especially in the MIX group B cell frequencies were significantly lower compared to the control in spleen, bone marrow and liver (Figure 13). In spleen target cell reduction was most prominent in three mice of the MIX and the CD4-LV group as well four mice in the CD8-LV group having B cell frequencies clearly below 20%. Also, in bone marrow all MIX, three CD4-LV and two CD8-LV mice showed B cell levels below 6% of the control background. Low target cell frequencies were also observed in isolated lung and liver cells for some vector-treated mice. However, abundance of B cells was generally low in these organs as indicated by the control and reduction of the B cells was less prominent (Figure 13).

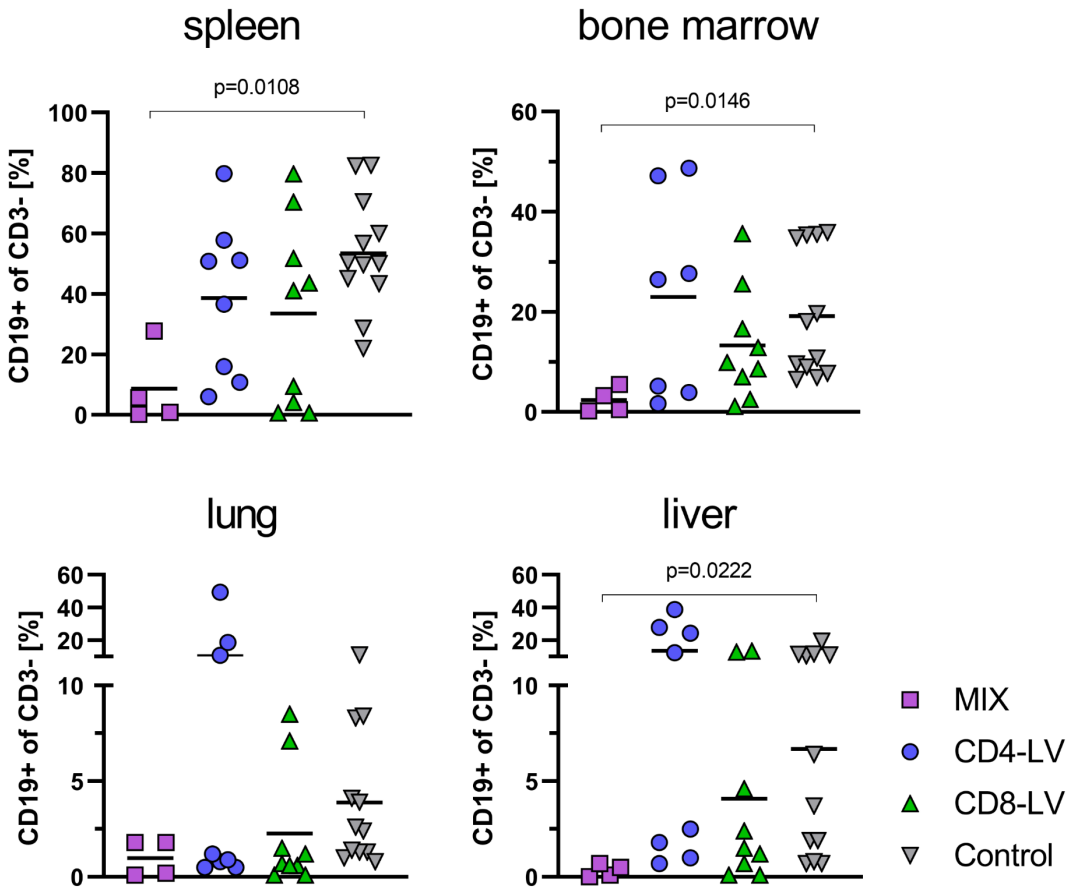

Figure 13: B cells in organs.
B cell levels in the spleen, bone marrow, lung and liver of huSGM3 mice after vector administration are shown for the day of final analysis determined by FACS. n= 4 (MIX), 7-8 (CD4-LV), 9 (CD8-LV) and 12 (Control) in 2 independent experiments. Statistics were determined by non-parametric Kruskal-Wallis (Dunn's multiple comparisons test) with indicated significant p-values. Figure modified from (147).

To further enhance the detection of CAR T cells in the major T lymphocyte residing organ, isolated splenocytes were co-cultivated in the presence of irradiated CD19 positive Raji or Nalm-6 tumor cells for over two weeks to allow for antigen induced proliferation of the CAR T cells. Flow cytometry analysis revealed a significant expansion of CAR T cells in all groups compared to the control (Figure 14). For two MIX, three CD4-LV and four CD8-LV treated mice and none in the control, reaching up to 26% CD4+ and 53% CD8+ CAR T cells in the culture. Importantly, the emerging CAR T cells were majorly restricted to the respective targeted subtypes of the vectors with only MIX treated mice containing CD4+ as well CD8+ CAR T cells (Figure 14).

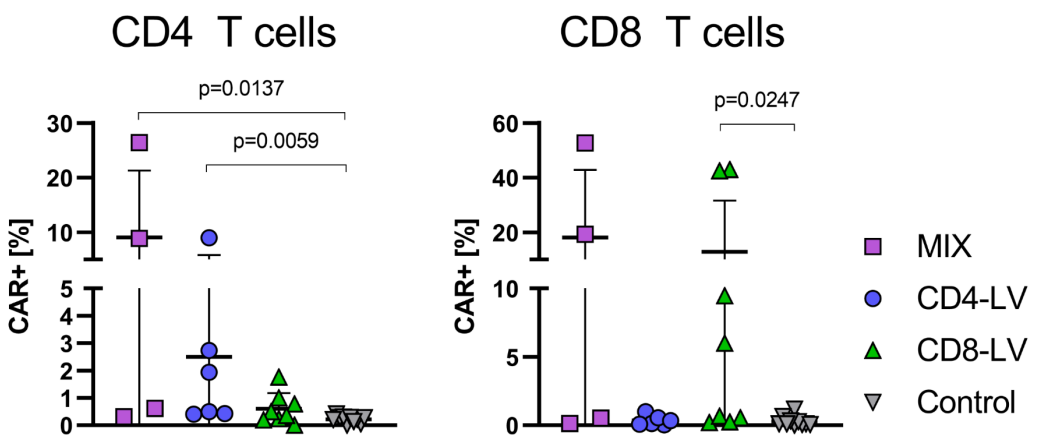

Figure 14: CAR T cell expansion in tumor cell co-culture.
In vitro expanded CAR+ CD4 or CD8 T cells after cultivation of isolated splenocytes from huSGM3 mice injected with indicated vector particles with irradiated CD19+ Raji cells measured by flow-cytometry. Data are shown for each mouse performed in technical triplicates, with mean and standard deviation of the group. n= 4 (MIX), 6 (CD4-LV), 8 (CD8-LV) and 10 (Control) of two experiments. Statistics were determined by non-parametric Kruskal-Wallis (Dunn's multiple comparisons test) with indicated significant p-values. Figure modified from (147).

2.2.1.3 Gene delivery verification on genomic level

To verify the successful *in vivo* gene delivery of the CAR by the different vectors on genomic level, isolated bulk splenocytes and bone marrow cells were assessed for integration of the transgene by qPCR. Correlating to the target cell reduction and the expansion assay data from the organs, vector copy numbers (VCN) above the threshold of the control mice confirmed overall significant vector integration (Figure 15). In general, VCN were rather low, which underlined the low abundance of CAR T cells in the organs and the difficult detection by flow cytometry. With a mean transgene integration number of 0.04 and 0.03 in the spleen and bone marrow for the MIX group, abundance of integrates was similar in those organs. As well for CD4-LV treated mice the mean VCN was at 0.095 and 0.054 for the isolated splenocytes and bone marrow cells. However, this was almost one log higher for CD8-LV generated CAR T cells in spleen (0.031) as in the bone marrow (0.004). Although, control injected mice were absolutely devoid of CAR T cells a mean VCN of 0.0013 and 0.00013 in spleen and bone marrow could be calculated that reflected the sensitivity limit for the measurement of these samples in this assay. Interestingly, among the vector treated groups the highest VCN was found in the CD4-LV group, although these mice showed the least prominent CAR T cell presence in the blood (Figure 15).

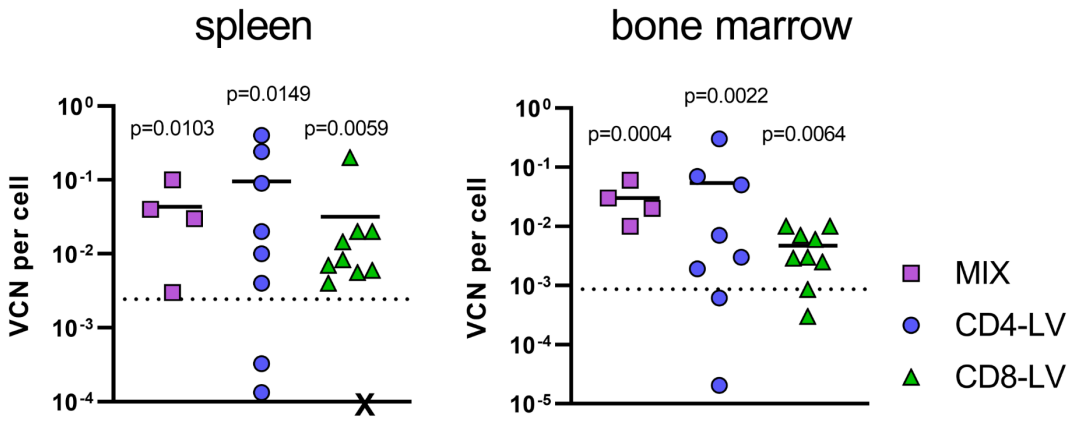

Figure 15: VCN in spleen and bone marrow.
VCN per cell of the CAR transgene was measured by qPCR for the respective organ from huSGM3 mice injected with indicated vector particles. The dotted lines represent the upper 95% confidence interval of the control group. Individual mice are plotted with mean of the group. n= 4 (MIX), 7-8 (CD4-LV), 9 (CD8-LV) and 12 (Control) in 2 independent experiments. X indicates a calculated VCN of 0 that could not be plotted on a logarithmic scale. Statistics were determined by non-parametric Kruskal-Wallis (Dunn's multiple comparisons test) with indicated significant p-values compared to the Control. Figure modified from (147).

2.2.2 Distinct cytokine pattern for CD4-LV treated mice

Analysis of human plasma cytokines in the blood on day 17 after vector application revealed a distinct myeloid cell associated cytokine pattern for CD4-LV treated mice. The pro-inflammatory cytokine IL-2, which is related to T cell activity, was rather low in all mice ranging below 150 pg/mL with the exception for two mice at 200 pg/mL and one mouse around 700 pg/mL in the CD4-LV injected group (Figure 16). As well for TNF-α, a pro-inflammatory and pyrogenic acting systemic cytokine, was found at low levels below 80 pg/mL and moderately increased in some mice treated with CD4-LV, CD8-LV but as well PBS. Interestingly, cytokines that are related to activity of myeloid cells, in particular monocytes, were notably increased in the plasma of CD4-LV treated mice. For instance, the pleiotropic cytokine IL-10, that acts mainly anti-inflammatory, was found to be about 2-fold increased compared to the other groups. In addition, the acute released pro-inflammatory cytokine IL1-β was also overall slightly elevated in the CD4-LV group ranging from 10 – 60 pg/mL, whereas the levels in all MIX mice, most CD8-LV and control mice were located below 20 pg/mL with exception of two mice each in the latter two groups. Furthermore, CD4-LV injected mice showed significantly elevated IL-15 compared to CD8-LV and control treated mice with overall about 3-25 fold increase. An interesting observation was also made in the CD4-LV group with overall 2-fold decreased GM-CSF compared to the other groups and might underline

ongoing activation and differentiation of monocytes and thereby GM-CSF consumption (Figure 16).

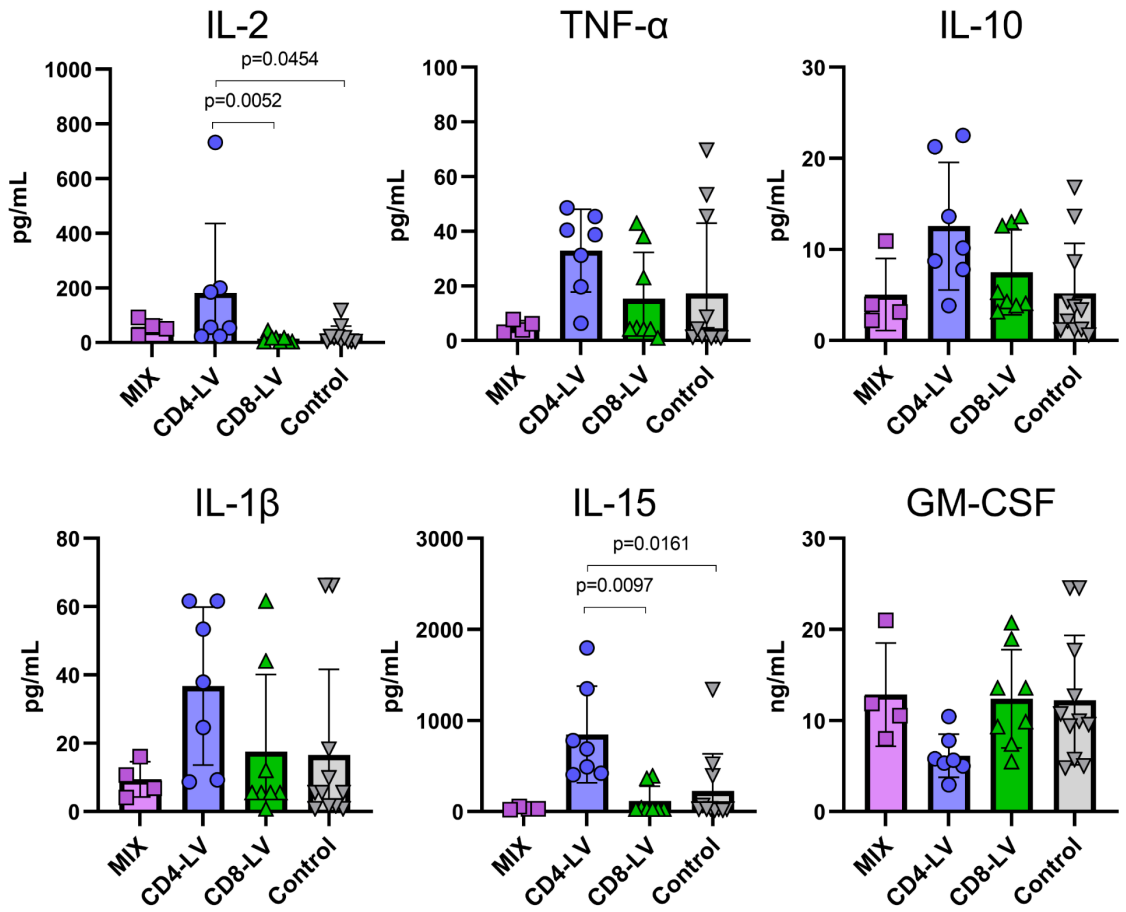

Figure 16: Plasma cytokines in huSGM3.
Plasma cytokines of huSGM3 mice on day 17 after vector administration were measured by bead-based multi-analysis kit. Concentration of the respective cytokines are shown for each mouse with mean and standard deviation of the group. n= 4 (MIX), 7 (CD4-LV), 8 (CD8-LV) and 11 (Control). Statistics were determined by non-parametric Kruskal-Wallis (Dunn's multiple comparisons test) with indicated significant p-values. Figure derived from (147).

Taken together, this indicates an activity by the myeloid population in the system that was pronounced for CD4-LV. Therefore, addressing this particular cell population might improve *in vivo* gene delivery with targeted LVs to T cell.

2.3 *In vitro* T cell transduction in the presence of myeloid cells

In the next step, to investigate if the pronounced presence of myeloid cells in the huSGM3 might be an obstacle for *in vivo* CAR T cell generation, an assay format was established to assess their impact on CD4-LV and CD8-LV mediated T cell transduction. Since human monocytes resemble a key feature in the huSGM3 mice

and the constituently expression of human GM-CSF in this model promotes macrophage differentiation, both cell types were selected for this assay. Macrophages were polarized from monocytes obtained from primary PBMC using a GM-CSF polarization protocol. Further, polarized macrophages were characterized for CD206 and CD209 surface expression by flow cytometry, which are typical markers for *in vitro* GM-CSF induced monocyte polarization and are associated with phagocytotic activity (148). In general, GM-CSF mediated polarization resulted in about 90% expression of CD206 or CD209 in the experiment and only macrophages which showed at least 40% CD209 expression were used to ensure assay robustness (Figure 17). In addition, to avoid alloreactivity donor matched activated T cells were used and transduced in the presence of the respective myeloid cell type.

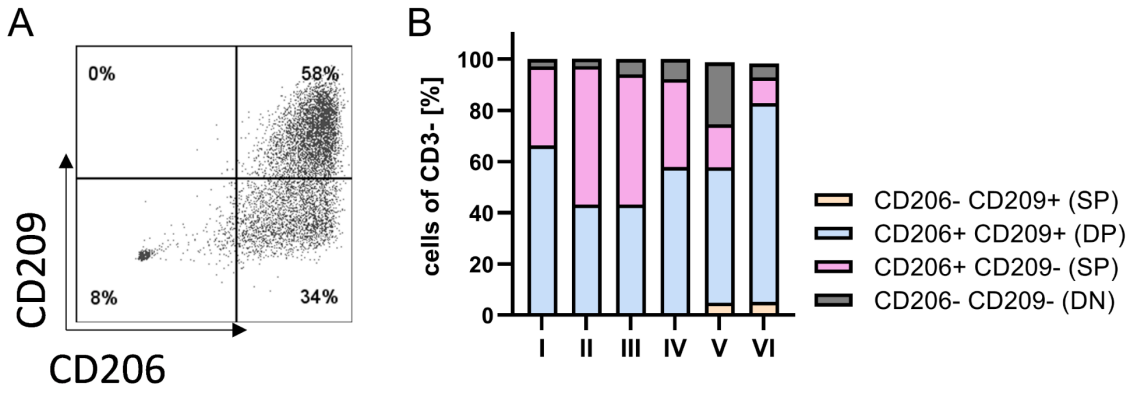

Figure 17: Characterization of *in vitro* polarized macrophages.
Macrophages, polarized from primary monocytes with GM-CSF, were characterized for surface expression of CD206 and CD209 by flow-cytometry. **A)** Representative FACS plot with indicated frequency of the respective quadrant, which was set based on isotype staining control. **B)** Marker expression on polarized macrophages of five different donors used in four independent experiments. Figure derived from (147).

2.3.1 Reduced T cell transduction in the presence of monocytes and macrophages

First, to recapitulate the different engraftment efficiency of myeloid cells in the huNSG and huSGM3 mice, different amounts of monocytes and macrophages were tested in the assay. The myeloid cell to T cell ratio was chosen based on the composition in the blood of humanized mice (4%) and of healthy human donors (10%) and an artificial ratio (50%) was included as well. To compensate for donor-variable transduction efficiency, results were normalized to the transduction in absence of myeloid cells.

Transduction of T cells in the presence of 50% monocytes was slightly reduced. For CD4-LV down to 88% and significantly for CD8-LV down to 64% as compared to the transduction in absence of monocytes. However, this was not notably visible in the physiological represented ratios 4% and 10% (Figure 18A). Whereas this effect was more pronounced when polarized macrophages were used in the culture. A dose dependent reduction of transduction could be observed for both vector types with the strongest reduction in the presence of the highest macrophage number. Interestingly, the impact on CD8-LVs was much more pronounced and transduction was reduced almost 2-fold at the highest ratio, whereas CD4-LV mediated transduction was reduced by about one third (Figure 18B).

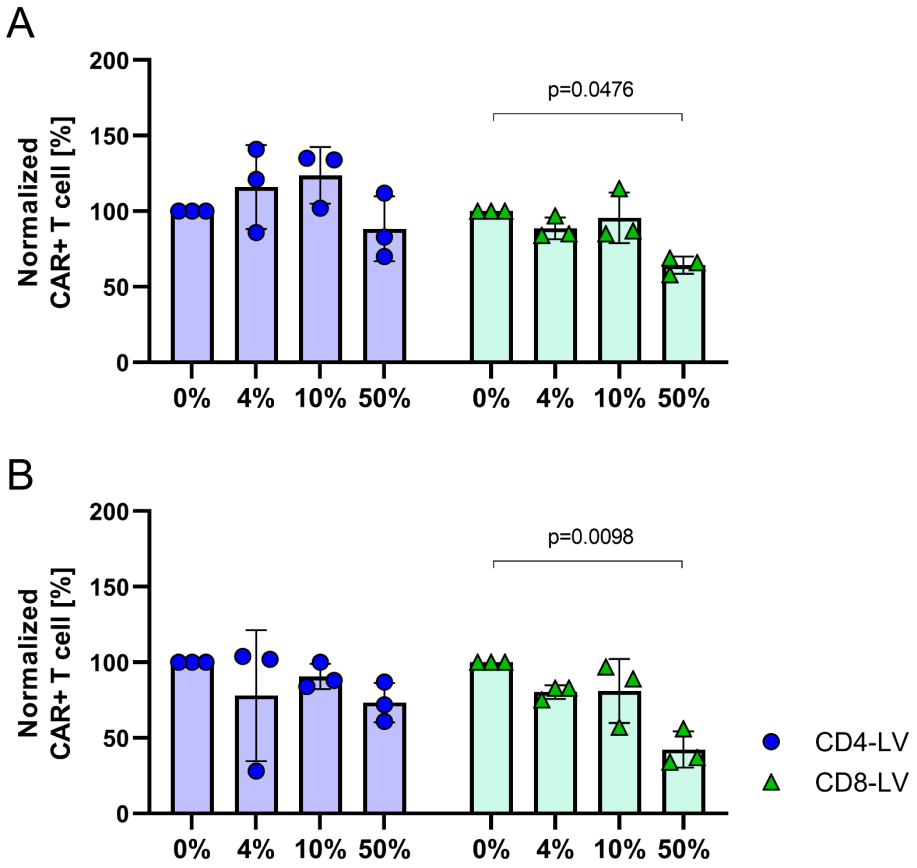

Figure 18: Reduced T cell transduction in presence of monocytes and macrophages. Normalized transduction of T cells co-cultivated with the indicated percentages of monocytes **(A)** or macrophages **(B)** using CD4-LV (blue) or CD8-LV (green) produced in conventional packaging cells. Mean with standard deviation from 3 donors performed in one to two different experiments in technical triplicates. Statistics were determined by 2-way ANOVA (Tukey's multiple comparisons test) with indicated significant p-values. Panel **B** modified from (147).

2.3.2 Phagocytosis shielding of CD4-LV and CD8-LV

To improve gene transfer efficiency to T cells in the presence of macrophages, the vector surface was refined to reduce immunogenicity of the targeted vector particles. By removing MHC I expression through β2 microglobulin (β2M) gene knockout and incorporating human CD47 into the vector surface, MHC mismatched induced immunogenic response as well phagocytosis-mediated uptake by phagocytes can be reduced. This was described before to improve vector particle half-life *in vivo* in mice as well *in vivo* gene delivery by VSV-G pseudotyped LVs into liver of non-human primates (149). In there, vector surface modification was achieved through vector particle production in β2M $^{-/-}$, CD47^{high} HEK-293T cells. To apply these modifications also on CD4-LV and CD8-LV, the vectors were produced in this modified HEK cell line to generate phagocytosis shielded CD4-LV (CD4-LV^{sh}) and CD8-LV (CD8-LV^{sh}).

Flow cytometry analysis of the cell surface marker CD47 and β2M expression on conventional HEK-293T and modified β2M $^{-/-}$, CD47^{high} HEK-293T cells confirmed the surface modification. A slight expression of human CD47 and a strong expression of β2M was found on the HEK-293T, whereas the modified cells significantly overexpressed human CD47 with an approximately 23-fold higher mean fluorescence intensity (MFI) and an over 14-fold lower MFI for β2M (Figure 19).

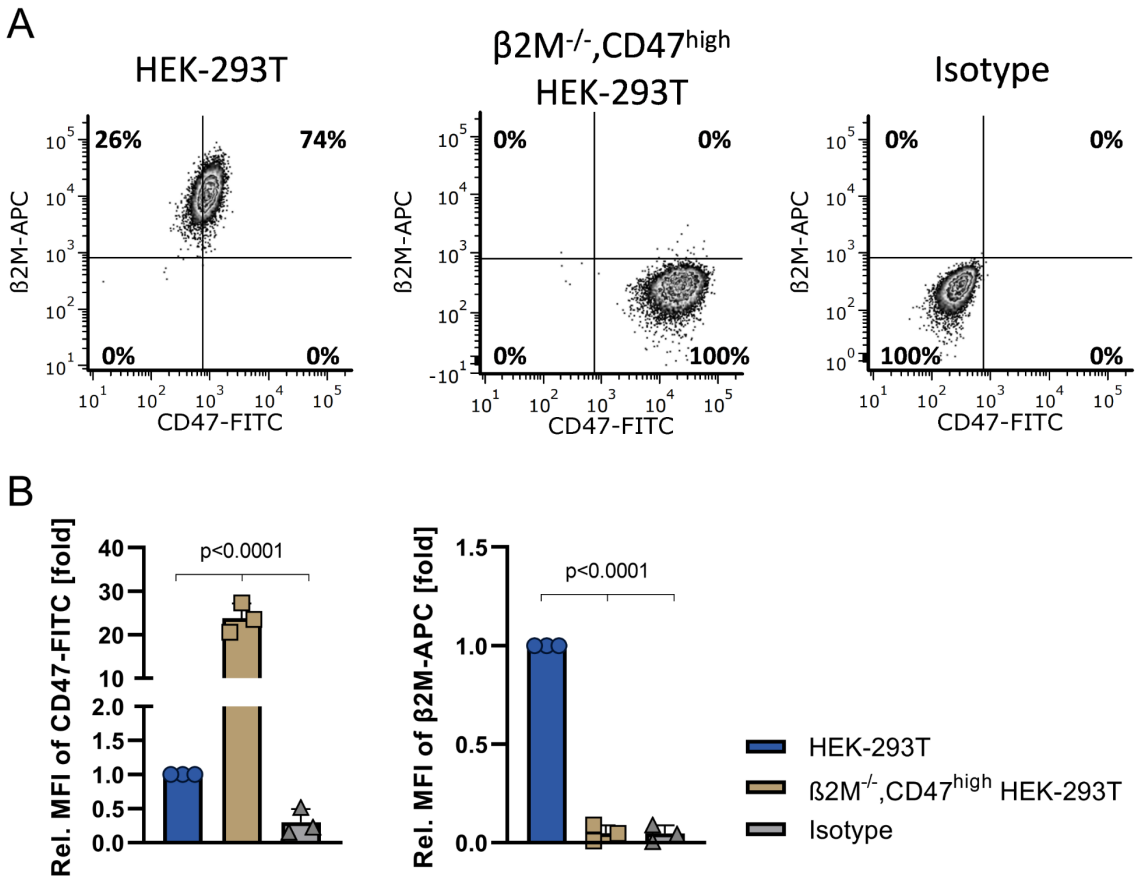

Figure 19: CD47 and β2M surface expression on vector packaging cell lines.
Surface expression of human CD47 and β2M on HEK-293T and β2M$^{-/-}$, CD47^{high} HEK-293T determined by flow-cytometry. **A)** Representative FACS plots with indicated frequency for CD47 and β2M expression on viable and singlet pre-gated HEK cells with isotype-stained cells as control. **B)** Relative mean-fluorescence intensity (MFI) for the markers as fold-change to HEK-293T cells. Data are shown as mean with standard deviation from three independent staining. Statistics were determined by one-way ANOVA (Dunnett's multiple comparisons test) with indicated significant p-values.

Targeted vectors produced in the different producer cells were then characterized for basic vector properties. Particle size and concentration in the vector stocks were assessed by nanoparticle tracking analysis and transducing units (t.u.), determined on the respective receptor expressing cell line, were compared. No significant difference in size was observed between shielded and non-shielded vectors with a mean size of 136 nm and 127 nm respectively (Figure 20A). However, particle concentration of the shielded vector stocks contained 1.8-fold more particles than the non-shielded stocks and showed an approximately 4.8-fold higher gene transfer activity (Figure 20B, C). To evaluate the potency of the vector stocks and compensate for higher particle counts in the shielded vector stocks, normalized gene transfer activity was calculated by dividing the gene transfer activity through the particle concentration. Although, normalized gene transfer activity in 1x10^{6} shielded vector particles was about 2.9-fold higher than in

non-shielded vector stocks, data distribution suggest a non-significant difference (Figure 20D).

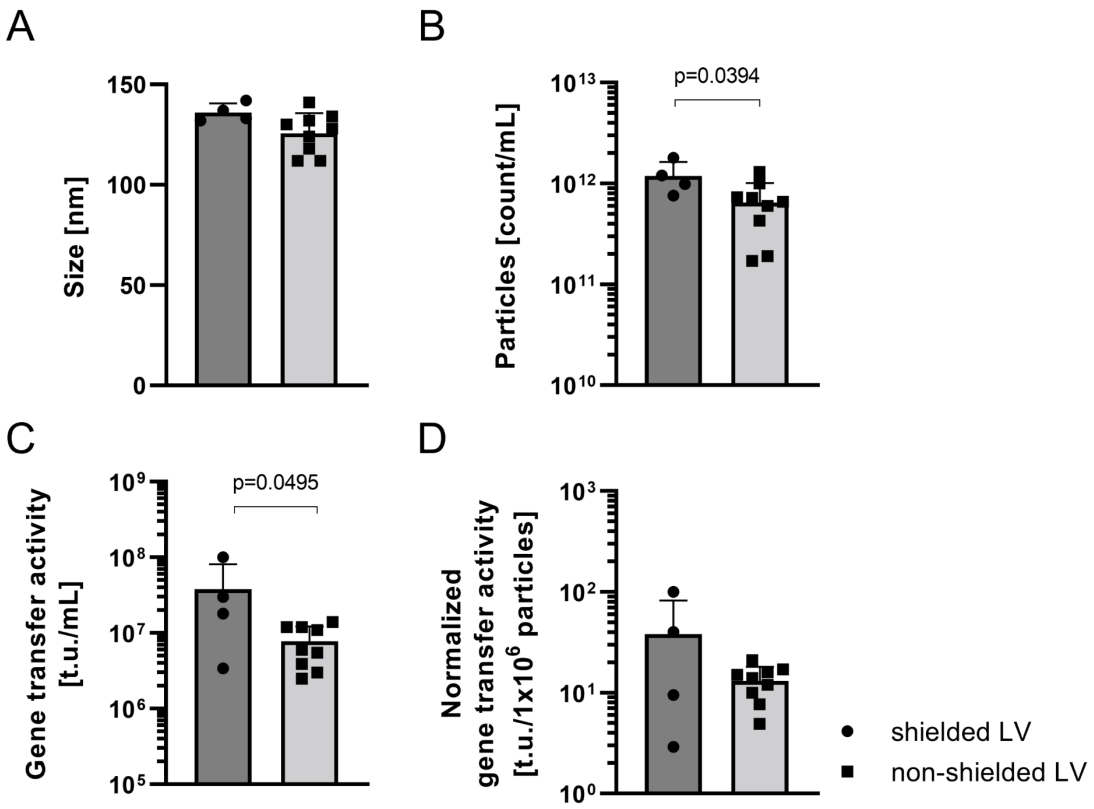

Figure 20: Characterization of shielded and non-shielded vector particles.
Shielded and non-shielded CD4-LV or CD8-LV produced in HEK-293T and β2M$^{-/-}$, CD47^{high} HEK-293T, respectively, were characterized for vector particle size **(A)** and particle concentration in the concentrated vector stock **(B)** by nanoparticle tracking analysis. Gene transfer activity of each LV stock was determined on the respective cell line **(C)** and normalized gene transfer activity as transducing units per 1x10^6 particles **(D)** was calculated. Each data point represents an independently produced vector stock plotted with the mean and standard deviation of n=4 (shielded LV) and n=9 (non-shielded LV). Statistics were determined by unpaired t test with indicated significant p-values. t.u.(transducing units).

2.3.3 Phagocytosis shielding of CD4-LV and CD8-LV improves T cell transduction in presence of macrophages

In the next step, to investigate if the vector surface modification benefits T cell transduction efficiency in the presence of macrophages, non-shielded CD4-LV and CD8-LV were compared to shielded CD4-LV^{sh} and CD8-LV^{sh} in the established co-culture assay at the 1:1 ratio. To ensure comparability of particle mediated effects and avoid donor-dependent influences, the transduction was normalized to the respective control in the absence of macrophages. The non-shielded CD4-LV and CD8-LV showed a mean reduction of 27% and 53% CAR gene delivery in the presence of macrophages (Figure 21). Remarkably, CD4-LV^{sh} and CD8-LV^{sh} significantly improved

relative T cell transduction 1.8-fold and 2.7-fold in the macrophage co-culture compared to the non-shielded vectors. Even more, transduction in the presence of macrophages performed on average 35% and 28% better than in absence (Figure 21).

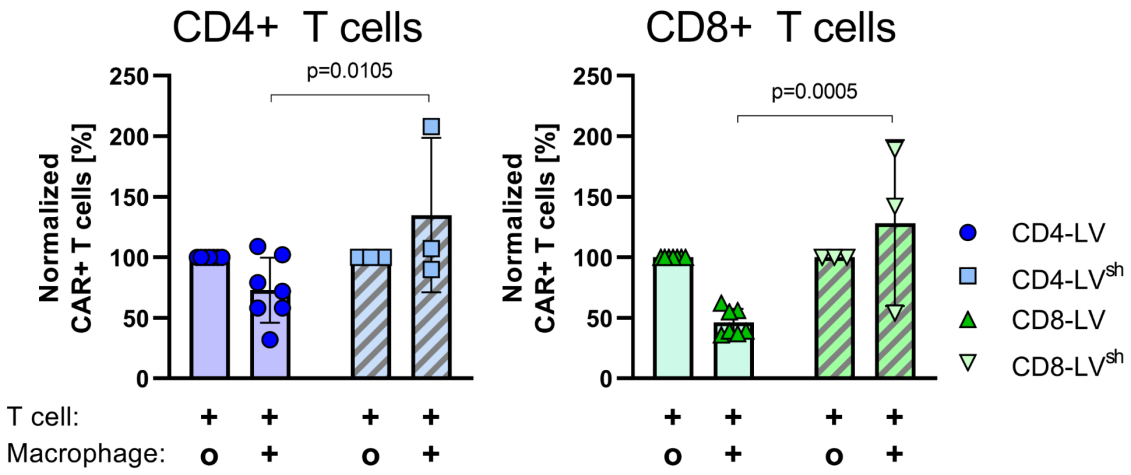

Figure 21: T cell transduction in presence of macrophages is improved by LV shielding. Comparison of conventional (blank bars) and shielded LVs (stripped bars) in transducing T cells in a 1:1 co-culture with (+) or without (O) macrophages. Mean with standard deviation from 3-7 donors performed in four independent experiments in technical triplicates. Statistics were determined by 2-way ANOVA (Bonferroni's multiple comparisons test) with indicated significant p-values. Figure modified from (147).

Taken together, this assay identified human macrophages, which were polarized with human GM-CSF from autologous monocytes as interceptor for T cell transduction with non-shielded T cell targeted LVs in a co-culture. Further, vector surface engineering of the CD4-LV and CD8-LV resulted in phagocytosis shielded CD4-LV^{sh} and CD8-LV^{sh} that significantly improved T cell transduction in presence of macrophages.

2.4 *In vivo* CAR T cell generation with phagocytosis shielded CD4-LV and CD8-LV

In the next step, the phagocytosis shielded CD4-LV^{sh} and CD8-LV^{sh} were tested in direct comparison to non-shielded CD4-LV and CD8-LV in the huSGM3 mice to evaluate if the vector surface modification improved CAR T cell generation *in vivo* in a human myeloid pronounced mouse model. To ensure comparability of particle mediated effects identical vector particle numbers of shielded and non-shielded particles were used, which differed only slightly in total transducing units (Table 2). Since the shielded LV stocks contained a higher particle concentration than the non-

shielded stocks, less vector stock volume was administered than technically possible. Therefore, an additional group of each shielded vector type was included with a 2-fold higher particle dose to see if higher *in vivo* gene transfer rates could be achieved (CD4-LV^{sh}(2x) and CD8-LV^{sh}(2x)). The same pretreatment and injection regime as described in Figure 9 was applied and CAR T cell generation was assessed as in the previous mouse experiment.

Table 2: Particle concentration and transducing units of injected shielded and non-shielded LV stocks.

Vector	Particle/mL	[a]T.u./mL	Injected particles / mouse	Injected t.u. / mouse
CD4-LV	4.3×10^{11}	[b]1.7×10^{7}	8.7×10^{10}	3.44×10^{6}
CD4-LV^{sh}	9.9×10^{11}	[b]6.5×10^{7}	8.7×10^{10}	5.71×10^{6}
CD8-LV	7.3×10^{11}	[b]2.6×10^{6}	1.46×10^{11}	4.99×10^{5}
CD8-LV^{sh}	1.8×10^{12}	[b]3.7×10^{6}	1.46×10^{11}	2.88×10^{5}

[a](T.u.) Transducing units.
[b]t.u. determined on PBMC.
Table modified from (147).

2.4.1 Improved *in vivo* gene delivery with CD4-LV^{sh} and CD8-LV^{sh}

Flow cytometry analysis of the blood revealed pronounced CAR T cells in the CD4 subset emerging in all CD4-LV groups on day 10, which dropped a week later (Figure 22). Strikingly, both shielded CD4-LV groups showed detectable CAR T cells in the blood of all mice on day 10 above 0.5% except for one mouse in each of the two groups. One CD4-LV^{sh}(2x) injected mouse exhibited CAR signals as early as day 4 that disappeared afterwards. However, injection of non-shielded CD4-LV resulted only in two out of five mice with notable CAR signal in CD4 T cells above the control background. Moreover, CAR frequency reached up to 2% for some mice in the CD4-LV^{sh} and CD4-LV^{sh}(2x) group, while in the CD4-LV group CD4 CAR T cells peaked at a maximum of 1%. In contrast, no detectable CAR T cells were observed in the blood of CD8-LV and CD8-LV^{sh} injected mice. Only mice, which received CD8-LV^{sh}(2x) developed detectable CD8 CAR T cells about 0.5% – 1% in the periphery. They emerged about one week later than in the CD4-LV group on day 17 in four out of five injected mice. In one mouse CD8 CAR T cells expanded further on day 24 up to 4% (Figure 22).

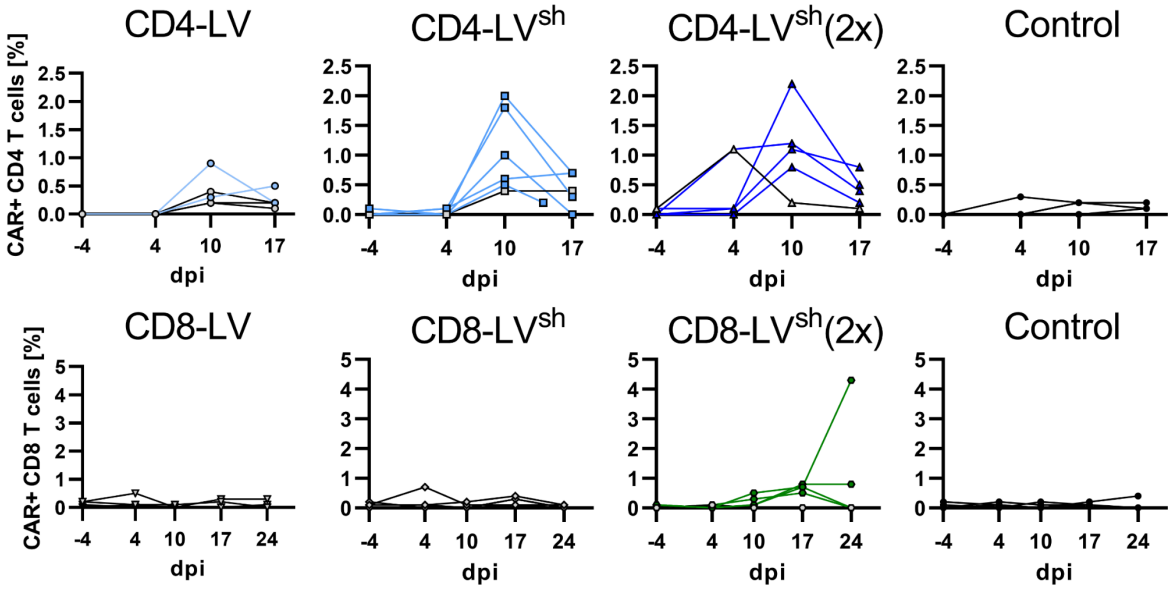

Figure 22: *In vivo* CAR T cell generation using shielded LVs.
huSGM3 mice were injected intravenously with identical particle numbers of conventional (CD4-LV, CD8-LV) and shielded (CD4-LV^{sh}, CD8-LV^{sh}) vectors. An additional group received a double dose of shielded vectors (CD4-LV^{sh}(2x), CD8-LV^{sh}(2x)). As control, PBS was injected into the mice. Kinetics of CAR+ T cells in blood determined by flow-cytometry are shown as percentage CAR+ of the respective T cell subtype. Mice determined as CAR negative in blood are depicted with grey symbols and black connecting lines. n= 5 (CD4-LV), 6 (CD4-LV^{sh}), 5 (CD4-LV^{sh} (2x)), 4 (CD8-LV), 5 (CD8-LV^{sh}), 5 (CD8-LV^{sh} (2x)) and 4 (Control) in one experiment. Figure modified from (147).

A more detailed analysis was enabled by including counting beads during flow cytometry measurement and allowed the assessment of total cell counts in blood. Although injection of 2-fold more CD4-LV^{sh} did not show increased CAR T cell frequencies, they resembled about 2-fold higher CAR T cell numbers in the blood (Figure 23). About 1.7x10^3, 2.6x10^3 and 5.9x10^3 CAR T cells per mL blood in the CD4-LV, CD4-LV^{sh} and CD4-LV^{sh}(2x) group were detected in the periphery at the peak time point on day 10, whereas detectable CAR T cells in the CD8-LV^{sh}(2x) group were present at a concentration of about 1.5x10^3 counts per mL blood on day 24 (Figure 23A). Further, CAR expression in blood was exclusively found on CD3 expressing T cells and on the respective T cell co-receptor expressing CD4 or CD8 subset underlining the receptor specific *in vivo* gene transfer of the targeted LVs in the huSGM3 mouse system (Figure 23B, C).

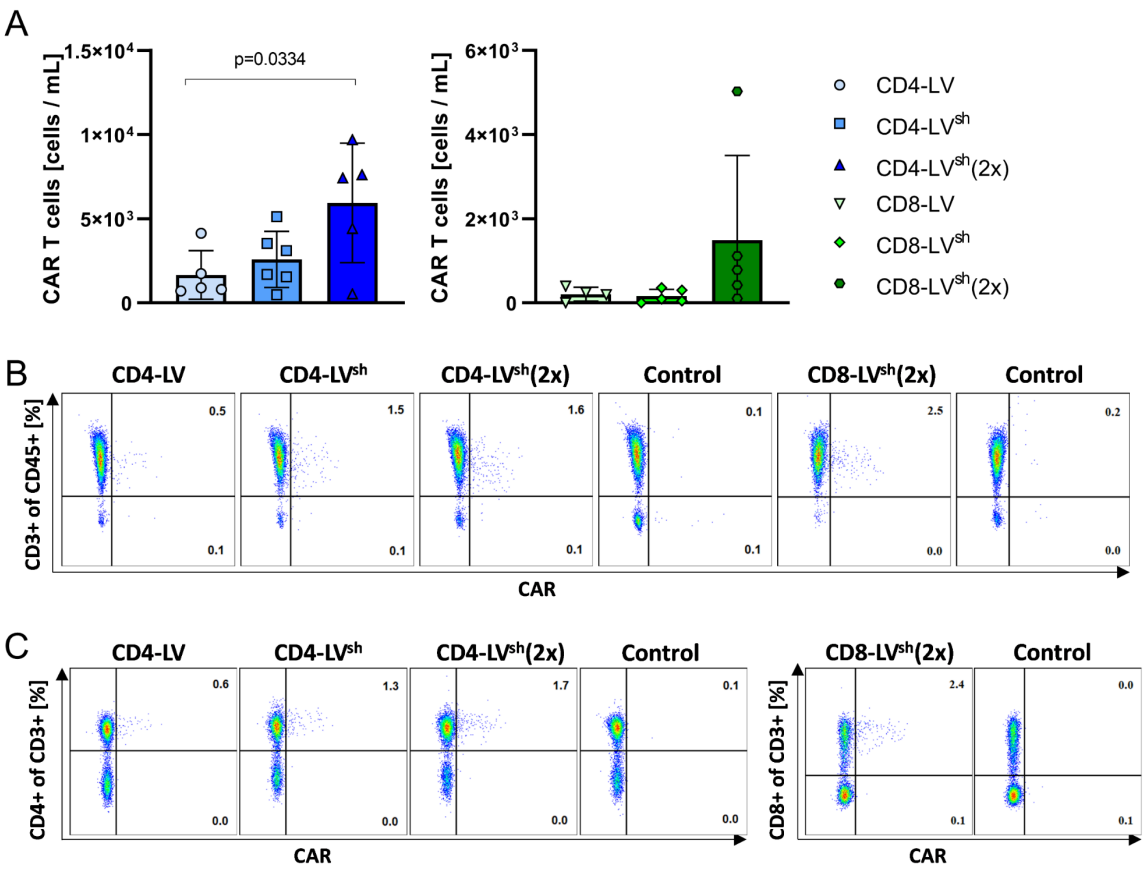

Figure 23: Absolute *in vivo* CAR T cell numbers in blood of huSGM3 mice and FACS plots of CAR signal.
A) Absolute quantification of CAR T cells in blood after intravenous injection of non-shielded and shielded CD4-LV on day 10 and CD8-LV on day 24 using counting beads during flow-cytometry analysis. Each data point represents an individual mouse with mean and standard deviation of the group. **B)** Representative FACS plots of *in vivo* generated CAR T cells shown for human T cell specific transduction is presented as CD3+ of human CD45+ cells positive for CAR, detected via its myc-tag. **C)** Representative FACS plots for specific transduction in T cell subtype is shown as CD4+ or CD8+ of CD3+ cells positive for CAR. Statistics were determined by one-way ANOVA (Tukey's multiple comparisons test) with indicated significant p-values. n= 5 (CD4-LV), 6 (CD4-LV^{sh}), 5 (CD4-LV^{sh}(2x)), 4 (CD8-LV), 5 (CD8-LV^{sh}), 5 (CD8-LV^{sh}(2x)) in one experiment. Figure modified from (147).

Next, human monocytes were evaluated if they may act as a barrier for *in vivo* CAR T cell generation in CD4-LV injected huSGM3 mice. This vector group showed in the previous mouse experiment the strongest innate-associated immune response. Therefore, initial monocyte number in the blood before experiment start was correlated to the highest CAR T cell number detected in the blood on day 10. Indeed, a tendency for a negative correlation of initial monocytes with numbers of *in vivo* generated CAR T cells was found (Figure 24). Highest CAR T cells numbers developed in the blood of mice, which had initially the lowest monocyte count in the periphery, whereas least CAR T cells were generated in mice with higher monocyte number. However, 6 out of

16 mice developed low CAR T cells number despite low monocyte count prior vector injection, which might have been attributed to other factors (Figure 24).

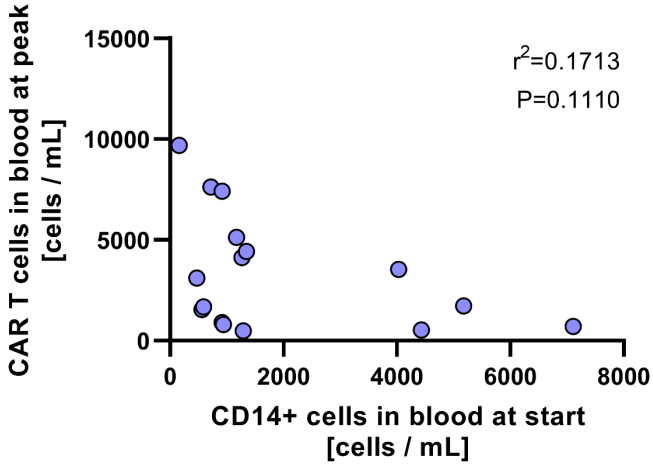

Figure 24: Correlation of monocyte level with *in vivo* CAR T cell generation with CD4-LV. Correlation of CD14+ cell number in the blood before experiment start (day -4) with numbers of *in vivo* generated CAR T cell in the blood on day 10 for CD4 targeted LVs. Individual mice are shown as data point for n=16. Correlation was determined by Pearson correlation analysis with indicated r^2 and P value. Figure modified from (147).

To confirm CAR T cell presence in the spleen an expansion assay with isolated splenocytes was conducted. On average, CAR T cells from CD4-LVsh injected mice expanded upon target antigen stimulation to 13% CAR+ in CD4 T cells with a maximum frequency of 33% (Figure 25). In comparison, samples from CD4-LV injected mice did not expand notably above the control background with only one mouse reaching about 10% CAR T cells in the CD4 subset. Interestingly, CD4-LV^{sh}(2x) did not show pronounced expansion of residual CAR T cells in the spleen, although this group showed the most pronounced *in vivo* CAR T cell generation in the blood. Only splenocytes of two mice indicated a CAR T cell expansion until 5% above the control background. For the CD8 targeted vector groups none of the mice injected with the non-shielded LV showed notable expansion of CAR T cells in the co-culture assay. While in the CD8-LV^{sh} group no detectable CAR T cells were observed in the blood, two mice showed an expansion of CAR+ T cells from the splenocytes reaching 1% and 4% in the CD8 subset. Highest CAR T cell expansion was seen for the CD8-LV^{sh}(2x) with an average CAR level of 11% and a maximum of 25% CAR+ CD8 T cells in splenocytes after the co-culture (Figure 25).

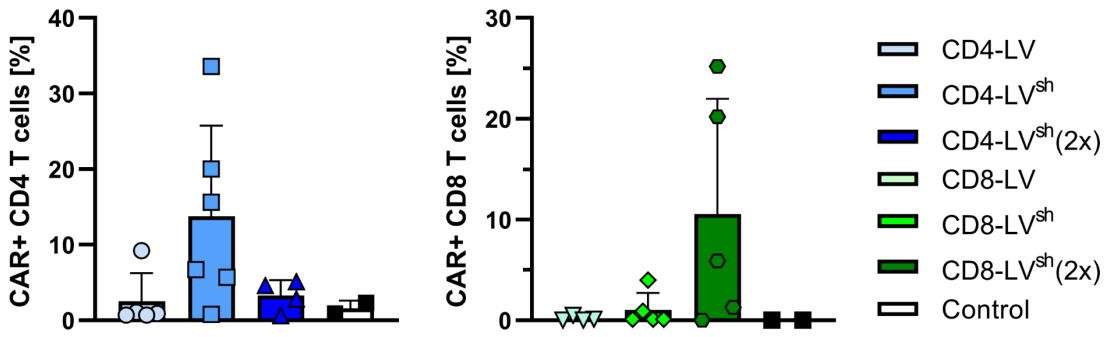

Figure 25: *In vitro* CAR T cell expansion from splenocytes.
Expansion of CAR T cells from splenocytes from LV injected huSGM3 mice upon co-culture with irradiated CD19+ Nalm6 tumor cells for seven days detected by flow-cytometry. Percentage of expanded CAR+ T cells of the respective subpopulation is shown for each mouse as data point performed in technical triplicates with mean and standard deviation of the group. n= 5 (CD4-LV), 6 (CD4-LV^{sh}), 5 (CD4-LV^{sh}(2x)), 4 (CD8-LV), 5 (CD8-LV^{sh}), 5 (CD8-LV^{sh}(2x)). Statistics were determined by one-way ANOVA (Tukey's multiple comparisons test). Figure modified from (147).

Further, qPCR analysis was performed to verify successful *in vivo* gene transfer into T cells. Isolated T cells from the spleen showed in CD4-LV^{sh} injected mice over 2-fold higher VCN compared to the conventional CD4-LV group (Figure 26). However, VCN in the CD4-LV^{sh}(2x) group were notably below the single dose of the CD4-LV^{sh} group. This fits well with the data from the expansion assay with splenocytes. Strikingly, the phagocytosis shielded CD8-LV^{sh} showed substantial CAR gene integration in all injected mice with over 2-fold higher VCN than the non-shielded CD8-LV, which had only two mice with VCN above the control group. In addition, mice receiving two-times higher vector dosage showed up to 10-fold higher VCNs in CD3+ splenocytes (Figure 26).

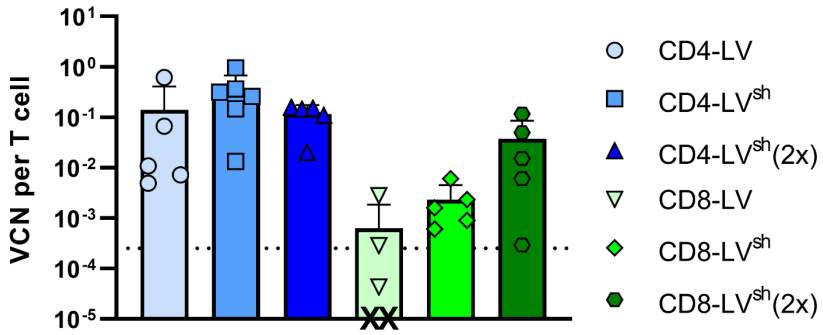

Figure 26: VCNs in T cells from spleen.
VCNs of the CAR transgene measured by qPCR in enriched T cells from spleen. Dotted line represents the upper standard deviation of the control group. X indicates data point below the axis. Individual mice are shown with mean and standard deviation of the group. n= 5 (CD4-LV), 6 (CD4-LV^{sh}), 5 (CD4-LV^{sh}(2x)), 4 (CD8-LV), 5 (CD8-LV^{sh}), 5 (CD8-LV^{sh}(2x)) and 4 (Control) from one experiment. Statistics were determined by one-way ANOVA (Dunnett's multiple comparisons test). Figure modified from (147).

Overall, the *in vivo* generation of CAR T cells with CD4 and CD8 targeted LVs could be improved in huSGM3 mice by shielding the targeted LVs from phagocytosis. This was confirmed on protein-level by flow-cytometry analysis directly in the blood and in splenocytes after tumor antigen exposure in an expansion assay, but as well on genomic level by qPCR analysis.

2.4.2 Pronounced B cell reduction with shielded LVs

Functionality of *in vivo* generated CAR T cells could be confirmed by a reduction of CD19 expressing endogenous human B cells in blood. Similar to the previous mouse experiment, kinetic of B cells correlated with the appearance of CAR T cells in the periphery. In this experiment, B cell reduction started from day 10 for the CD4-LV groups and from day 17 for the CD8-LV groups (Figure 27). Moreover, improved gene transfer of the shielded vectors was reflected by a slightly faster and more pronounced target cell reduction in CD4-LV^{sh} and especially in CD4-LV^{sh}(2x) injected mice. Three out of five CD4-LV, all CD4-LV^{sh} and four out of five CD4-LV^{sh}(2x) injected mice exhibited B cell levels below 50% of the initial level, including some mice without detectable CAR T cells in the periphery. No mice injected with the non-shielded CD8-LV showed notable B cell reductions below the control background and only one mouse from the CD8-LV^{sh} group demonstrated a slight CD19+ target cell reduction, whereas all CAR positive mice in the CD8-LV^{sh}(2x) group experienced pronounced B cell decrease (Figure 27).

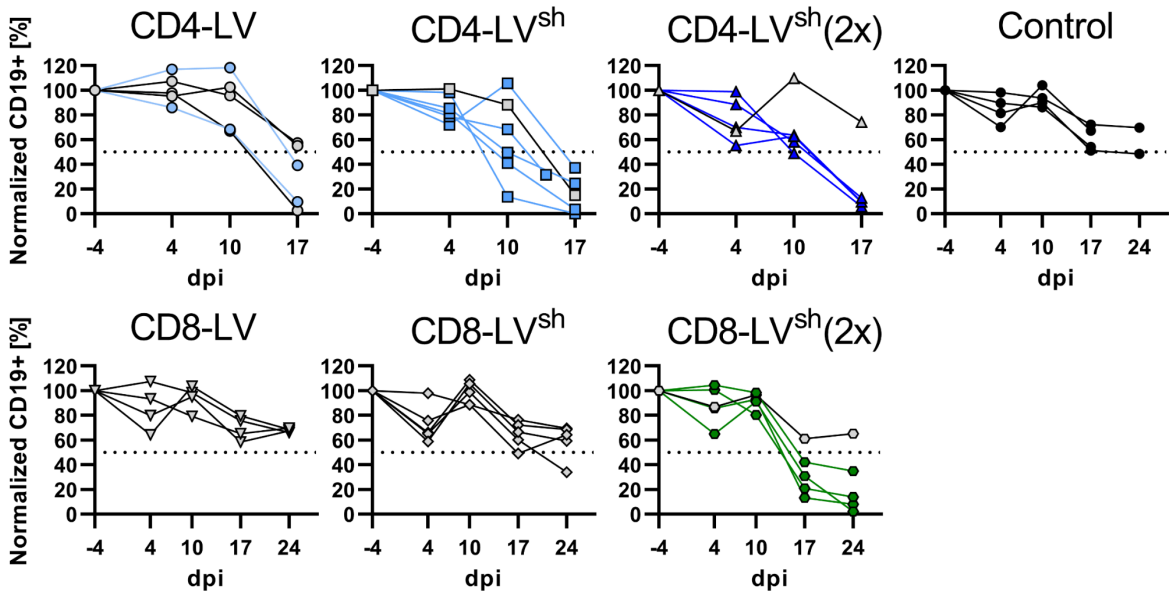

Figure 27: Functionality of *in vivo* generated CAR T cell with shielded LVs.
huSGM3 mice were injected intravenously with the indicated vectors as a single or a double dose (2x). As control, PBS was injected into the mice. Kinetics of normalized CD19+ cells of CD3- population were determined by flow-cytometry. Dotted line shows cut off for determining reduction of B cells in mice. Mice determined as CAR negative in blood are depicted with grey symbols and black connecting lines. n= 5 (CD4-LV), 6 (CD4-LV^{sh}), 5 (CD4-LV^{sh} (2x)), 4 (CD8-LV), 5 (CD8-LV^{sh}), 5 (CD8-LV^{sh} (2x)) and 4 (Control) in one experiment. Figure modified from (147).

Further, in the bone marrow B cell levels were overall significantly lower in mice injected with both shielded CD4-LV^{sh} dose compared to the control, whereas the non-shielded CD4-LV group had only three out of five mice with notable reduced B cells (Figure 28A). Remarkably, mice injected with the shielded CD8-LV^{sh} also showed pronounced B cell reduction, which was significantly below the non-shielded CD8-LV group underlining the improved CAR T cell generation for the shielded CD8 targeted LVs as well. Similar pattern was as well observed in the spleen. B cell frequencies in CD4-LV injected mice were similar to the control, whereas two mice in the CD4-LV^{sh} and three mice in the CD4-LV^{sh}(2x) group displayed noticeable B cell reduction. The difference between shielded and non-shielded CD8-LV groups was even more pronounced with more prominent B cell reduction in CD8-LV^{sh}(2x) treated mice (Figure 28B).

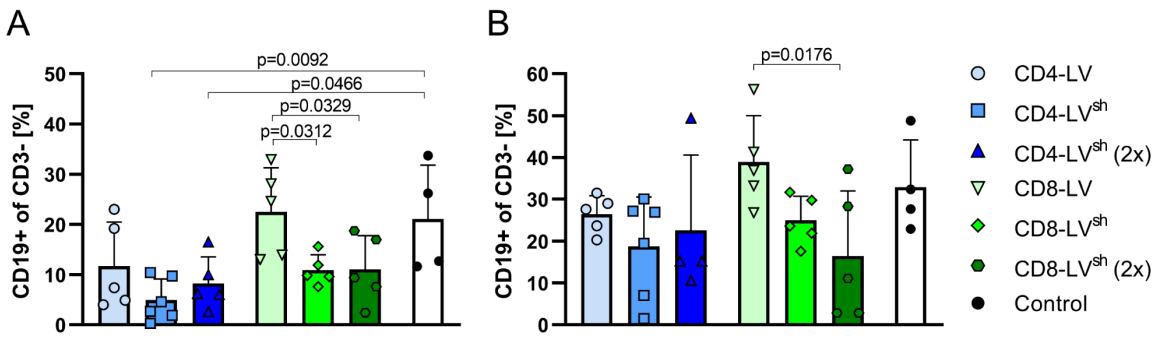

Figure 28: B cell depletion in bone marrow and spleen.
B cell levels in bone marrow **(A)** and spleen **(B)** at final analysis determined by flow-cytometry gated on CD19+ of human CD3- cells. Individual mice are shown with mean and standard deviation for n= 5 (CD4-LV), 6 (CD4-LV^{sh}), 5 (CD4-LV^{sh}(2x)), 4 (CD8-LV), 5 (CD8-LV^{sh}), 5 (CD8-LV^{sh}(2x)) and 4 (Control) in one experiment. Statistics were determined by one-way ANOVA (Dunnett's multiple comparisons test) with indicated significant p-values. Figure modified from (147).

In summary, functional readout of CAR T cell activity in the periphery and organs confirmed the improved *in vivo* CAR T cell generation by shielding the CD4-LV and CD8-LV from phagocytosis. Especially, for CD8-LV^{sh}, which could not be shown otherwise by direct CAR T cell detection via flow cytometry analysis.

2.4.3 No pathological cytokine release in plasma

As systemic administration of viral-like particles and as well the presence of CAR T cells can lead to systemic overreaction and severe cytokine release in the body human plasma cytokines related to T cell and myeloid cell associated activation were assessed.

Overall, systemic pro-inflammatory cytokines, such as IL-6, IFN-γ, IL-2 and TNF-α were notably increased in the plasma of all vector-injected mice on day 17 compared to the control group, which only received PBS (Figure 29). However, they did not reach above 300 pg/mL in most cases. Only one mouse injected with CD4-LV^{sh} experienced up to 800 pg/mL IL-6 in the blood. Exceptionally, an IFN-γ level close to 25ng/mL in the plasma, was measured in one CD8-LV^{sh} injected mouse, although this might rather be an artifact from the measurement. Nevertheless, no mice showed signs for severe side effects, based on assessment of body weight and visual appearance. Interestingly, for the myeloid associated cytokines, IL-1β and IL-10 were more increased in the shielded CD4-LV^{sh} group than in the non-shielded CD4-LV and CD8 targeted LVs. This was also the case for IL-15, although some mice from the CD8-LV^{sh}

group also exhibited substantially increased IL-15 level (Figure 29). Similar to the finding from the mouse experiment described above in Figure 16, GM-CSF was significantly decreased only in the CD4 targeted vector groups, regardless from phagocytosis shielding or not (Figure 29).

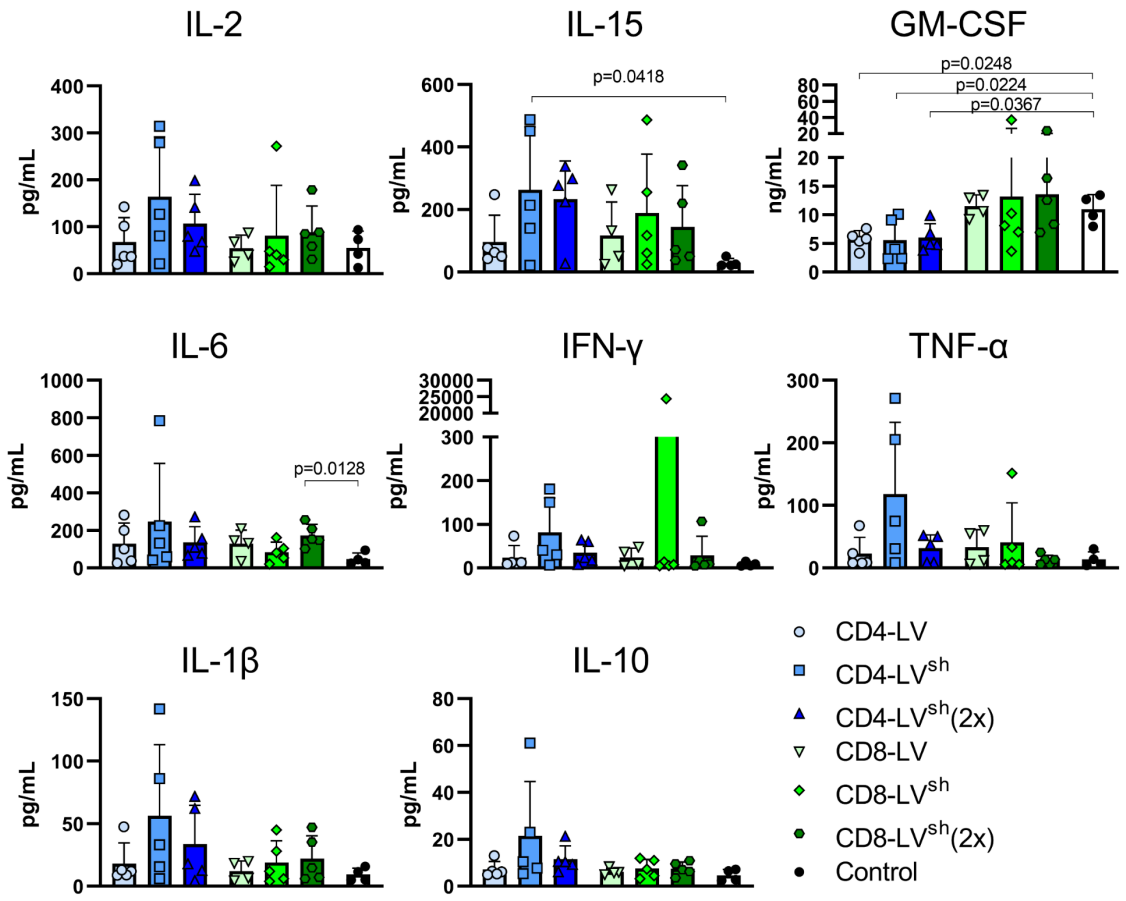

Figure 29: Plasma cytokines in LV injected huSGM3 mice.
Plasma cytokines of huSGM3 mice on day 17 after vector administration were measured by bead-based multi-analysis kit. Individual mice are shown with mean and standard deviation of the group. Statistics were determined by one-way ANOVA with indicated significant p-values. n= 5 (CD4-LV), 6 (CD4-LV^{sh}), 5 (CD4-LV^{sh} (2x)), 4 (CD8-LV), 5 (CD8-LV^{sh}), 5 (CD8-LV^{sh}(2x)) and 4 (Control) from one experiment. Figure modified from (147).

In addition, antiviral cytokine response was assessed to determine ongoing antiviral immune response in mice. In general, IFN-α and IFN-β level were low in all mice and at a similar range as the control mice (Figure 30). However, an interesting correlation was observed for one mouse in the CD4-LV^{sh} and one in the CD4-LV^{sh}(2x) group with initially high levels of about 160 pg/mL IFN-α and 670 pg/mL IFN-β before vector injection that declined to background level on day 10 (Figure 30). These mice showed particularly low levels of CAR T cell generation in the periphery (Figure 22), suggesting

an initially antiviral primed immune system limiting viral vector based *in vivo* gene delivery.

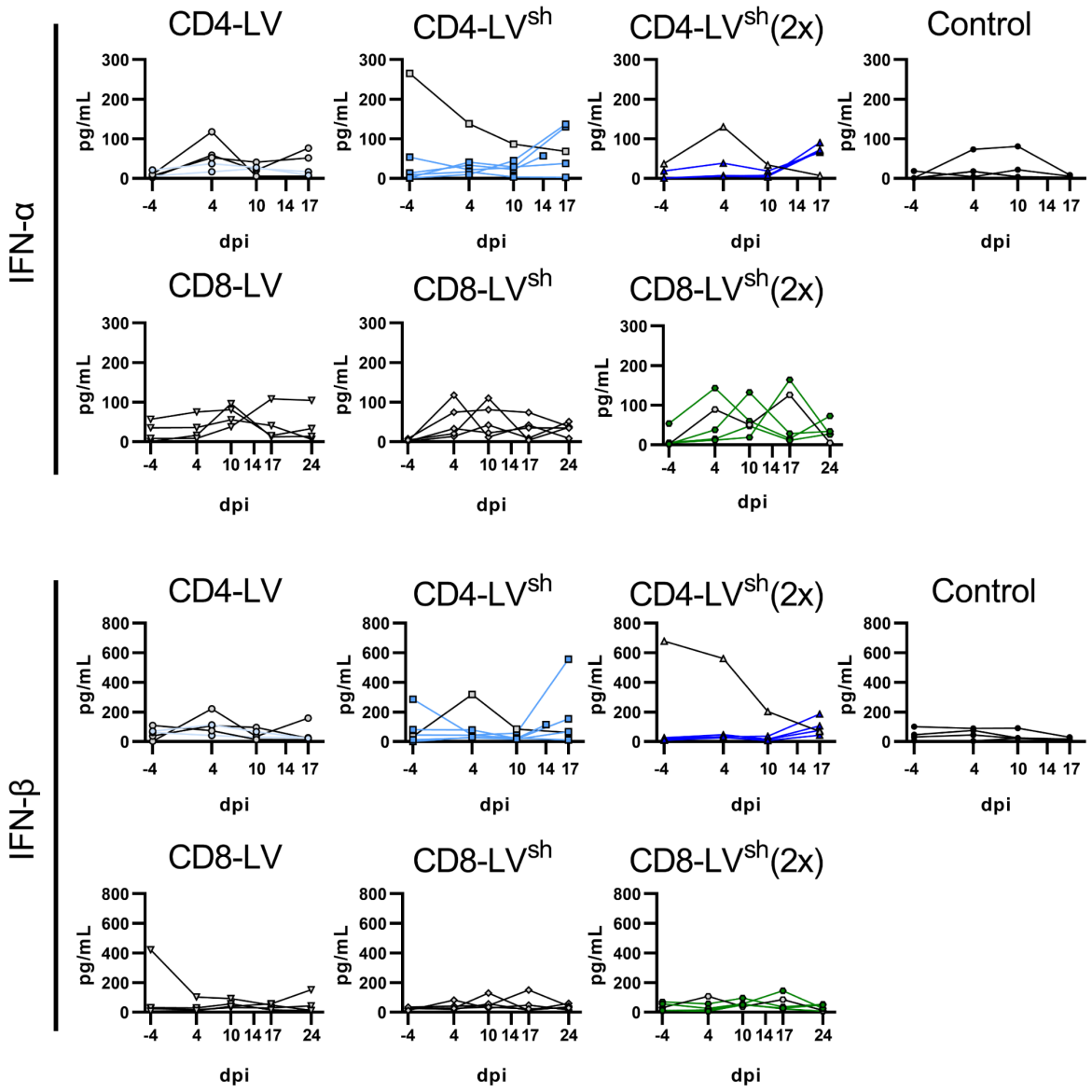

Figure 30: Kinetic of anti-viral cytokines in huSGM3 mice.
Plasma cytokines of huSGM3 mice injected with the indicated LVs were determined by bead-based multi-analysis kit. The concentrations for IFN-α and IFN-β over time are shown for each mouse. Mice determined as CAR negative in blood are depicted in grey with black connecting lines. n= 5 (CD4-LV), 6 (CD4-LV^{sh}), 5 (CD4-LV^{sh} (2x)) and 4 (Control) from one experiment. Figure modified from (147).

Taken together, systemic injection of lentiviral vectors induced a mild increase of T cell and myeloid cell associated pro-inflammatory cytokines. This was not pathological and did not induce severe adverse effects in the mice. Phagocytosis shielding of the vector did not reduce cytokine response, but was rather more pronounced in shielded CD4-LV^{sh}.

In summary, in the first part of this thesis, the *in vivo* CAR T cell generation with receptor targeted LVs was characterized in detail in the huSGM3 mouse model. The pronounced presence of human myeloid cells was identified as a limitation for effective *in vivo* gene delivery in this model. Finally, *in vivo* CAR T cell generation could be clearly improved upon vector surface modification with less immunogenic properties. In addition, no severe acute cytokine release or other adverse events were observed upon *in vivo* CAR T cell generation in huSGM3 mice, which has been described as a robust model for recapitulating *ex vivo* generated CAR T cell induced CRS (86).

2.5 Modeling of CAR T cell induced acute cytokine release syndrome

In the second part of this thesis the side effects of CAR T cell therapy are addressed. In particular, the modulation of acute cytokine release syndrome in appropriated models. Therefore, *in vitro* and *in vivo* models were designed and established that robustly capture clinical relevant parameters in CAR T cell therapy. In this regard, the novel approach of CAR T cells generated *ex vivo* in a short time scale were characterized and assessed for safety using these models.

2.5.1 Impact of CAR co-stimulatory domain on CAR T cell cytotoxicity in continuous killing assay

In the first step, different intracellular co-stimulatory activation domains in the CD19CAR construct were compared for strongest cytotoxicity and expansion effects, since these are important parameters leading to CRS. Therefore, the CD28 intracellular signaling in the $CD19CAR_{28z}$ was substituted by the 4-1BB co-stimulatory domain resulting in the $CD19CAR_{BBz}$ CAR construct (Figure 31). In this step the CD28 transmembrane domain was changed to a CD8a transmembrane as well, to reflect the configuration present in the approved CAR T cell product tisagenlecleucel (Kymriah), whereas the $CD19CAR_{28z}$ construct reflects the design of axicabtagene ciloleucel (Yescarta) (Figure 31). In addition, a third generation $CD19CAR_{28BBz}$ was cloned with both co-stimulatory domains (Figure 31).

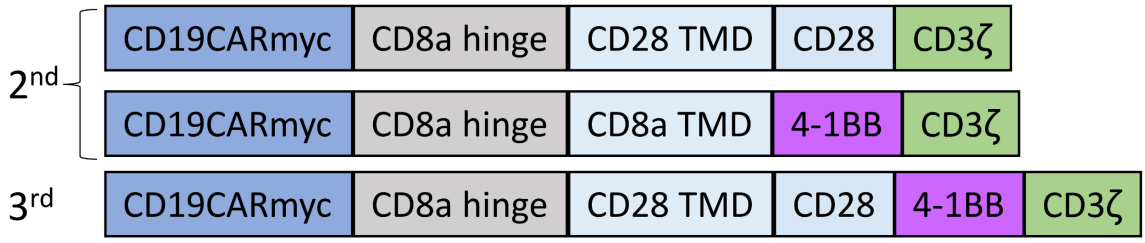

Figure 31: CAR co-stimulatory domains.
Schematic representation of three CAR constructs with different intracellular co-stimulatory domains compared in the continuous killing assay in Figure 32. 2nd generation CAR constructs only consist of one, whereas the 3rd generation construct includes two co-stimulatory domains in addition to the CD3ζ activation domain. TMD (transmembrane domain).

To compare the efficiency of the different CD19CAR constructs, CAR T cells were tested in a continuous killing assay with CD19 expressing Nalm6 tumor cells. In there,

increasing amounts of new tumor cells were added to the co-culture. CAR T cells were generated by transduction with VSV-LV, which transduces both CD4 and CD8 T cells, or with CD4-LV or CD8-LV, which transduces only the respective T cell subset.

Over the course of the killing assay CD19CAR28z showed the strongest cytotoxicity effect and could effectively control tumor cell growth in all vector groups until day 7 (Figure 32A). In the VSV-LV transduced group CD19CAR$_{28BBz}$ performed slightly weaker followed by the CD19CAR$_{BBz}$ construct. Interestingly, when separate T cell subsets were modified with the CAR, CD19CAR$_{BBz}$ CAR T cells performed substantially less efficient after day 3 with Nalm6 cells overgrowing the culture (Figure 32A). This is well in agreement with the CAR T cell level, which were increased in the conditions with pronounced tumor cell eradication, especially for the CD19CAR$_{28z}$ construct (Figure 32B). The assessment of the exhaustion marker PD-1, which is upregulated on T cells upon prolonged antigen induced activation, further gives inside into the activity of the CAR T cells. This was most prominent for the CD19CAR$_{28z}$ and least in CD19CAR$_{BBz}$ T cells (Figure 32C).

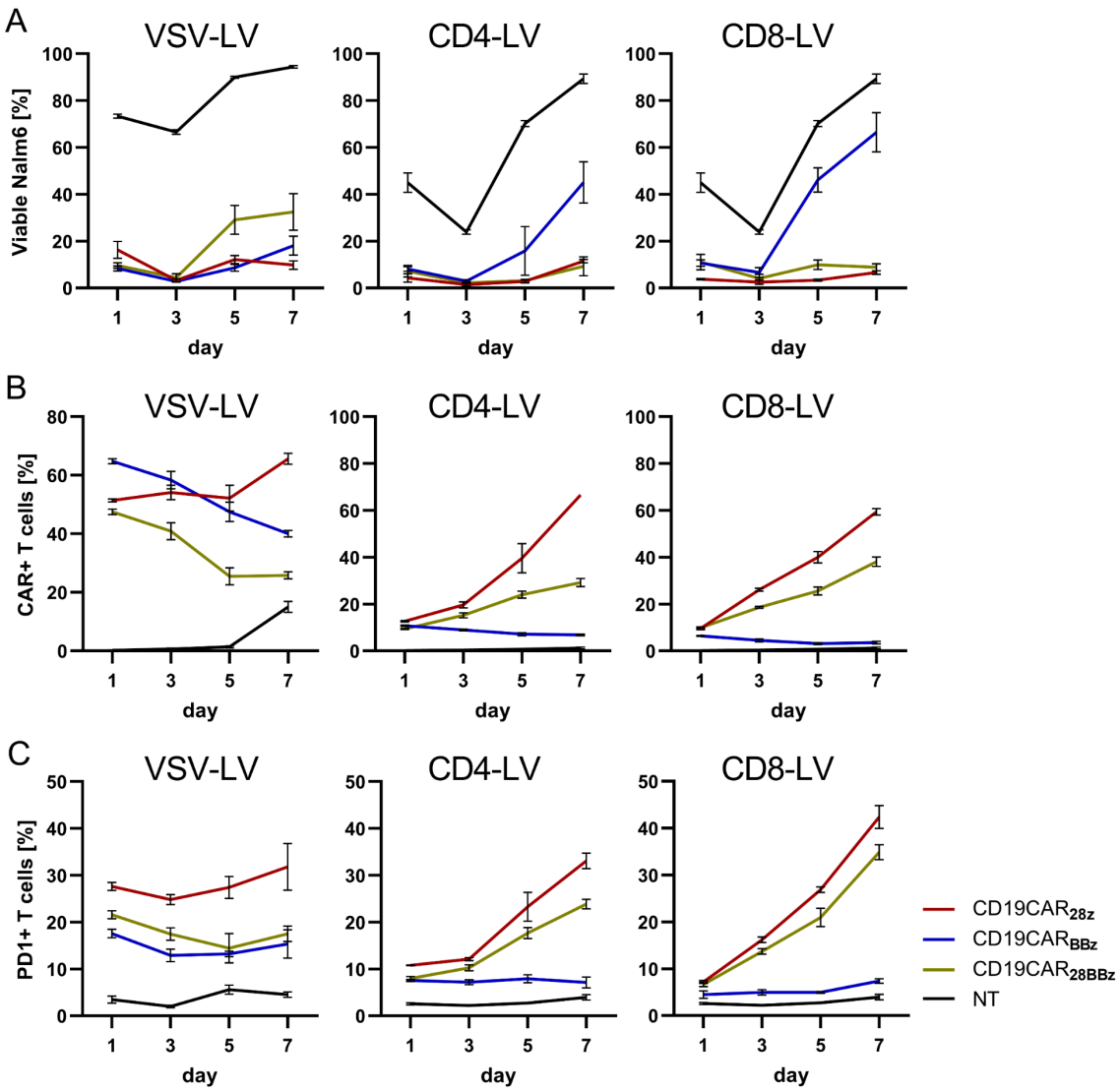

Figure 32: Continuous killing assay comparing different CAR co-stimulatory domains. CAR T cells with different co-stimulatory domains ($CD19CAR_{28z}$, $CD19CAR_{BBz}$, $CD19CAR_{28BBz}$) were generated by VSV-LV, CD4-LV or CD8-LV transduction. Killing assay conditions were normalized separately between the VSV-LV and T cell targeted LV group. Not transduced T cells (NT) were used as a negative control. For the killing assay $1x10^4$ CAR T cells were seeded with CellTrace® Violet (CTV) labeled CD19+ Nalm6 cells at a 1:1 (Effector:target) ratio. On day 1, 3 and 5 after co-culture 2-fold increasing labeled Nalm6 cells were added at the respective day to the culture. Kinetic of cytotoxicity was determined by viability of CTV labeled tumor cells **(A)** and CAR T cell level **(B)** and PD1 expression **(C)** were assessed within CTV negative and CD3+ cells by flow-cytometry. Data are shown from one donor performed in technical triplicates with respective mean and standard deviation.

Taken together, this continuous killing assay revealed the strongest cytotoxic activity as well expansion and PD-1 upregulation for $CD19CAR_{28z}$ T cells compared to other co-stimulatory domains. Therefore, this construct was identified as most promising in inducing CRS and was used to study and evaluate suitable models for the assessment of CD19CAR T cell induced adverse effects. Furthermore, these results revealed an interesting impact of the co-stimulatory domains on CAR T cells generated separately

in the CD4 or CD8 subset. CD19CAR$_{BBz}$ seems to work poorly when transduced by CD4-LV or CD8-LV whereas transduction by VSV-LV with this construct still showed efficient tumor cell killing. However, this needs to be investigated in further studies, where a mixture of CD4-LV and CD8-LV might be a better comparison than VSV-LV to consider the different vector particle entry. To simplify and reduce the conditions, VSV-LV was used for transduction in further experiments, since it transduced both T cell subsets and achieved high transduction efficiency.

2.5.2 Short-term generation protocol yields substantial CAR T cells

Current approved CAR T cell products are manufactured *ex vivo* by viral vector transduction of isolated peripheral T cells and further *in vitro* expansion that can take up to 4 weeks. Using a protocol, which was established and described by Laura Kapitza in her PhD dissertation (150), CAR T cells were generated within three days which are referred to as short-term CAR T cells in this thesis. In there, PBMC are activated for two days with anti-CD3 and anti-CD28 activation antibody in the presence of IL-7 and IL-15 and afterwards incubated for one day with VSV-LV (Figure 33). Since transduction is not expected to be completed within the short vector incubation time, short-term CAR T cells were further reactivated and cultivated for additional three days to achieve fully transduced CAR T cells (Figure 33).

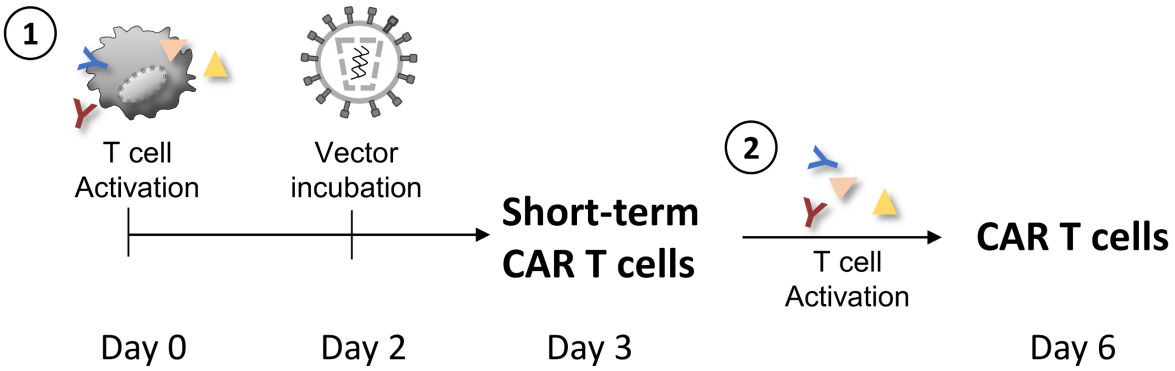

Figure 33: Generation of short-term CAR T cells.
① Short-term CAR T cell were generated by activation of 8x10^4 PBMC for two days with anti-CD3 and anti-CD28 activation antibody in the presence of IL-7 and IL-15, following incubation with 0.5µL VSV-LV stock for one day in cytokine supplemented medium. ② Further reactivation and cultivation in presence of the activation antibodies and cytokines until day 6 resulted in fully transduced CAR T cells. Excessive vector in the supernatant were washed off prior experiments.

To evaluate if the shortened CAR T cell generation protocol already resulted in substantial T cell transduction, vector particles and CAR expression were determined by using a staining protocol established by Elham Adabi, a colleague from the group. Thereby, an antibody specific for the VSV glycoprotein (VSV-G) on the vector surface was used to detect cell bound vector particles and the CAR was identified by its myc-tag. Characterization of CAR and vector particle signal on short-term CAR T cells revealed that a majority of the vector incubated T cells were single-positive for the vector particles after 24h (Figure 34). Only a small part of about 15% T cells were double-positive for CAR and vector particles and a minor fraction of less than 5% was solely positive for CAR on the surface (Figure 34B). However, upon removing excessive unbound vector particles in the culture and further activation and cultivation for three more days, these cells converted to about 50% single positive CAR T cells with no detectable vector particles on the surface (Figure 34). Interestingly, this is comparable to transduction levels achieved for CAR T cells generated conventionally within 6 days with the same vector particle amount in our research group (data not shown).

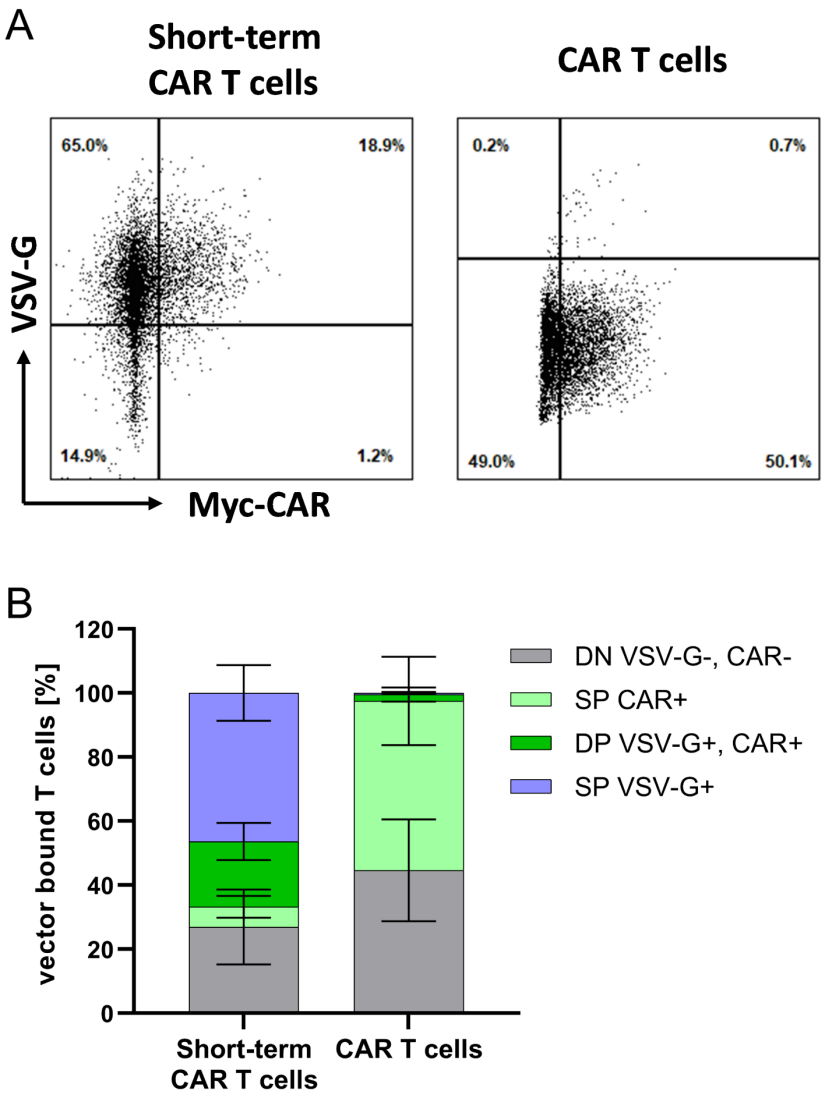

Figure 34: Characterization of Short-term CAR T cells for vector and CAR signal.
Short-term CAR T cells and further cultivated CAR T cells were evaluated for vector particle and CAR signal on cell surface. **A)** Representative dot plots for vector and CAR signal with indicated cell frequencies inside the quadrants. Gates were set according to the non-transduced negative control. **B)** Stacked bar diagrams summarize the data for short-term CAR T cells after production and after further activation and cultivation (CAR T cells) with single positive VSV-G (blue), single positive CAR (bright green), double positive (dark green) and double negative (grey) frequencies. Mean and standard deviation of four donors measured in technical triplicates from two independent experiments are shown.

This shows that the short-term CAR T cells are rather a vector particle-bound cell product than cells fully equipped with the CAR. Therefore, safety of such short-term CAR T cells during tumor cell killing is still unclear and needs to be addressed in appropriated models.

2.5.3 *In vitro* CRS model with monocyte supplementation

To evaluate the cytotoxicity of short-term CAR T cells including their capability for CRS induction, a co-culture killing assay was designed to recapitulate key immune cell components involved in cytokine release. Since CAR expression on short-term CAR T cells is not complete, effector cells were calculated based on vector positive and CAR positive cells. In addition to the conventional killing assay, co-cultures of CAR T cells and Nalm6 tumor cells were supplemented with 10% monocytes. To avoid alloreactivity, monocytes were dervied from the same donor as the T cells for short-term CAR T cell generation. The data set was completed with the help of Angela Braun, a colleague from the group.

2.5.3.1 Presence of monocytes does not influence CAR T cell cytotoxicity, but induces clinically relevant cytokine release

Interestingly, short-term CAR T cells displayed pronounced killing of tumor cells after one day of co-culture compared to the control T cells with less than 20% remaining viable tumor cells (Figure 35A). Further assessment of CAR expression revealed that substantial amount of about 60% T cells were CAR positive after the killing assay with preferentially two-fold higher frequency for CD8 negative than CD8 positive T cells (Figure 35B). In comparison to the initial CAR signal after short-term CAR T cell production, frequencies of CAR expressing T cells increased over 2-fold after tumor cell co-culture (Figure 34, 35). Therefore, vector particle bound T cells presumably converted to CAR T cells within the co-culture time, which resulted in efficient tumor cell killing. Importantly, cytotoxicity and CAR expression level were not influenced by the addition of monocytes to the culture (Figure 35).

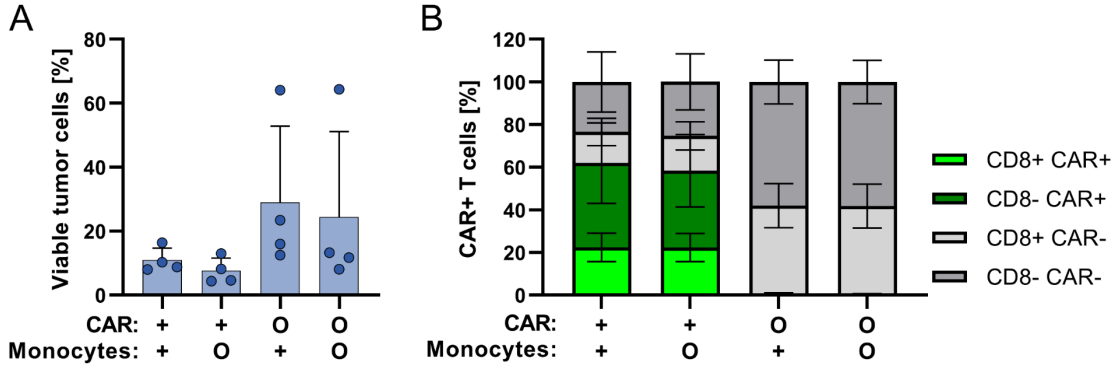

Figure 35: *In vitro* cytotoxicity assay with monocyte supplementation.
Short-term CAR T cells (+) or not transduced T cells (O) were co-cultured with $1x10^5$ CellTrace® Violet (CTV) labeled CD19+ Nalm6 cells at 5:1 (Effector:target) ratio in the presence (+) or absence (O) of 10% monocytes for 24 – 26h. Bar diagrams show **(A)** cytotoxicity as viability of CTV labeled tumor cells and **(B)** CAR expression on CD8 positive or negative short-term CAR T cells determined by flow cytometry. Data are shown for four donors with mean and standard deviation of the group, measured in at least technical duplicates from two independent experiments. Data of the figure were obtained with the help from Angela Braun.

Analysis of human cytokines secreted during killing activity revealed tremendously elevated levels of CAR T cell associated pro-inflammatory IFN-γ, GM-CSF, IL-2 and TNF-α in the cell culture supernatant compared to T cell control (Figure 36). IFN-γ reached between 20 – 126 ng/mL, GM-CSF levels were approximately 9500 pg/mL, IL-2 was elevated to about 1300 pg/mL and TNF-α was found at around 3400 pg/mL in the supernatant. Presence of the anti-inflammatory IL-10, which was secreted during inflammation, was also significantly elevated for short-term CAR T cells and detected at 100 pg/mL in the culture. Strikingly, the clinical CRS-relevant cytokine IL-6 was significantly elevated when monocytes were supplemented to the co-culture assay. On average 600 pg/mL was measured in the supernatant, which was approximately 2-fold higher than in the absence of monocyte during killing and about 24-fold increased compared to T cell control. Moreover, IFN-γ level was also on average 2-fold higher, although not significantly increased in the presence of monocytes (Figure 36).

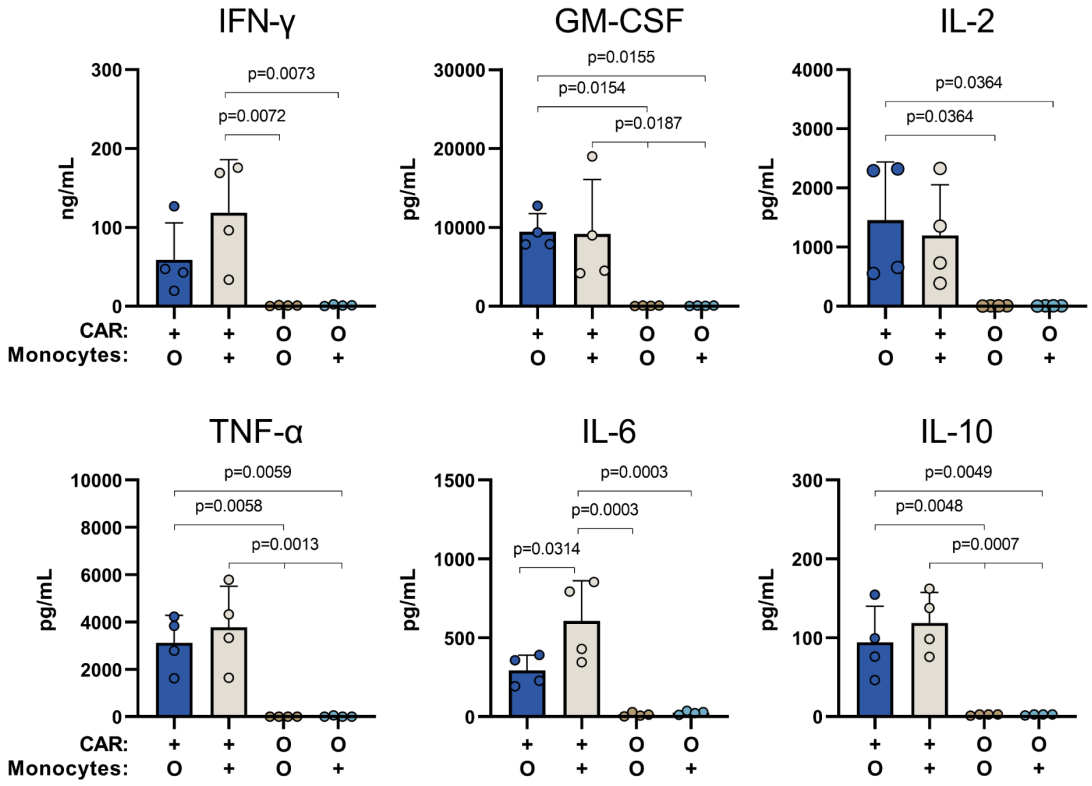

Figure 36: *In vitro* cytokine release.
Human cytokines in the supernatant after 24h-26h *in vitro* cytotoxicity assay were measured by bead-based multi-analysis kit. Short-term CAR T cells (+) or not transduced T cells (O) in the presence (+) or absence (O) of monocytes. Bar diagrams show human cytokines for four donors with mean and standard deviation of the group, measured in technical duplicates. Statistics were determined by one-way ANOVA (Tukey's multiple comparisons test) with indicated significant p-values.

Therefore, the established *in vitro* CRS assay confirmed functionality of short-term CAR T cells, which has been likely facilitated by T cells completing transduction and expressing the CAR. Nevertheless, a high cytokine release was observed during cytotoxic activity with induction of clinically relevant CRS-related cytokines in the presence of monocytes. However, to assess the safety risk of short-term CAR T cells in more detail, they need to be evaluated in a pre-clinical *in vivo* model to see if it truly leads to systemic adverse events.

2.5.4 CRS tumor model in NSG-SGM3 mice with short-term CAR T cells

In the next step, a CRS mouse model was set up to further evaluate short-term CD19CAR T cells for their potential to induce systemic adverse events. Immunodeficient NSG-SGM3 mice were pre-engrafted with luciferase positive Nalm6 tumor cells for 10 days to establish a tumor model before short-term CAR T cells were

injected (Figure 37). Since the amount of target cell is expected to correlate with the CAR T cell activity and therefore the cytokine release, a high tumor load was chosen to achieve a sensitive CRS model.

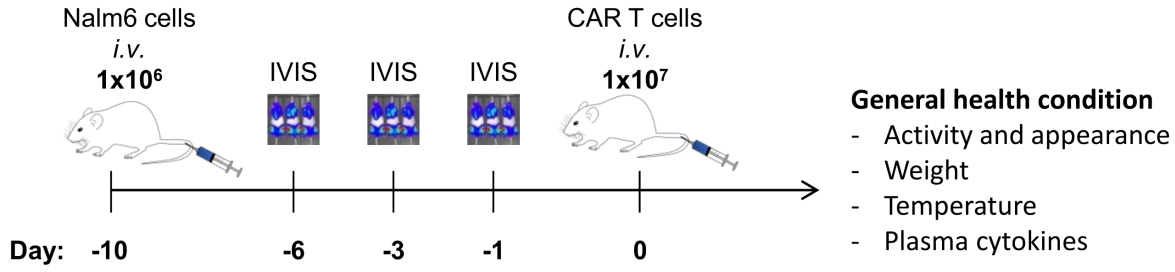

Figure 37: Schematic experimental setup for CRS mouse model.
NSG-SGM3 mice were engrafted intravenously (*i.v.*) with $1x10^6$ EBFP and luciferase expressing Nalm6 tumor cells for 10 days. Tumor load was monitored by *in vivo* bioluminescence imaging system (IVIS) at the indicated days. On day 0 $1x10^7$ short-term CAR T cells or respective amount of T cells without vector particle incubation were administrated *i.v.* and mice were monitored for general health condition until pre-defined termination criteria were reached.

Tumor growth was carefully assessed by *in vivo* bioluminescence imaging system (IVIS) showing that the tumor cells were located mainly in the bone marrow areas of the front and back legs as well the hip and the sternum (Figure 38A). One day before CAR T cell injection tumor signal reached about $1x10^8$ p/s and mice were distributed into the experimental groups (Figure 38B). Afterwards, $1x10^7$ short-term CAR T cells (determined as vector and CAR positive cells) were administrated intravenously into the mice. As control equal amount of total T cells, which were activated and cultured at the same condition, were injected.

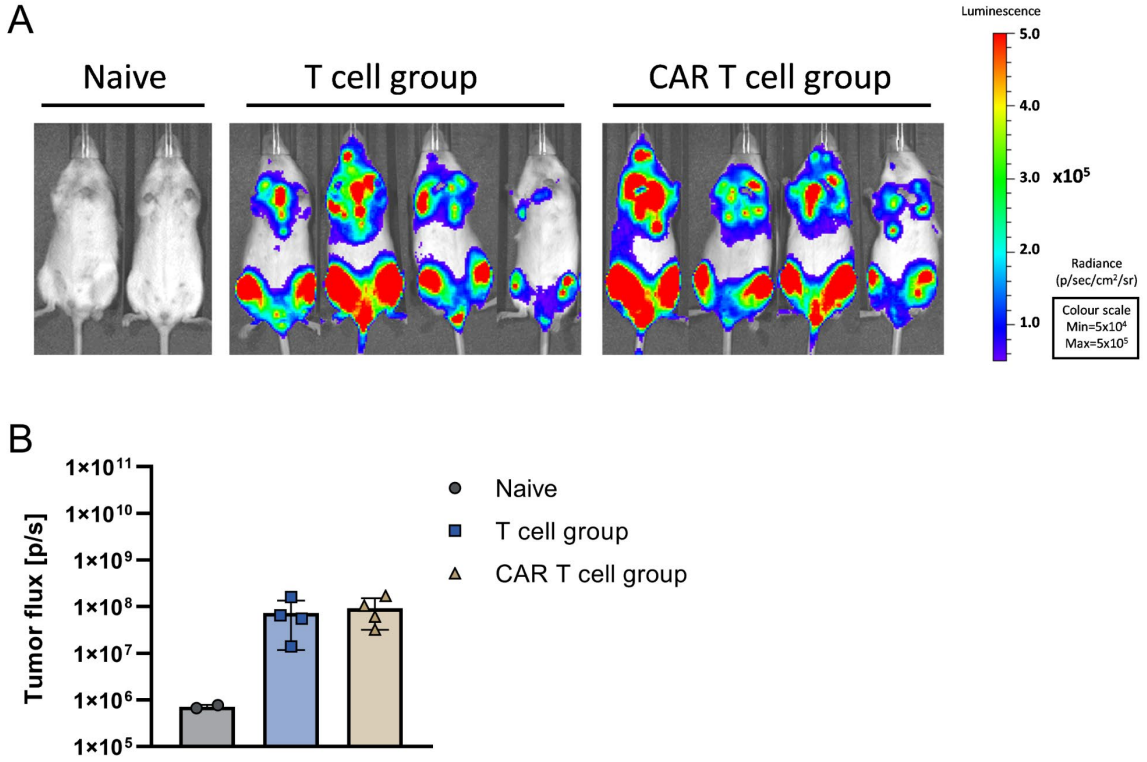

Figure 38: Tumor cell engraftment in NSG-SGM3 prior short-term CAR T cell treatment. Tumor burden in NSG-SGM3 mice pre-engrafted with EBFP and luciferase expressing Nalm6 tumor cells for nine days was determined by *in vivo* bioluminescence imaging system (IVIS). One day bevor administration of short-term CAR T cells or T cells mice were allocated into the groups. Mice without tumor cell engraftment (naive) were used to determine background signals in IVIS imaging. **A)** IVIS images of the ventral side of each mouse are shown with colour scale for tumor signal intensity. **B)** Bar diagrams summarize quantification of the tumor flux with single data points for each mouse including mean and standard deviation of the group. n = 2 (naive), 4 (T cell group), 4 (CAR T cell group).

Mice were then monitored tightly for overall health condition including animal activity and appearance, weight, temperature and plasma cytokines on the final day. In here, the acute induced side effect of short-term CAR T cells were investigated with the main readout as survival. Accordingly, mice were sacrificed once they had reached the pre-defined termination criteria.

2.5.4.1 Distribution of short-term CAR T cells in blood and bone marrow

An interesting observation was made when the administered human T cells and CAR T cells were examined in the periphery by flow cytometry analysis one day after injection. Qualitative and quantitative assessment of human CD3 cells showed a clear absence in the blood of short-term CAR T cell treated mice (Figure 39). In contrast,

human T cells were clearly detected in the T cell group, which made up 3% of all viable cells in the periphery resembled about 35 human T cells per µL blood (Figure 39).

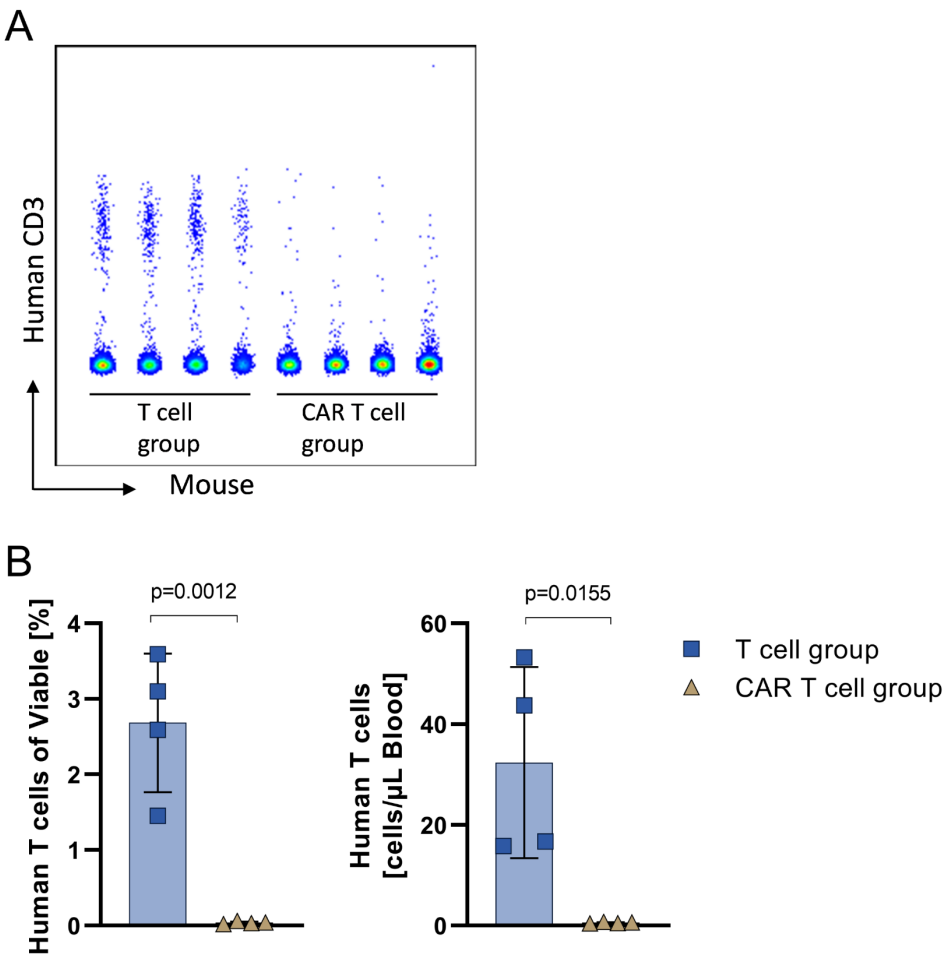

Figure 39: T cell presence in blood of NSG-SGM3 one day post short-term CAR T cell treatment.
T cells in the blood of NSG-SGM3 mice pre-engrafted with EBFP and luciferase expressing Nalm6 tumor cells one day after short-term CAR T cell or T cell administration were determined by flow-cytometry. **A)** Dot plot of human CD3+ T cells within all viable cells for each mouse. **B)** Bar diagram shows frequency of human T cells within viable cells and absolute quantification of human T cells per µL blood. Single data points represent individual mice including mean and standard deviation of the group. n = 4 (T cell group), 4 (CAR T cell group). Statistics were determined by unpaired t test with indicated significant p-values.

A likely explanation might be the migration of CAR T cell to the tumor residing bone marrow. However, this could not be clearly confirmed by flow cytometry analysis due to low abundance of human cells and strong autofluorescence signal in the bone marrow samples (Figure 40A). Only few events of human T cells were found in the bone marrow with a frequency below 0.05% of all viable cells (Figure 40B, C). In contrast, EBFP expressing Nalm6 could be detected at around 4% in the bone marrow

(Figure 40D). Since T cell treated mice were sacrificed at a different time point, it was not possible to conclude if it was a CAR specific migration or not.

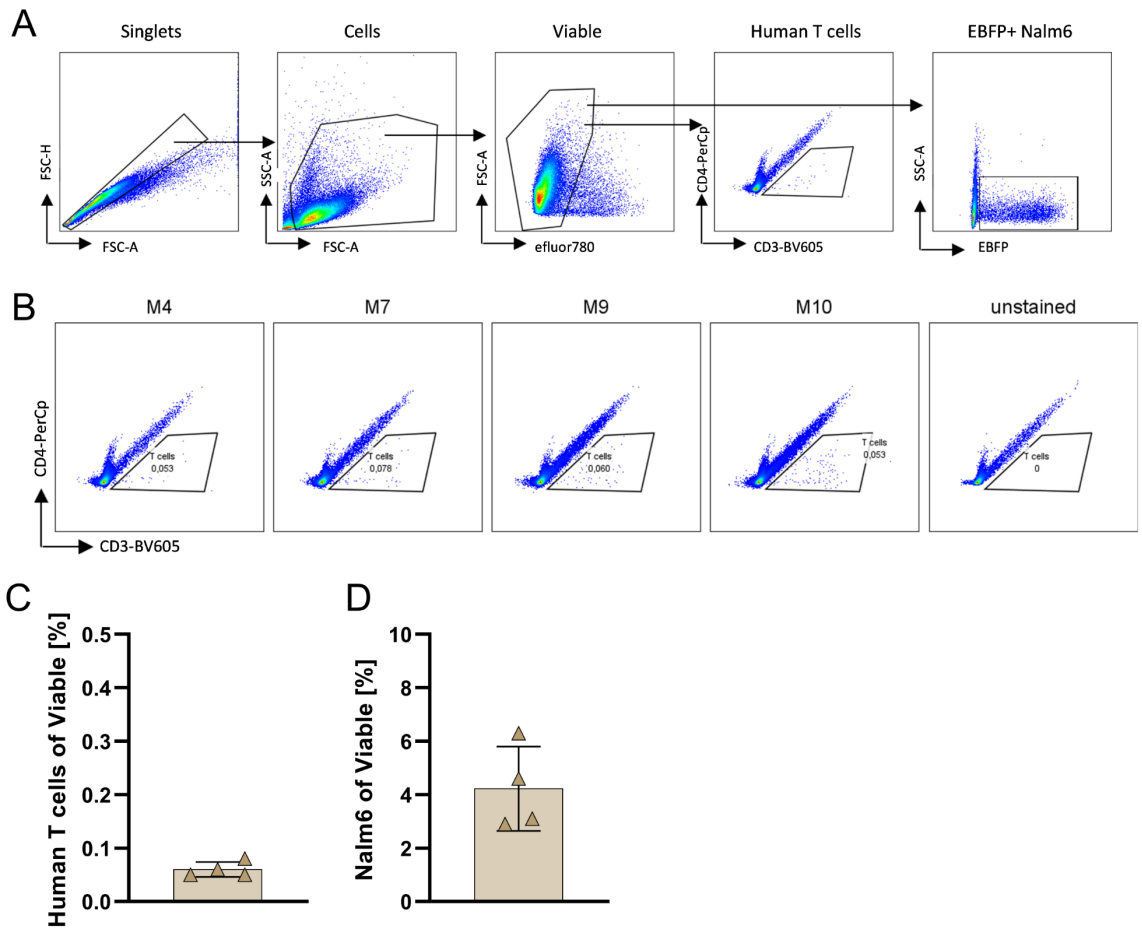

Figure 40: Gating strategy and T cell presence in bone marrow of NSG-SGM3 mice one day post short-term CAR T cell treatment.
Bone marrow of NSG-SGM3 mice pre-engrafted with EBFP and luciferase expressing Nalm6 tumor cells one day after short-term CAR T cell administration were analyzed for the presence of human T cells and tumor cells by flow cytometry. **A)** Gating strategy in bone marrow samples to identify human T cells and EBFP+ tumor cells. **B)** FACS plots of human CD3+ T cells within all viable cells for each mouse with unstained cell sample as control. Bar diagrams show frequency of human T cells **(C)** and tumor cells **(D)** within viable cells. Single data point represents individual mice including mean and standard deviation of the group. n = 4 (CAR T cell group).

2.5.4.2 Short-Term CAR T cell induced acute side effects

After injection of short-term CAR T cells mice developed within 24h severe acute adverse events and had to be sacrificed. In contrast, control T cell injected mice survived until day 12 and had to be terminated due to the high tumor burden (Figure 41A). For the general health assessment, visual appearance, cage activity and weight loss were scored in a body index, which represents adverse effects with increasing scoring number. All mice treated with short-term CAR T cells showed very high body

scoring one day after administration, whereas the T cell treated mice showed a similar scoring as the naive mice (Figure 41B). Only later, T cell treated mice showed a high scoring index due to the increased tumor load and had to be terminated.

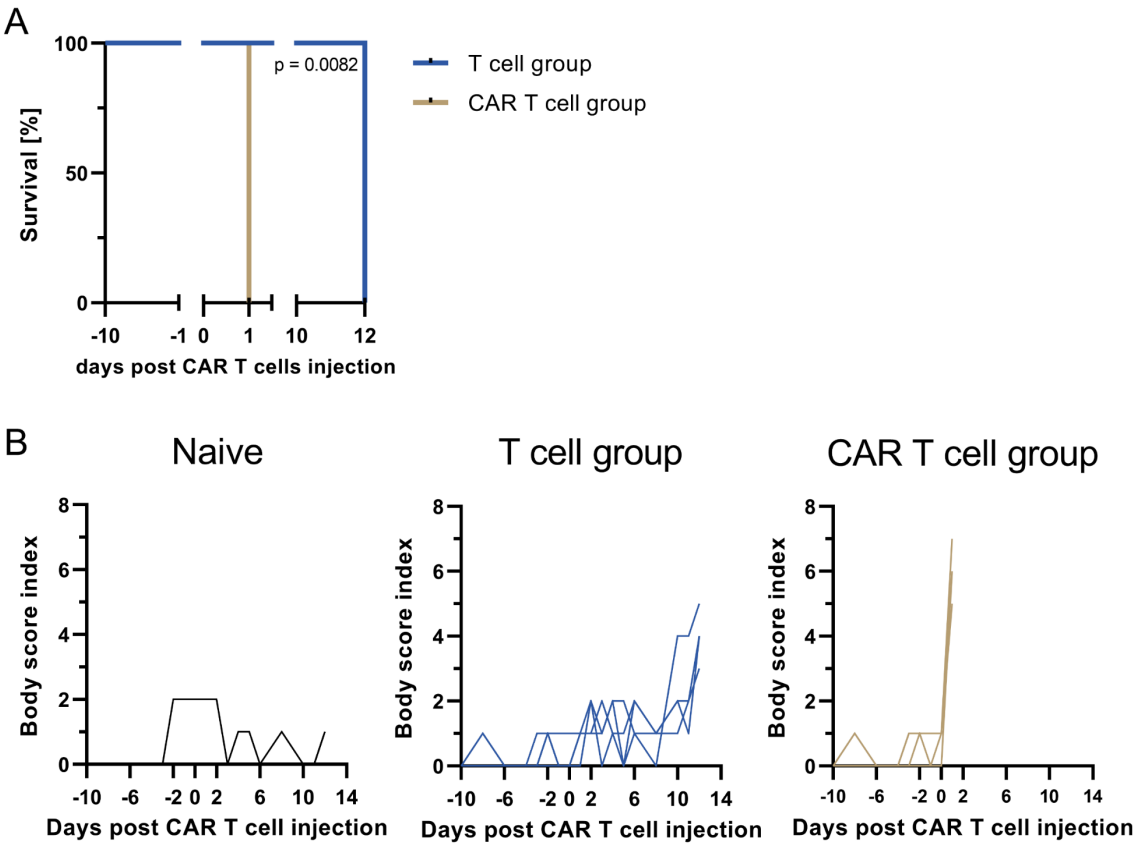

Figure 41: Survival and body score index in NSG-SGM3 mice after short-term CAR T cell treatment.
Tumor pre-engrafted NSG-SGM3 mice after short-term CAR T cell or T cell administration or mice without prior treatment (Naive) were monitored for their general condition. Once reaching pre-defined termination criteria, which are described in more detailed in the methods section 4.4.2.4, mice were sacrificed. **A)** Kaplan-Meier survival curve showing survival of CAR T cell or T cell treated groups post administration. **B)** Kinetic of body score index was determined based on visual appearance, cage activity and weight loss of the mice. n = 2 (naive), 4 (T cell group), 4 (CAR T cell). Statistic for survival curve were determined by Gehan-Breslow-Wilcoxon with indicated significant p-value.

To dissect the scoring in more detail, relative weight loss and temperature change from experiment start were examined. Mice treated with short-term CAR T cells showed on average about 10% weight loss within 24h, whereas T cell treated mice experienced weight loss at the end of the experiment (Figure 42A). Only the naïve mice showed a stable weight development throughout the experiment (Figure 42A). Strikingly, short-term CAR T cell treated mice displayed a very distinct temperature drop of over 2°C from the baseline within 24 hours (Figure 42B). Since, mice, as all small rodents, require constant body activity and food acquirement to maintain their body

temperature, fever or unwell being will manifest rather as temperature drop then temperature increase (151). Such temperature change was not observed for the naïve nor for the T cell treated mice (Figure 42B).

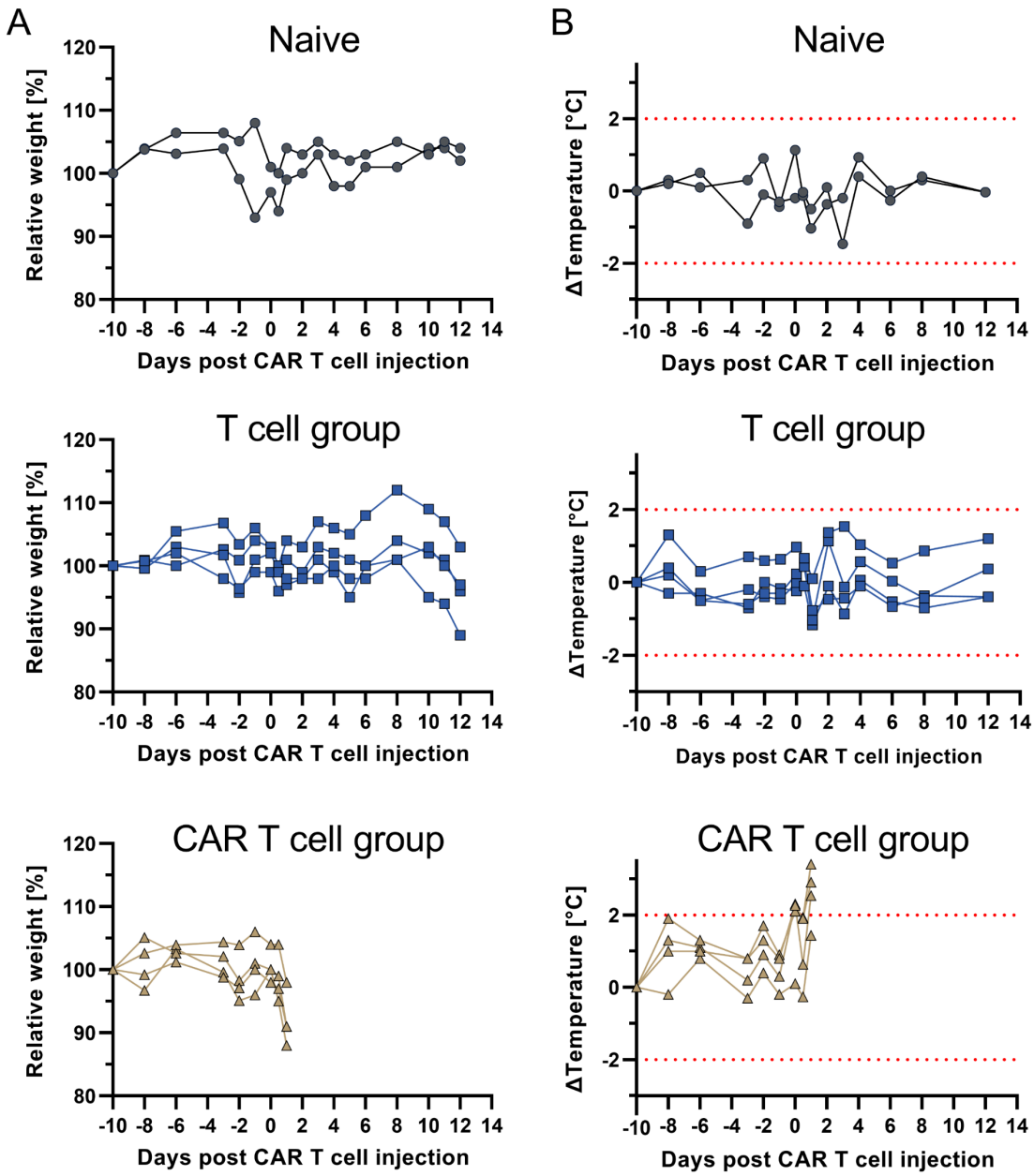

Figure 42: Weight and temperature development after short-term CAR T cell treatment. Tumor pre-engrafted NSG-SGM3 mice after short-term CAR T cell or T cell administration or mice without prior treatment (Naive) were monitored for body weight and body surface temperature development. **A)** Weight was normalized to initial start weight prior experiment start on day -10. **B)** Temperature presented as delta temperature (subtracted from the value prior experiment start on day -10) was assessed in technical triplicates and depicted as mean value. Red dotted lines indicate threshold for determining body temperature change as adverse event. n = 2 (naive), 4 (T cell group), 4 (CAR T cell group).

2.5.4.3 Acute human cytokine release after CAR T cell application

To verify if a cytokine release syndrome was causative for the early mortality of short-term CAR T cell treated mice, typical CRS associated human cytokines were assessed in the plasma on the day of termination. Mice of the T cell group were bled on the same day to assess xenogeneic baseline activity. Results showed a very high and significant increase in various CRS-related human cytokines in all mice treated with short-term CAR T cells compared to the T cell control (Figure 43). In particular, IFN-γ was over 130-fold increased in the CAR T cell group reaching on average 70 ng/mL in plasma. Similarly, other CAR T cell associated pro-inflammatory cytokine, such as TNF-α (114-fold) and IL-2 (6-fold) and the anti-inflammatory cytokine IL-10 (54-fold) were substantially increased (Figure 43). Interestingly, monocyte associated cytokines, such as IL-1β were not notably elevated, but on the other hand IL-6, a major CRS-related cytokine, was significantly increased, but to a lower level (<10 pg/mL) (Figure 43). Taken together, this argues for an acute ongoing cytokine release syndrome shortly after administration of short-term CAR T cells.

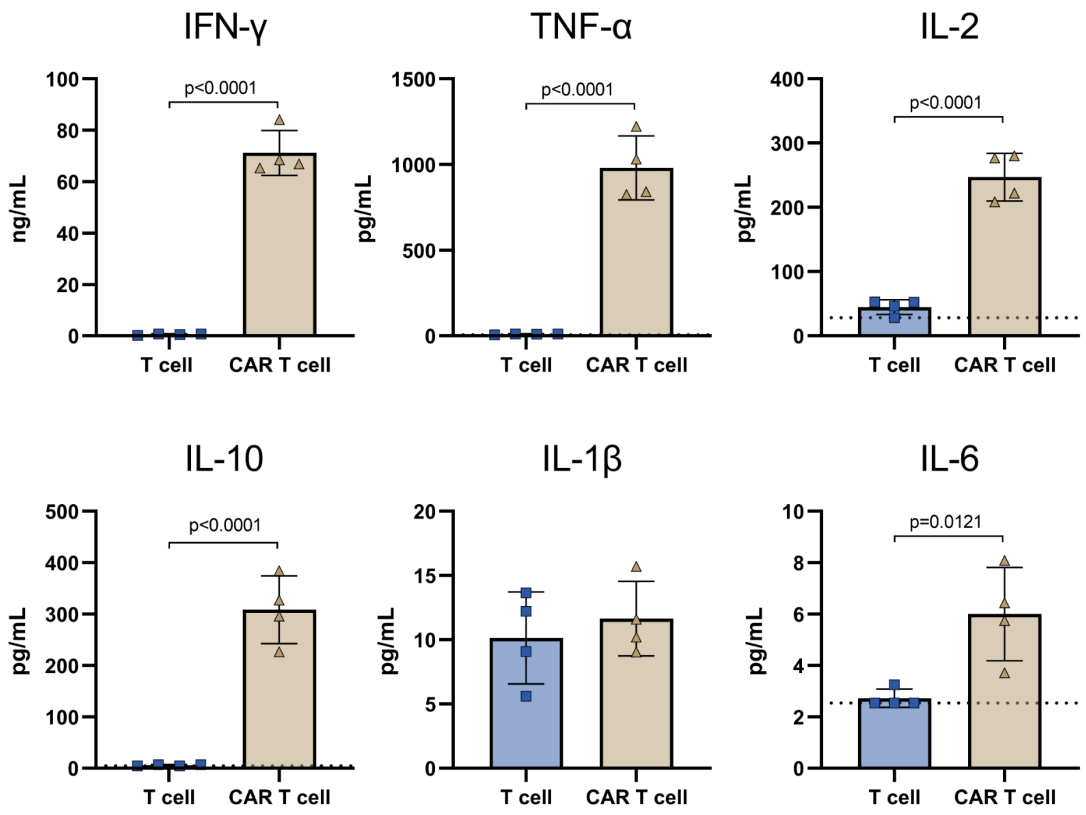

Figure 43: Human plasma cytokines in NSG-SGM3 mice one day post CAR T cell treatment.
Human plasma cytokines in tumor pre-engrafted NSG-SGM3 mice after short-term CAR T cell or T cell administration were measured by bead-based multi-analysis kit. Plasma was collected one day after treatment. Bar diagrams show cytokine levels for each mouse with mean and standard deviation of the group. Dotted lines represent lower detection limit in the cytokine assay. n = 4 (T cell group), 4 (CAR T cell). Statistics were determined by unpaired t test with indicated significant p-values.

2.5.4.4 Involvement of murine immune system during cytokine release after CAR T cell application

Since systemic adverse events during cytokine release syndrome is a multicellular interplay of the whole immune system, the residing murine immune cells in the NSG-SGM3 model might have been involved during cytokine release syndrome too. In particular, this refers to murine myeloid cells including monocytes, macrophages, DCs and neutrophils which were detected in the spleen of NSG-SGM3 mice (Figure 8). To examine if they also contributed to the ongoing CRS, multiple murine cytokines were measured in the plasma of short-term CAR T cell and T cell treated and naïve mice. However, due to limited plasma volume from the intermediate bleeding on day one after administration, murine cytokines were assessed in the plasma derived from the respective termination day of the mice. Results show that especially murine MCP-1 and G-CSF were significantly elevated in CAR T cell treated mice with on average over

9-fold and 59-fold increase compared to the other groups (Figure 44). Interestingly, murine IL-6 was elevated in the CAR T cell and T cell treated mice compared to the naïve mice, but notably more in the CAR T cell group (Figure 44).

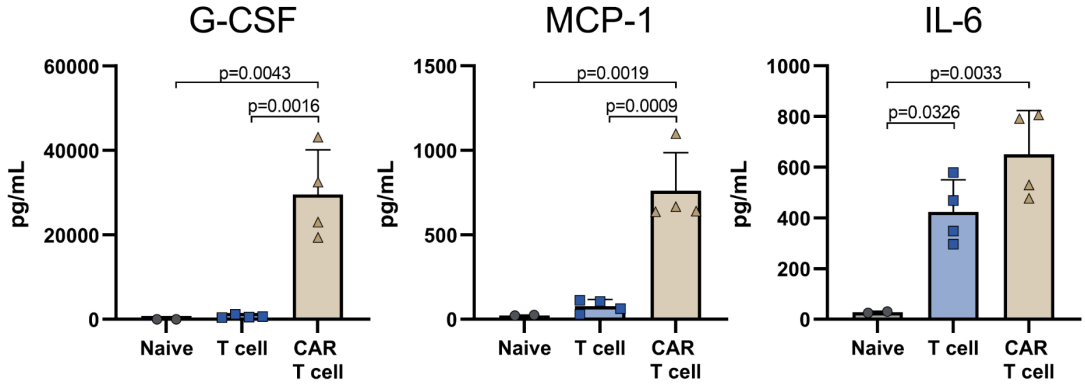

Figure 44: Mouse plasma cytokines in NSG-SGM3 on final day post CAR T cell treatment
Mouse plasma cytokines in tumor pre-engrafted NSG-SGM3 mice after short-term CAR T cell or T cell administration or mice without prior treatment (naive) were analyzed by bead-based multi-analysis kit. Plasma was collected on the final days, which was on day one for mice treated with CAR T cells and on day 12 for mice treated with T cells and naïve mice. Bar diagrams show cytokine for each mouse with mean and standard deviation of the group. n = 2 (naïve), 4 (T cell group), 4 (CAR T cell). Statistics were determined by one-way ANOVA (Tukey's multiple comparisons test) with indicated significant p-values.

Although plasma samples were derived from different time points between the CAR T cell and the T cell group, it revealed in both cases elevated murine cytokines, thus underlining the involvement of murine immune cells during systemic adverse events. Especially MCP-1 and G-CSF, but as well the slightly greater release of IL-6 in short-term CAR T cell treated mice might have contributed to the acute morbidity.

2.5.4.5 No indication of tumor lysis syndrome

A common side effect in hematologic cancer treatment is tumor lysis syndrome, which occurs during therapy due to excessive lysis of tumor cells and release of cellular content into the system that lead to organ failure. Therefore, tumor load of the mice was assessed by IVIS at the time point when short-term CAR T cell treated mice showed severe acute adverse effects. No visible difference in tumor load could be observed in mice treated with short-term CAR T cells or T cells one day after administration (Figure 45). Both groups had similar tumor flux around $2x10^8$ p/s (Figure 45) which had increased 2-fold compared to the measurement from 2 days before (Figure 38).

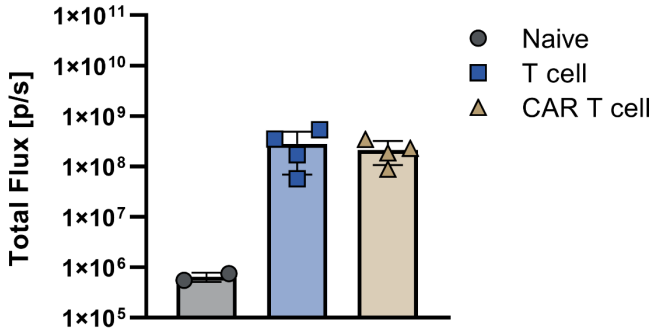

Figure 45: Tumor burden in NSG-SGM3 one day post short-term CAR T cell treatment. Tumor burden in NSG-SGM3 mice pre-engrafted with EBFP and luciferase expressing Nalm6 tumor cells one day after short-term CAR T cell or T cell administration or mice without prior treatment (naive) were determined by *in vivo* bioluminescence imaging system (IVIS). Bar diagram summarizes quantification of the tumor flux with single data point for each mouse including mean and standard deviation of the group. n = 2 (naive), 4 (T cell group), 4 (CAR T cell).

This confirms that the observed cytokine release syndrome was rather the result of an overactivation by the administered short-term CAR T cells and not by excessive tumor cell lysis.

3 Discussion

As the field of CAR T cell therapy progresses, new model systems and evaluation platforms are becoming more and more crucial for accurate assessment of benefits and risks of novel CAR T cell strategies, as well as the identification of potential barriers. In the following section the strength and relevance of different model systems, established in this thesis, will be discussed. Further, their effective use to unravel safety risks of short-term CAR T cells and roadblocks for *in vivo* CAR T cell generation will be explained as well the implementation as assessment tool for pre-clinical studies.

3.1 Advances in model systems for CAR T cell therapy

A common issue in CAR T cell therapy is CRS induction after CAR T cell administration, which can reach life-threatening conditions in patients. Although this can be managed by application of cytokine receptor blocker, e.g. tocilizumab, or in severe case of corticosteroids, CRS should be avoided. In particular for new CAR T cell approaches, such as CAR T cells manufactured within few days, this risk should be carefully evaluated. First model systems for evaluation are *in vitro* cultures, which can be designed to recapitulate key features of CRS and allow fast and high throughput screening. In this thesis an assay was established that allowed simultaneous assessment of cytotoxicity and sensitive readout for CRS related human cytokines of short-term CAR T cells. Setting up a co-culture of labeled tumor cells and CAR T cells allowed a simple readout for cytotoxicity. Strikingly, supplementation with 10% autologous monocytes, which are key player involved in CRS induction and development (88, 85, 86). Besides IFN-γ, IL-10 and TNF-α, addition of monocytes significantly increased IL-6 level during short-term CAR T cell specific tumor cell killing (Figure 36). Importantly, the presence of monocytes did not influence CAR T cell cytotoxicity. A similar co-culture has been described by Sachdeva and colleagues (89) where tumor cells and CAR T cells were cultivated together in one chamber of a transwell and allogeneic monocytes in a separate chamber to allow only cytokine mediated interaction. In this way they could study only cytokine mediated effects between CAR T cells and monocytes. Artifacts due to the allogeneic mismatch were likely overcome by the absence of cellular contact between these cells. However, cytokine levels for IFN-γ, IL-10 and TNF-α were about 10 to 200 times lower than those found in this thesis. This could be due to the different CAR T cell manufacturing

protocol (conventional vs. shortened; CAR insertion in TRAC locus vs. not guided CAR insertion), target receptor of CAR (CD22 vs. CD19) or more likely because of the differences in experimental assay layout, such as time point and monocyte ratio. Another study also reported the use of additional monocyte derived macrophages and dendritic cells in the co-culture of tumor cells and CAR T cells with enhanced CRS readout (88). However, the selected cell types were not accurately reflecting human's blood composition, which contains rather monocyte than macrophages and DCs. Therefore, the proposed assay in this thesis seems to allow a more accurate CRS readout compared to *in vitro* CRS models described by others. Furthermore, the additional readout for CAR T cell cytotoxicity gives a more complete evaluation of benefit and risk of the CAR T cells investigated.

Although *in vitro* models can be designed to recapitulate some key parameters of CRS, the systemic implication of an organism cannot be modeled in cell culture assays. In this thesis an *in vivo* CRS model was developed using NSG-SGM3 mice, which has been reported recently as a sensitive PBMC humanized model for monoclonal antibody mediated CRS (152). The NSG-SGM3 model was adapted in this thesis for modeling CAR T cell induced CRS by engraftment of tumor cells to a high burden in mice. This model robustly recapitulated typical symptoms for CRS after CAR T cell administration, including high levels of CRS-relevant cytokines in plasma, drop in temperature and weight and overall high body scoring resulting in high mortality (Figure 41, 42, 43, 44). Interestingly, strong rise in human IFN-γ, IL-10, IL-2 and TNF-α, but as well elevation of murine IL-6, MCP-1 and G-CSF was observed and underlines a multicellular immune response and interactions between human CAR T cells and murine cells in this xenogeneic mouse model system. A similar cytokine pattern was reported by Giavridis and colleagues (85) after CAR T cell administration into tumor bearing SCID-beige mice. Both mouse strains are immunocompromised, but with a different degree of remaining innate murine cells in the system. Murine T cell and B cell development is impaired by the same *scid* mutation in both strains (153, 154). This could also be confirmed in splenocytes of NSG-SGM3 mouse by immunophenotyping in this thesis (Figure 8). In contrast, deficiency of murine NK cells is mediated by the *beige* mutation in SCID-beige mice (155), whereas in NSG-based mouse models this is achieved by the IL-2 receptor common gamma chain knockout, which additionally also impairs murine macrophage presence and functionality (133). However, in this thesis immunophenotyping of murine splenocytes from NSG-SGM3 mice confirmed

the presence of residual macrophages, dendritic cells and neutrophils (Figure 8), which likely contributed to the elevated murine IL-6 levels. Although it has been reported that murine macrophages in SCID-beige mice are capable for iNOS activity and rather defective in NSG mice (156, 154, 85), similar levels of elevated murine cytokines (IL-6, MCP-1 and G-CSF) were found in NSG-SGM3 mice during CRS in this thesis. Moreover, the proposed model in this thesis might be refined with human monocyte supplementation to recapitulate innate cytokines, such as IL-6, also from the human compartment. Since the NSG-SGM3 model was designed to support human myeloid engraftment and persistence, this approach might provide a more complete humanized CRS model.

Such a model would be closely related to the CD34+ stem cell humanized NSG-SGM3 model described by Norelli and colleagues (86, 90). In there, autologous human myeloid-, T- and B cells develop from the engrafted human stem cells and reconstitute a sophisticated human immune system. Using this model the authors recapitulated CRS relevant adverse events after administration of stem-cell derived autologous or PBMC-derived CAR T cells. Similar to the model proposed in this thesis mice experienced weight loss, temperature drop, increased mortality and high release of human plasma cytokines, but in addition also neurotoxicity-related events, such as seizure and paralysis (86, 90). Importantly, huSGM3 mice also showed tremendously elevated human IL-6, which were secreted by endogenous human monocytes upon CAR T cell treatment (86, 90). Therefore, to date this study described the most accurate CRS mouse model for human CAR T cell therapy so far. However, the high cost for purchasing ready-to use humanized NSG-SGM3 mice, challenges in acquiring umbilical cord blood derived stem cells and achieving robust humanization in the own laboratory is limiting the broad application in research for screening experiments. Therefore, the proposed model in this thesis might provide a cost-effective alternative to stem cells humanized NSG-SGM3 mice for CAR T cell induced CRS studies.

3.2 Potential risks for short-term CAR T cells

Current approaches to refine CAR T cell therapy focus on the reduction of manufacturing time from weeks down to several days. In this study results showed that CAR T cells, which were manufactured by lentiviral vectors within three days, consisted of mainly vector particle-bound cells with only a minor fraction of the cells being positive

for CAR. Only upon further cultivation and reactivation of these cells, CAR is expressed and vector particles removed, showing that transduction is not fully completed after manufacturing and is rather still ongoing. This is in line with previous work by Ghassemi and colleague (157) where similar findings were observed for rapidly manufactured CAR T cells by lentiviral vector incubation. They showed that transient detection of the CAR protein on short-term CAR T cells is due to vector particle binding and does not mediate any killing activity when further downstream reverse transcription and genome integration of the transgene is inhibited (157). However, they used the CAR protein, which is incorporated on the LV envelope during LV production (158, 159), as surrogate marker for lentiviral vector detection. In this study, using an anti-VSV-G antibody allowed a more accurate characterization of short-term CAR T cells. All vector particles bound on the T cell surface must have VSV-G incorporated, since this is the glycoprotein mediating binding and cell entry of the vector particle. In contrast, not all bound vector particles will have the CAR incorporated, since they might have derived from a vector production HEK cell with unsuccessful CAR plasmid transfection.

Although current studies reveal that CAR T cells generated within few days are having a beneficial phenotype and outperforming long-term cultivated CAR T cells *in vivo* for expansion and anti-tumor activity, less is known about potential side effects of these cells (Figure 46). Especially the fact that transduction is not completed within the short manufacturing time make these CAR T cells somewhat unpredictable. Therefore, the question arises, if side effects commonly observed with CAR T cells are shared by short-term CAR T cells?

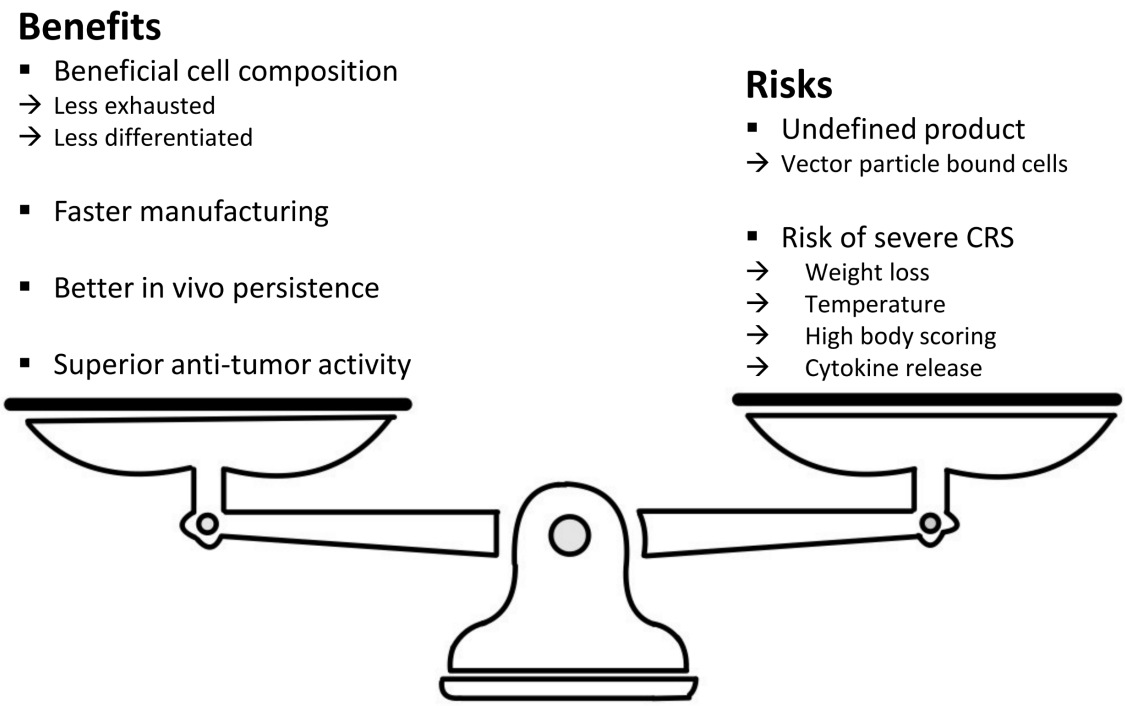

Figure 46: Benefits and risks of short-term CAR T cells.
To shorten manufacturing process of CAR T cells, time for T cell activation, viral vector transduction and CAR T cell expansion are reduced. That results in a unique cell composition of short-term CAR T cells compared to conventional generated CAR T cells and can offer certain benefits but risks as well.

In this thesis using an *in vitro* killing assay confirmed the tumor cell killing activity of short-term CAR T cells manufactured within three days and is in line with other studies (100, 157, 160, 161). Already within 24h CAR specific tumor cell lysis could be observed for short-term CAR T cells. Moreover, high release of human CRS relevant cytokines was observed with tremendous increase of IFN-γ, TNF-α, IL-10 and IL-6.

To assess if these CAR T cells exhibit a safety risk and lead to clinically relevant manifestation of CRS, they were tested in an *in vivo* CRS model, which was established in this thesis. Strikingly, all mice treated with short-term CAR T cells rapidly developed typical signs for CRS associated mortality already 24h after administration. Strong fur ruffleness, squinted eyes and reduced active response confirmed ongoing adverse events in the mice. This was further underlined by sudden weight and temperature drop within the time frame. These physical signs are typical symptoms for ill-being in mice (162, 151) and also described during CRS induced by monoclonal antibodies (163, 152, 164) and conventionally generated CAR T cells (85, 86, 90).

Furthermore, mice treated with short-term CAR T cells displayed tremendously elevated human cytokines in the plasma for TNF-α, IL-10 and especially IFN-γ and

thereby reflecting the cytokine patterns observed in the clinic during therapy with conventionally manufactured CAR T cells (77, 79, 80). Interestingly, high plasma levels of these cytokines were also reported in a recently published clinical study with B-ALL patients treated with CAR T cells, which were manufactured within 36h (160, 161). Although in the mouse study of this thesis the key human CRS cytokine IL-6 was significantly elevated in short-term CAR T cell treated mice its moderate levels suggest rather a subordinate role in CRS promotion. Most likely this is due to the missing human monocytes in this model, which are one of the major source for IL-6 during CRS (85, 86). But strikingly, similar to the study from Giavridis and colleagues (85), also a massive increase in some murine inflammatory cytokines was observed in this thesis (Figure 44). Immunophenotyping of residual murine immune cells in splenocytes of a NSG-SGM3 mouse showed residual macrophages and monocytes in the system (Figure 8), which presumably released high levels of murine IL-6 found in short-term CAR T cell treated mice (Figure 44). In addition, highly increased murine MCP-1, a chemoattractant for monocytes, and murine G-CSF, an activator for granulocytes, was found in CRS affected mice. Both these cytokines can be secreted by activated endothelial cells (165, 166). This is in line with clinical implication of endothelial activation in patients with severe CRS and ICANS (92).

A limitation of the study conducted in this thesis was the different time points for termination of short-term CAR T cell and control T cell treated mice, which was due to the experimental design to assess survival. Therefore, murine cytokine analysis had to be performed on plasma samples from the respective end time points of the mice, since plasma sample volume from the intermediate bleeding day of T cell treated mice were not sufficient to perform both human and mouse cytokine analysis. Since prolonged engraftment of activated human T cells in a xenogeneic mouse model results in GvHD (137–139), this is likely an explanation for the significant increase in murine IL-6 for the T cell treated control mice on the late final analysis day. Further experiments, not designed for survival assessment, where T cell control mice are terminated on the same day as short-term CAR T cell treated mice, are required for a final conclusion about the involvement of murine cytokines in this model.

Another interesting observation made in this thesis was an almost complete absence of short-term CAR T cells in the periphery one day after administration. In contrast, human T cells could be very well detected in the blood of the control T cell mice (Figure

39). A likely, explanation is the migration of short-term CAR T cells to the tumor-residing niche in the bone marrow, where most of the tumor cells are located (Figure 38, 40D). Indeed, presence of few human T cells could be confirmed in the bone marrow despite the short time between administration and analysis of short-term CAR T cells. Interestingly, recent data also showed a more pronounced migration into the bone marrow for rapidly manufactured CAR T cells than for conventional CAR T cells (160). The authors correlated this to a higher degree of the chemokine receptor CXCR4 expression on CAR T cells, which is involved in migration and has been shown to increase homing into the bone marrow niche for CAR T cells, but as well CAR NK cells when overexpressed (167, 168).

A surprising outcome in the thesis was the fast kinetics of severe CRS appearance within 24 hours after short-term CAR T cell administration. This has not been reported so far for any preclinical studies with rapid manufactured CAR T cells (100, 157, 160) nor with conventionally manufactured CAR T cells in pre-clinical CRS mouse models (85, 86). Norelli and colleagues (86) evaluated this in CD34+ huSGM3 mice and observed critical heath condition within a week post therapy infusion. Also, Giavridis and colleagues (85), who used a similar experimental setup as in this thesis regarding tumor burden, humanization platform and CAR T cell dosage, observed onsetting mortality earliest 42h post CAR T cell administration. Their results for conventional CAR T cells are well in line with clinical data for conventional CAR T cells, which also show first signs of CRS, starting with fever, around two to four days post infusion that reaches its peak within a week (77, 79, 80). However, patients with very high and life-threatening grade of CRS (grade 4 or more), already develop first signs within 25 hours post CAR T cell therapy (79, 80). This would support that a life-threatening grade of CRS was ongoing in short-term CAR T cell treated mice in this thesis and is in line with the tremendous elevation of human IFN-γ in the plasma. Although, the high number of short-term CAR T cells used in this thesis might have contributed to the intense and fast occurring CRS in the mice. Recent clinical data for rapidly manufactured CAR T cells in patients also showed CRS peaks occurring about a week post treatment (160, 161). Note, these first clinical studies were conducted with quite low CAR T cell dosage from 10^4 to 10^5 cells/kg bodyweight range in patients, yet induced severe CRS in some patients (160, 161). In comparison the dosage used in this thesis was approximately 5 $x10^8$ cells/kg and thus over 1000-fold higher, nevertheless conventional CAR T cell dosage of up to 2 $x10^7$ cells/kg have been used in clinical trials (77, 69, 169). Therefore,

administering higher dosages of rapidly manufactured CAR T cells in patients may not be safe. Nonetheless, further preclinical studies using the CRS models presented in this thesis could give a deeper understanding about dosage regime and anti-tumoral activity for such new type of CAR T cell manufactured product. In addition, careful investigation, characterization and establishment of parameter for quality control of rapid manufactured CAR T cells are needed in the future to ensure a safe product for the patient.

3.3 Roadblocks for *in vivo* CAR T cell generation

In vivo CAR T cell therapy is a novel approach that has the potential to avoid *ex vivo* manufacturing and thus enable CAR T cell therapy for patients worldwide. Preferentially, this requires T cell targeted vector particles systemically that deliver the genetic material for the CAR selectively to the T cells. Currently this strategy is still in the preclinical phase and rigorous evaluation and improvements are ongoing. In this thesis *in vivo* CAR T cell generation with CD4-LV and CD8-LV has been evaluated in CD34+ stem cell humanized NSG-SGM3 mice, which develop pronounced human myeloid cells (145, 146). Accordingly, this enabled studying the influence of the innate immune cells on *in vivo* CAR T cell generation.

In principle, *in vivo* CD19CAR T cell generation using CD4-LV and CD8-LV was achieved in huSMG3 mice with some mice developing substantial CAR T cells in the blood, but not detectable in other hematopoietic organs. However, cultivation of splenocytes in the presence of irradiated CD19+ tumor cells showed expanding CAR T cells from spleen even up to 10 weeks after vector administration. This highlights the long persistence of *in vivo* generated CAR T cells in the system, which must have been in a resting state and proliferated in the presence of tumor antigens. Interestingly, B cell reduction was observed as a more sensitive readout for CAR T cell presence than CAR detection by flow-cytometry. Downmodulation of CAR on the cell surface and CAR T cells in a resting status are likely explanations (170), especially in the stem cell humanized platform, which are known to develop a quiescent and non-activated human immune system (171).

Intriguingly, *in vivo* CAR T cell generation efficiency in huSGM3 mice was overall much lower compared to the parental huNSG model according to previous publications using

the same vector (108, 17). In the huNSG model about 70% to 88% of the mice showed successful *in vivo* generation of CAR T cells and B cell reduction after systemic administration of the CD4-LV or CD8-LV (Table 3). In contrast, only 46% and 62% of the mice in the huSGM3 model developed detectable CAR T cells with even slightly less frequent B cell depletion in the mice (Table 3). Since one particular feature of the NSG-SGM3 mouse model is the enhanced humanization and human myeloidpoiesis upon CD34+ stem cell engraftment, the more pronounced level of human myeloid cells was suspected to be causative for the low *in vivo* CAR T cell generation in huSGM3 mice.

Table 3: Overview of *in vivo* CAR T cell generation in huNSG and huSGM3 mice.

Mouse model	Vector	Number of animals	[a]CAR+ mice	[b]B cell depletion	Reference
huNSG	CD4-LV	8	7 (88%)	7 (88%)	(17)
	CD8-LV	10	7 (70%)	8 (80%)	(108)
huSGM3	[c]CD4-LV	13	6 (46%)	5 (39%)	(147) / This thesis
	[c]CD8-LV	13	8 (62%)	4 (31%)	
	[d]CD4-LV^{sh}	6	6 (100%)	5 (83%)	
	[d]CD4-LV^{sh}(2x)	5	4 (80%)	4 (80%)	
	[d]CD8-LV^{sh}	5	2 (40%)	1 (20%)	
	[d]CD8-LV^{sh}(2x)	5	4 (80%)	4 (80%)	

[a]Mice are stated as CAR+ when two out of five independently assessed parameters (flow cytometry of blood, spleen and bone marrow, qPCR and expansion assay) were positive for the presence of CAR.

[b]B cell depletion was determined if at least two out of three organs exhibited reduced B cell levels.

[c]Data from chapter 2.2 and 2.4 combined.

[d]Data from chapter 2.4.

Table modified from (147).

Using an *in vitro* co-culture assay the negative impact of human monocytes and macrophages on T cell transduction with CD4-LV and CD8-LV could be confirmed. However, significance was only observed in the presence of a rather artificial ratio of 50% myeloid cells in the co-culture, which does not represent the frequency in human blood. Probably the excess of vector particles used in the assay, which is artificial

compared to the *in vivo* setting, might have masked the inhibitory effects at lower ratios. Although the ratio of 50% might not represent the composition in human blood, it still might be a biological relevant composition for tissue residing macrophages in biodistribution relevant organs, such as Kupffer cells in liver, red pulp macrophages in spleen and alveolar macrophages in lung (172). Moreover, the interference was also only observed for *in vitro* polarized macrophages, which also exhibited the marker expression of CD206 and CD209 (Figure 17). These receptors were found by mass-spectrometry based phagocytosis analysis to be associated with a highly phagocytic active phenotype on macrophages (148). Therefore, reducing phagocytic clearance seemed to be a promising strategy to improve T cell gene transfer in presence of macrophages.

An interesting approach was initially described by the group of Dennis E Discher using human CD47 decorated nanoparticles (173) and lentiviral vectors (174) to reduce phagocytic uptake and therefore increase half-life in NOD-derived mouse strain. As a “marker of self” (175) or “don’t’ eat me signal” (176) CD47 acts through the phagocyte receptor CD172a (SIRPα) and reduces clearance by macrophages. Later on, this approach was further refined by removing MHC-I decoration in addition to human CD47 overexpression on the LV particle surface (149). This was achieved by applying these modifications to the packaging cell line HEK-293T, resulting in the $\beta2M^{-/-}$, $CD47^{high}$ HEK-293T cell line. Phagocytosis shielded VSV-LV showed improved half-life of the vector in immunodeficient NOD mice and finally also improved *in vivo* gene transfer into the liver of non-human primates after intravenous administration (149). In this thesis, this vector shielding strategy was successfully combined with T cell receptor targeted LVs resulting in shielded $CD4\text{-}LV^{sh}$ and $CD8\text{-}LV^{sh}$ that significantly improved T cell specific transduction in presence of macrophages in the co-culture (Figure 21).

Remarkably, systemic administration of $CD4\text{-}LV^{sh}$ and $CD8\text{-}LV^{sh}$ also improved *in vivo* CAR T cell generation in huSGM3 mice and outperformed non-shielded CD4-LV and CD8-LV. For $CD8\text{-}LV^{sh}$ this was confirmed with more sensitive detection readouts in the organs (Figure 26), whereas for $CD4\text{-}LV^{sh}$ this was observed also in the periphery by flow-cytometry analysis. Interestingly, these results are in slight discrepancy to the mouse experiment in Figure 10 in which CD8-LV performed better than CD4-LV. A likely explanation is the difference in vector potency between the CD8-LV in both experiments. An at least 2-fold lower titer was found for CD8-LV used in Figure 22 than

in Figure 10 (Table 1, 2). Nevertheless, it did not affect the interpretation of the results from the *in vivo* comparison between shielded and non-shielded LVs. Moreover, vector particle numbers were normalized between the groups of shielded and non-shielded LVs with similar transducing units injected into the mice (Table 2). Hence, the improved *in vivo* CAR T cell generation is likely mediated by the vector surface modification rather than by a higher intrinsic vector stock potency. This is further supported by basic vector stock characterization of shielded and non-shielded CD4-LV and CD8-LV that showed that incorporation of human CD47 and absence of MHC I did not significantly influence particle size and normalized gene transfer activity (Figure 20). Intriguingly, increasing the dosage of shielded CD4-LV and CD8-LV profoundly increased *in vivo* CAR T cell generation efficiency and suggests that saturation for *in vivo* generation of CAR T cells has not yet been reached. Overall, shielding of CD4-LV and CD8-LV restored *in vivo* CAR T cell generation efficiency in huSGM3 mice similar to the frequencies observed in huNSG (Table 3).

Interestingly, *in vivo* gene transfer efficiency was particularly reduced for CD4-LV in huSGM3 mice and could be profoundly improved by phagocytosis shielding (Figure 47). A possible reason for this effect might be low level expression of CD4 on monocytes (177) which can be bound by CD4-LV and therefore be eliminated more efficiently than CD8-LV. Moreover, direct CD4 binding on monocytes may activate monocyte and induce macrophage differentiation (178), which have even a higher phagocytic activity. Therefore, it is possible that CD4-LV binding might trigger an innate immune response and thereby restrict gene delivery in the huSGM3 model. In addition, phagocytosed vectors may also trigger an innate immune response via PRR, such as ssRNA and induce TLR-7 signaling (179). In this thesis, a tendency of initially high monocyte numbers in the blood were found to correlate with low *in vivo* CAR T cell generation for CD4-LV injected mice (Figure 24). In addition, a distinct myeloid associated human cytokine pattern was observed exclusively in CD4-LV injected mice (Figure 16). Elevated human IL-1β and IL-15 in the plasma of huSGM3 mice can be confidently traced back to human monocytes and macrophages in the chimeric humanized system, while elevated human IL-10 might be contributed by human T cells as well. Moreover, reduction of transgenically expressed human GM-CSF in the system is also an indication for monocyte activation and subsequent macrophage differentiation resulting in overall GM-CSF consumption.

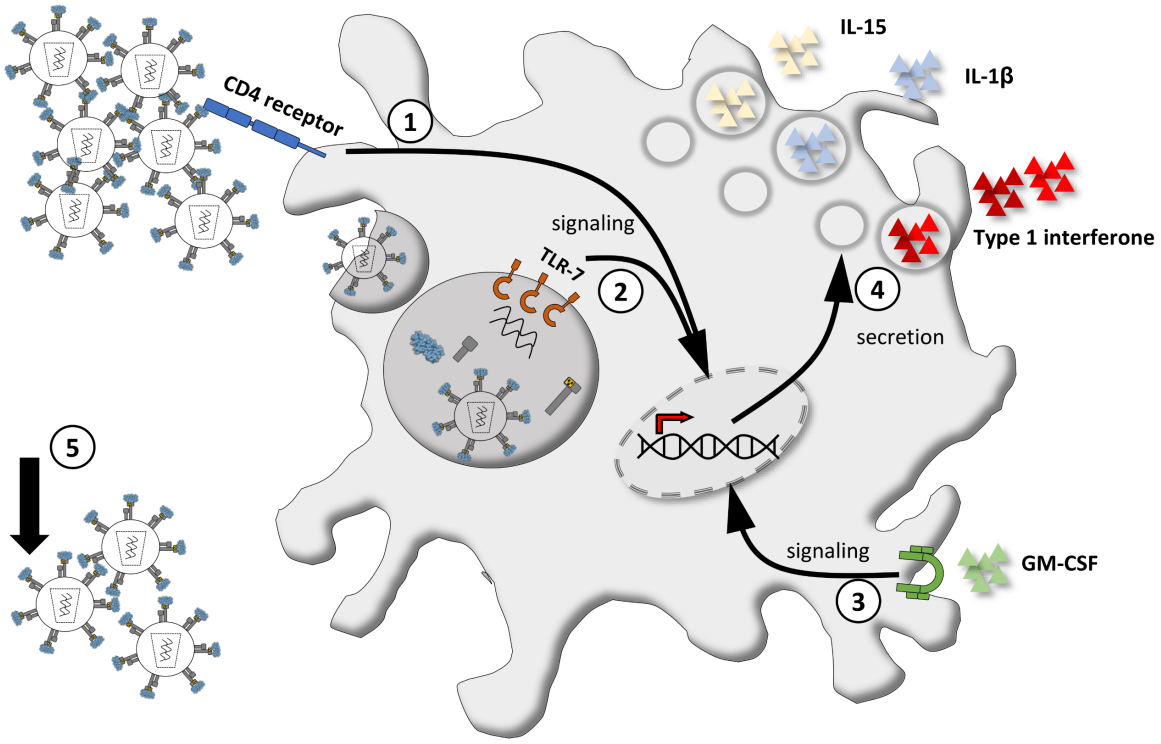

Figure 47: Working model for CD4-LV sequestration and immune response by monocytes during *in vivo* CAR T cell generation.
In vivo CAR T cell generation with CD4-LV is limited by myeloid cells in the system. Sequestration of CD4-LVs appears through direct binding to CD4 on the cell surface ①, but as well by phagocytosis and subsequent degradation in the lysosome. In response, CD4 binding and ssRNA sensing through TLR-7 ② induces immune cell activation and upregulation of inflammatory and anti-viral gene transcription. In addition, activated monocytes can bind and take up GM-CSF, which further leads to differentiation into professional antigen-presenting macrophages ③. This results into secretion of immune modulatory cytokines, such as IL-15, IL-1β or type-1 interferons ④, and overall reduced availability of CD4-LV that limits *in vivo* CAR T cell generation in the system ⑤.

Although binding of CD4-LV to monocytes might appear, no transduction and CAR expression was observed on these cells. This is expected since monocytes are less susceptible for HIV-1 derived lentiviral vector transduction and require the accessory viral protein vpx for efficient transduction (180–182). This bypasses antiviral restriction factors in myeloid cells such as SAMHD1 (183, 184). Moreover, *in vitro* transduction of monocytes and macrophages with lentiviral vectors applies high vector particle numbers (185, 186, 181), whereas vector particle to cell ratio is low in the *in vivo* setting and decreases the likelihood of *in vivo* monocyte transduction with CD4-LV.

An important aspect for *in vivo* gene therapy is specificity of gene delivery. An infamous example showed the accidental transduction of a B cell leukemic cell during *ex vivo* CD19CAR T cell manufacturing of one patient, which resulted in a CAR resistant

leukemic clone and ultimately led to relapse and failure of the therapy and death of the patient (120). Thus, specific gene transfer into the therapeutic relevant cells is highly important for gene therapy itself and vital for *in vivo* gene delivery where no preselection of the target cell is possible. In here, systemic injection of CD4-LV and CD8-LV in huSGM3 mice resulted in specific CD4 or CD8 CAR T cell generation *in vivo*, without visible CAR expression in human CD3 negative population. Importantly, shielding of the vector by overexpression of CD47 on the vector surface did not alter specificity. Nevertheless, concerns regarding off-target transduction using highly CD47 decorated LVs might arise for SIRP-α expressing cells. For instance, phagocytes but also certain tumor cell types including human lung carcinoma cells and glioblastoma are described to express SIRP-α (174). Although, binding of the vector to the off-target cell is possible, activation of membrane fusion is highly unlikely. Fusion via the paramyxoviral fusion glycoprotein is triggered exclusively upon binding and conformational change of the targeting glycoprotein (187). Only in that case, this is leading to membrane fusion, entrance of the LV into the cell and successful transduction.

Another potential limitation for *in vivo* CAR T cell generation is a pre-activated immune system that can further restrict lentiviral vector mediated gene transfer. In this thesis, a noteworthy observation was made for two mice with elevated IFN-α or IFN-β levels prior vector application, likely induced by a preexisting viral infection (Figure 47). Interestingly, in these mice the high type I interferon level correlated with poor *in vivo* CAR T cell generation. This is in line with studies showing that type I IFN responses can limit viral infection (188), but as well *in vivo gfp* gene delivery by VSV-LV in syngeneic mouse models (189). They also showed that this is originated from plasmacytoid DCs (189), which can also develop in the human compartment in huSGM3 mice (190). In addition, Brown and colleagues (189) demonstrated that *in vivo* gene delivery can be improved in mice incapable to respond towards IFN-α.

In conclusion, human innate immune cells present a serious hurdle for *in vivo* CAR T cell generation. Being aware of its implications will make further advancing of this approach to the clinical phase more likely.

4 Material and Methods

4.1 Materials

Detailed information to chemicals, reagents, instruments and softwares used in this thesis are given below.

4.1.1 Chemical and Reagents

Name	Supplier
10X TAE buffer	Paul-Ehrlich-Institut
2-log DNA Ladder	New England Biolabs (NEB)
4 µm CountBright Plus Absolute Counting Beads	Thermo Fisher Scientific
4Cell® Nutri-T	Sartorius
Agarose	Biozym
Ammoniumchloride (0.86%)	Paul-Ehrlich-Institut
Ampicillin	Roche
BD PharmLyseTM	BD Biosciences
Bovine serum albumin (BSA)	Sigma-Aldrich
Bromophenol blue	Merck Millipore
CFSE	Thermo Fisher Scientific
Cut Smart buffer	New England Biolabs
Dimethyl sulfoxide (DMSO), 99.9% p.a.	Sigma-Aldrich
D-luciferin	Perkin Elmer
DNA loading dye, purple (6X)	New England Biolabs
Dulbecco's Modified Eagle Medium (DMEM), high glucose	Biowest
Fc receptor (FcR) blocking reagent, human	Miltenyi Biotec
FcR blocking reagent, murine	Miltenyi Biotec
Fetal bovine serum (FBS)	Biochrom
Formaldehyde	Sigma-Aldrich
GM-CSF (Sargramostim)	Sanofi Aventis
H2O, cell culture grade	Sigma-Aldrich
Histopaque®-1077	Sigma-Aldrich
IL-15, human	Miltenyi Biotec
IL-2, human	Miltenyi Biotec
IL-7, human	Miltenyi Biotec
IL-7, human	Peprotech
Isoflurane CP	CP-Pharma
LB medium	Paul-Ehrlich-Institut

Name	Supplier
L-glutamine (200 mM)	Sigma-Aldrich
Midori Green Direct DNA loading dye	Nippon Genetics
N-2-hydroxyethylpiperazine-N'-2-ethanesulfonic acid (HEPES)	Sigma-Aldrich
PBS, without (w/o) Mg2+/Ca2+	Lonza, Paul-Ehrlich-Institut
Penicillin/streptomycin	Paul-Ehrlich-Institut
Polyethyleneimine, branched, 25 kDa	Sigma-Aldrich
RPMI 1640	Biowest
Sodium azide (NaN3) solution, 10% in cell-culture grade H2O	Paul-Ehrlich-Institut
Sodium pyruvate	Gibco
Sucrose	Sigma-Aldrich
Trypan blue	Sigma-Aldrich
UltraComp eBeads™ compensation beads	Thermo Fisher Scientific

4.1.2 Kits

Kits	Company
Anti-APC MicroBeads	Miltenyi Biotec
Anti-FITC MicroBeads	Miltenyi Biotec
CellTraceTM Violet Cell Proliferation Kit	Thermo Fisher Scientific
Customized LEGENDplex™ Multiplex Assay Kit	BioLegend
DNeasy® Blood and Tissue Kit	Qiagen
Fixable Viability Dye, eFluor™ 780	Thermo Fisher Scientific
GeneJET Gel Extraction Kit	Thermo Fisher Scientific
GeneJET Plasmid Miniprep Kit	Thermo Fisher Scientific
LightCycler® 480 Probes Master, 2X	Roche
Liver Dissociation Kit, mouse	Miltenyi Biotec
Lung Dissociation Kit, mouse	Miltenyi Biotec
NucelobondTM XtraMidi Kit	Macherey Nagel
Pan T Cell Isolation Kit, human	Miltenyi Biotec

4.1.3 Cytokine panels

Customized LEGENDplex™ Multiplex Assay Kits from BioLegend

Species reactivity	Panel	Cytokines
Anti-human	Panel 1	IL-1β, IL-1α, IL-2, IP-10, MCP-1, IL-10, MIP-1α, IL-17A, IL-6, GM-CSF, IL-15, IFN-γ, TNF-α
	Panel 2	IL-1β, IL-2, IP-10, IL-10, MIP-1α, IL-17A, IL-6, GM-CSF, IL-15, IFN-γ, TNF-α, IFN-α2, IFN-β
	Panel 3	IL-1β, IL-2, IL-10, IL-6, GM-CSF, IL-15, IFN-γ, TNF-α, IFN-α2, IFN-β
Anti-mouse	Panel 4	IL-1β, IL-1α, MCP-1, IL-17A, IL-6, GM-CSF, TNF-α, G-CSF, CXCL1, IL-4, CCL3, CCL4, CXCL5

4.1.4 Buffer and solution

Name	Formulation
Blocking solution	2% BSA in PBS w/o Mg^{2+}/Ca^{2+}
FACS fix solution	1% formaldehyde in PBS w/o Mg^{2+}/Ca^{2+}
FACS wash buffer	2% FBS, 0.1% NaN_3 in PBS w/o Mg^{2+}/Ca^{2+}
LB medium	1% tryptone, 0.5% yeast extract, 1% NaCl in H2O, pH 7.2
PBS/Ethylenediaminetetraacetic acid (EDTA)	2 mM EDTA in PBS w/o Mg^{2+}/Ca^{2+}
SOC medium	1% tryptone, 0.5% yeast extract, 1% NaCl, 2.5 mM KCl, 10 mM $MgCl_2$, 10 mM $MgSO_4$, 20 mM glucose in dH2O
Sucrose solution	20% (w/v) sucrose in PBS w/o Mg^{2+}/Ca^{2+}
TAE buffer	40 mM Tris, 20 mM acetic acid, 1 mM $EDTANa_2$ in dH2O
TE buffer	10 mM Tris-HCl, 1 mM EDTA in dH2O
Transfection reagent	18 mM branched polyethyleneimine in H2O
Trypsin working solution	0.25% Trypsin in PBS/EDTA

4.1.5 Cell culture media

Name	Formulation
DMEM complete	DMEM supplemented with 10% FBS, 2mM L-glutamine
RPMI complete	RPMI 1640 supplemented with 10% FBS, 2mM L-glutamine
Freezing medium	10% DMSO, 90% FBS
TCM	RPMI complete supplemented with 25 mM HEPES, 0.4% penicillin/streptomycin

Name	Formulation
4Nutri+	4Cell® Nutri-T supplemented with 0.4% penicillin/streptomycin
Jurkat medium	RPMI complete supplemented with 1 mM sodium pyruvate, 1 mM NEAA

4.1.6 Consumables

Name	Supplier
1.4 ml tubes	Micronic
500 ml Rapid-Flow Bottle Top Filters, 0.45 µm SFCE	Thermo Fisher Scientific
BD Falcon Round Bottom Tubes, 5 ml	BD Biosciences
BD Microtainer® Blood Collection Tubes, Lithium Heparin	BD Biosciences
Cell culture dishes, ⌀ 15 cm	VWR
Cell strainer, 70 µm	Corning
CellStar® conical centrifuge tubes, 15 ml and 50 ml	Greiner Bio-One
Centrifuge tubes, 225 ml	VWR
Cryovials, 2 ml	Greiner Bio-One
Frame Star 96 well plate, Roche style	4titude
Insulin syringes, U-100; 0.33 mm (29G) × 12.7 mm	BD Biosciences
Micro-centrifuge tubes, 1.5 ml	Eppendorf
MS, LS columns	Miltenyi Biotec
Pasteur pipetes, glass, 14.6 cm	VWR
PCR tubes, 0.2 ml	Eppendorf
Petri dishes, ⌀ 10 cm	Greiner Bio-One
Pipet tips, filtered (10 µl, 100 µl, 300 µl, 1000 µl)	Biozym
Serological pipets (5 ml, 10 ml, 25 ml)	Greiner Bio-One
Sterian cannulas (24G, 30G)	B. Braun
Syringe filters, Minisart, PTFE (0.45 µm, 0.2 µm)	Sartorius
Tissue culture flasks (T25, T75, T125)	Greiner Bio-One
Tissue culture plates (6-, 12-, 24-, 48-, 96-well)	Thermo Fisher Scientific

4.1.7 Antibodies

Species specificity	Marker	Fluorophore	Clone	Dilution	Supplier
Anti-human	Anti-CD14	PerCp	TÜK4	1:100	Miltenyi Biotec
	Anti-CD14	APC	REA599	1:200	Miltenyi Biotec
	Anti-CD19	PE-Vio770	LT19	1:200	Miltenyi Biotec
	Anti-CD19	AlexaFluor700	HIB19	1:100	Thermo Fisher Sceintific
	Anti-CD206	BV421	DCN228	1:100	Miltenyi Biotec
	Anti-CD209	PE	REA617	1:100	Miltenyi Biotec

Species specificity	Marker	Fluorophore	Clone	Dilution	Supplier
	Anti-CD28	unlabeled	15E8	1:33	Miltenyi Biotec
	Anti-CD3	BV605	HIT3a	1:200	BD Bioscience
	Anti-CD3	PerCp	BW264/56	1:200	Miltenyi Biotec
	Anti-CD3	FITC	BW264/56	1:200	Miltenyi Biotec
	Anti-CD3	unlabeled	OKT3	1:100	Miltenyi Biotec
	Anti-CD4	FITC	VIT-4	1:200	Miltenyi Biotec
	Anti-CD4	Vioblue	VIT4	1:200	Miltenyi Biotec
	Anti-CD4	PerCp	VIT-4	1:200	Miltenyi Biotec
	Anti-CD4	PE-CF594	RPA-T4	1:100	BD Bioscience
	Anti-CD45	BV510	2D1	1:200	Biolegend
	Anti-CD47	FITC	REA220	1:200	Miltenyi Biotec
	Anti-CD8	BV786	RPA-T8	1:200	BD Bioscience
	Anti-CD8	FITC	BW135/80	1:200	Miltenyi Biotec
	Anti-CD8	APC	BW135/80	1:200	Miltenyi Biotec
	Anti-myc	PE	9B11	1:100	Cell Signalling
	Anti-myc	FITC	SH1-26E7.1.3	1:200	Miltenyi Biotec
	Anti-PD-1	PE-Vio770	PD1.3.1.3	1:100	Miltenyi Biotec
	Anti-β2M	APC	2M2	1:1000	Biolegend
Anti-Mouse	Anti-CD11b	FITC	M1/70	1:100	Biolegend
	Anti-CD11c	PE	N418	1:100	eBioscience
	Anti-CD19	BV605	1D3	1:100	BD Bioscience
	Anti-CD3	BV421	17A2	1:100	BD Bioscience
	Anti-CD4	Alexa Fluor700	RM4-5	1:100	BD Bioscience
	Anti-CD8a	PerCP-Cy5.5	53-6.7	1:100	BD Bioscience
	Anti-IgG	AlexaFluor647	polyclonal	1:200	Jackson ImmunoResearch
	Anti-Ly-6C	APC	1G7.G10	1:100	Miltenyi Biotec
	Anti-Ly-6G	PE-Vio770	REA526	1:100	Miltenyi Biotec
Undefined	Anti-VSV-G	Unlabeled	8G5F11	1:1000	Kerafast

4.1.8 Plasmids

Plasmid number	Name	Description	Reference
P1.01-01	pCMVΔR8.9	HIV-1 packaging plasmid	U. Blömer (191)
P4.04-01	pCG-Fnse-Δ30	Encodes MV-FnseΔ30	(121)

Plasmid number	Name	Description	Reference
P1.07-01	pMD2.G	Encodes the glycoprotein G of VSV	D. Trono
P4.09-01	pCAGGS-NiVFcΔ22	Encodes NiV-FcΔ22	(122)
P2.01-21	pS-CD19CAR.28BBz-W	HIV-1 transfer vector encoding the CD19-CAR with intracellular CD28 and 4-1BB costimulatory domain	This thesis
P2.01-28	pS-CD19CAR.BBz-W	HIV-1 transfer vector encoding the CD19-CAR with intracellular 4-1BB costimulatory domain	This thesis
P4.07-02	pCAGGS-NiVGcΔ34CD8mut4	Encodes NiV-GcΔ34 fused to the antihuman CD8-specific scFv OKT8 humVh1	(122)
P4.01-04	pHnse-DARPin.CD4.29.2	Encodes MV H Δ18 mutated fused to the CD4 specific DARPin 29.2 via (G4S)3 linker	(130)
P2.01-06	pS-CD19CAR.28z-W	HIV-1 transfer vector encoding the CD19-CAR with intracellular CD28 costimulatory domain	W. Wels (192)
P2.01-12	pS-Albumin-W	HIV-1 transfer vector encoding WPRE and human albumin gene	F. Thalheimer, Paul-Ehrlich-Institut

4.1.9 Oligonucleotide primers

Primer number	Name	Sequence (5' – 3')
1067	WPRE rev	GGC ATT AAA GCA GCG TAT CC
1108	3rd generation CAR CD28,4-1BB	TAG ACC TCC TAC CCC AGC C
1118	SIN rev	GAT ATA GGC GCC AGC AAC
2461	4-1BB forw. (AgeI)	ACG CCT ACC GGT CCA AGC GGG GCA GAA AGA AG
2462	4-1BB rev. (SbfI)	TTA CGC CCT GCA GGT TAT CTA GGT GGC AG
4001	Probe-albumin	[6FAM]-ACG TGA GGA GTA TTT CAT TAC TGC ATG TGT-[BHQ1]
4002	hAlb fwd	CAC ACT TTC TGA GAA GGA GAG AC
4003	hAlb rev	GCT TGA ATT GAC AGT TCT TGC TAT
4020S	WPRE for	CAC CAC CTG TCA GCT CCT TT
4021S	WPRE rev	GGA CGA TGA TTT CCC CGA CA
5007	Probe-WPRE	[Cy5]-CGC CGC CTG CCT TGC CCG CT-[BHQ2]

4.1.10 Enzymes and growth factors

Name	Company
Antarctic Phosphatase	New England Biolabs
GM-CSF (sargramostim)	Sanofi-Aventis
Human IL-15, research grade	Miltenyi Biotec
Human IL-2, premium grade	Miltenyi Biotec
Human IL-7	Peprotech
Human IL-7, premium grade	Miltenyi Biotec
Phusion HF polymerase	New England Biolabs
Restriction endonucleases	New England Biolabs
T4 Ligase	Thermo Fisher Scientific
Trypsin (Melnick, 2.5% solution)	Paul-Ehrlich-Institut

4.1.11 Cell lines and bacteria

Name	Description	Culture medium	Source
A301	Human T lymphoblast cell line, human CD4+	RPMI complete	A. Pfeiffer, Paul-Ehrlich-Institut
E. coli, Top10	Highly transformable laboratory strain of *Escherichia coli* (*E. coli*)	LB medium	Life technologies
HEK-293T	Human embryonic kidney cell line, transformed to express the SV40 large T antigen	DMEM complete	ATCC, CCL-11268
J76S8ab	Human T lymphoblast cell line genetically engineered to express human CD8ab	Jurkat medium	Inan Edes, Georg Speyer Haus, Frankfurt am Main
Nalm-6 EBFP-luc	Human adult acute B cell lymphoblastic leukemia cell line, genetically engineered to express eBFP and firefly luciferase	RPMI complete	Fielding lab, University College London
Raji	Human B lymphoblast cell line	RPMI complete	ATCC CCL-86

Name	Description	Culture medium	Source
ß2M$^{-/-}$, CD47^{high} HEK-293T	HEK-293T cells modified with knockout for ß2 microglobulin and overexpression of human CD47	DMEM complete	M. Milani and A. Cantore, IRCCS San Raffaele Scientific Institute, Italy

4.1.12 Instruments

Name	Company
Cell incubator BBD6220	Heraeus, Thermo Fisher Scientific
Centrifuge multifuge X3	Heraeus, Thermo Fisher Scientific
Freezer (-20°C, -80°C)	New Brenswick, Liebherr, Thermo Fisher Scientific
Fridge	AEG
Gel documentation imager	Intas
Gel tray	Paul-Ehrlich-Institut
Incubator shaker thermomixer comfort	Eppendorf
Infrared thermometer Contact Free 4	Aponorm
IVIS® Imaging System	Perkin Elmer
LSR Fortessa™ flow cytometer	BD Biosciences
MACS Quant Analyzer 10 flow cytometer	Miltenyi Biotec
MicroChemi 4.2	DNR
Micropipets research plus®	Eppendorf
Microwave	Sharp
Mini-Protean® 3	Bio-Rad
Mr. Frosty™ Freezing container	Nalgene
Multichannel pipets	Thermo Fisher Scientific
NanoSight™ NS300	Malvern Pananalytic
Nitrogen tank Chronos, Apollo	Messer
Orbital shaker	Celltron
Pipetbox Accu-jet	Brand
Pump Vacusafe	Integra
Semi-Dry blotting system Trans-Blot® SD	Bio-Rad
Spectrophotometer NanoDrop 2000c	Thermo Fisher Scientific
Table centrifuge	Heraeus
Table-top shaker Biometra® WT12	Biometra
Vortex Mixer Vortex Genie® 2	Scientific Industries
XGI-8 Gas Anesthesia system	Perkin Elmer

4.1.13 Software

Name	Company
Citavi 6	Swiss Academic Software
FACSDiva™, Version 8.0	BD Biosciences
FCS Express, Version 6	De Novo Software
FlowJo, Version 10	FlowJo LLC
GraphPad Prism 8	GraphPad Software
Intas Gel Doc	Intas
LEGENDplex™ Data Analysis Software Version 8	BioLegend
LightCycler® Software 4.1	Roche
Living Image	Perkin Elmer
Microsoft Office 2016, 365	Microsoft
NTA, version 3.3	Malvern Pananalytic
SnapGene 4.0.6	SnapGene

4.2 Molecular biology methods

4.2.1 Transformation of chemically competent bacteria

For transformation of chemically competent *E. coli* Top 10 bacteria with freshly ligated plasmids, 10 µL of ligation product were incubated with 100 µL of bacteria suspension on ice for 20 min. Then a heat shock was performed at 42°C for 1 min with subsequent resting on ice for 3 min. Afterwards 900 µL of S.O.C. medium was added to the bacteria and shaked at 600 rpm and 37°C for 1 h. For retransformation of purified plasmids, 100 µL competent bacteria were mixed with 1 µg of plasmid DNA, incubated on ice for 1 min and heat shock was performed at 37°C for 5 min with subsequent resting on ice for 3min. Then 50 – 100 µL of transformed bacteria were plated on LB agar plates supplemented with ampicillin and incubated overnight at 37°C. The next day clones were directly picked to inoculate 4 mL or 200 mL LB medium containing 100 µg/mL ampicillin and incubated at 37°C and 180 rpm shaking overnight. Otherwise, plates were stored at 4°C up to one month for later processing.

4.2.2 Plasmid DNA preparation

For plasmid DNA purification from overnight culture of transformed *E. coli* bacteria, the GeneJet® Mini Prep Kit (Thermo Fisher Scientific) or the NucleoBond® Xtra Midi Kit (Macherey Nagel) was used according to manufacturer's protocol. The DNA was eluted in TE buffer and concentration and quality of the plasmid was measured by UV/Vis spectroscopy using the NanoDrop 2000 spectrophotometer.

4.2.3 Restriction digest of DNA

Restriction digest of DNA was performed for verification of correct plasmid identity after purification (analytical digest) or for subsequent cloning work (preparative digest). Appropriated restriction enzymes and their optimal reaction conditions were used according to New England Biolabs instructions with exemplary reactions shown in table 4. Analytical digestions were carried out for at least 1 h at 37°C, while preparative digestions were performed for at least 4 h at 37°C. Afterwards, DNA fragments were separated by agarose gel electrophoresis or stored at -20°C until further use.

Table 4: Standard DNA restriction reactions

Component	Analytical digest	Preparative digest
DNA	1 µg	1 – 5 µg
Restriction buffer	2 µL	5 µL
Restriction enzymes	5 – 20 units	10 – 30 units
Fill up with H_2O	20 µL	50 µL

4.2.4 Agarose gel electrophoresis

Agarose gel electrophoresis was performed to separated DNA fragments after DNA restriction. Gels were prepared by dissolving 1% (w/v) agarose in heated TAE buffer and subsequent cooling down to RT. Samples and a reference lane with 6 µL of 2log ladder marker (NEB) was loaded into the gel pockets. To visualize samples during the electrophoresis run and DNA bands later under UV light, purple DNA loading dye (NEB) and 0.5 µL of Midori Green (Nippon Genetics) were added to the DNA samples prior gel loading. Gels were run at 100 – 120 V for 1 – 2 h in a Wide Mini Sub-Cell® GT chamber (Bio-Rad). Afterwards, separated DNA fragments were visualized by UV and LED light on a FastGene Blue-Green LED Illuminator table and photographed. For extraction of DNA fragments the respective band was cut out with a scalpel, stored in 1.5 mL reaction tube for further processing.

4.2.5 DNA isolation from agarose gel

Excised gel containing the DNA fragment of interest was isolated using the GeneJet® Gel Extraction Kit (Thermo Fisher Scientific) according to the manufacturer's protocol. Purified DNA was eluted in kit's elution buffer and concentration and quality was measured by UV/Vis spectroscopy using the NanoDrop 2000 spectrophotometer.

4.2.6 DNA dephosphorylation and ligation

Linearized DNA with compatible ends was dephosphorylated prior to ligation to avoid ligation of the same fragment. For this purpose, 0.5 – 5 µg of DNA was incubated with 5 U Antarctic phosphatase (NEB) in Antarctic phosphatase buffer and incubated at 37°C for 1 h. The enzyme was heat inactivated at 80°C for 2 min prior ligation. For ligation the Standard T4 DNA ligase enzyme was used. Reaction was performed with 3 times excess of insert DNA over backbone DNA (Table 5) and the amount of insert DNA used was calculated based on the following formula:

$$\text{Inser (ng)} = \frac{\text{molar ratio} \times \text{ backbone (ng)} \times \text{insert length (bp)}}{\text{backbone length (bp)}}$$

Ligation was carried out at 22°C for 1 h and inactivation of the enzyme was performed by heat inactivation at 65°C for 10 min. Ligation reaction was used for subsequent transformation of chemically competent bacteria (chapter 4.2.1).

Table 5: Ligation reaction

Component	Amount
Insert DNA	See formula calculation
Backbone DNA	20 – 50 ng
T4 ligation buffer	2 µL
T4 DNA ligase	0.5 µL
Fill up with H_2O	20 µL

4.2.7 DNA sequencing

To confirm correct DNA sequence after molecular cloning, DNA Sanger sequencing was carried out with GATC Services Eurofins Genomics according to the company's guidelines. After evaluation using SnapGene, correct sequences were used further work.

4.2.8 Isolation of genomic DNA

Genomic DNA was isolated from frozen cell pellets of mouse organs, which were stored at -80°C, using DNeasy® Blood and Tissue Kit according to the manufacturer's protocol. Following elution in 50 – 100 µL elution buffer, the concentration and purity of the genomic DNA was determined by UV/Vis spectroscopy using the NanoDrop 2000 spectrophotometer.

4.2.9 Polymerase chain reaction

Amplification of DNA fragments for subsequent molecular cloning was performed by polymerase chain reaction (PCR) with Phusion HF polymerase (NEB) and sequence-specific primers with extended sequences to introduce restriction sites into the DNA amplicons. PCR was performed with the reaction mix as outlined in table 6 and the cycle condition (1x 98°C for 30 sec; 25 cycles of [98°C for 10 sec, then 60°C for 15 sec and 72°C for 30 sec] afterwards at 72°C for 60 sec and then kept cool at 4°C) in a PCR thermal cycler (Bio-Rad). PCR product was analyzed by agarose gel electrophoresis (chapter 4.2.4) and purified as described in chapter 4.2.5.

Table 6: PCR reaction and cycle conditions

Component	Amount
Plasmid DNA template	5 – 10 ng
Primer fwd (10 µM)	2.5 µL
Primer rev (10 µM)	2.5 µL
dNTPs (10 mM)	1 µL
$MgCl_2$ (50 mM)	2.5 µL
5x Pusion HF buffer	10 µL
Phusion HF Polymerase (2 U/µL)	0.5 µL
Fill up with H_2O	50 µL

4.2.10 Quantitative polymerase chain reaction

To detect and quantify specific DNA sequences a TaqMan-based qPCR assay was performed with the LightCycler® 480 Probes Master and measured at the LightCycler 480 Instrument II (Roche). It allows the quantitative assessment of the target sequence during sequence amplification by using fluorescently labeled complementary target sequence probes in real time. Thereby transgene integration number per genome copy can be determined. Transgene integrates were identified by (WPRE)-specific primer and primer for human albumin served as internal reference. WPRE and human albumin were simultaneously measured from one well in technical duplicates as well for the standard using the plasmid pS-Albumin-W. Reaction setup is shown in table 7 with the PCR condition (1x 95°C for 5 min; 45 cycles of [95°C for 10 sec and 60°C for 40 sec] and the kept cool at 4°C). A linear standard curve was used to calculate the amount of

human cells (albumin) and vector integration (WPRE). The VCN was then calculated as a ratio (copies WPRE/ copies albumin) for human cells carrying the WPRE. For standardization purposes, all qPCR measurements in this thesis were performed by experienced technical staff.

Table 7: Quantitative polymerase chain reaction setup

Component	Amount
Genomic DNA	50 – 100 ng
WPRE fwd	0.2 µM
WPRE rev	0.2 µM
WPRE probe	0.2 µM
Human albumin fwd	0.2 µM
Human albumin rev	0.2 µM
Human albumin probe	0.2 µM
LightCycler® 480 Probes Master	1x

4.3 Cell culture work

All cell culture work was performed under sterile condition inside a safety work bench with laminal flow. All cells were cultivated at 37°C, 5% CO_2 and 90% humidity.

4.3.1 Freezing and thawing of cells

For cryopreservation of cells, respective cell numbers were centrifuged at 300 x g for 5 min. Cell pellets were resuspended in cold freezing medium and aliquoted at 1 mL in cryovials and frozen in MR. Frosty™ container (Thermo Fisher Scientific) at -80°C. After 24 h cryovials were transferred to the gas phase of liquid nitrogen for long term storage.

For thawing of cryopreserved cells, vials were incubated at 37°C in a water bath until half of the content was thawed. Remaining frozen cells were thawed by slowly adding pre-warmed RPMI complete to the cryovials. Cells were washed two times with 10 mL RPMI complete at 300 x g for 5 min to remove freezing medium and used for subsequent experiments or cell cultivation.

4.3.2 Cell lines

Suspension cell lines were cultivated vertically in T25 or T75 flasks with 10 mL or 30 mL of the respective cell culture medium and splitted every 3 – 4 days to maintain a cell density between 1 x 10^5 – 2 x 10^6 cells/mL. Adherent HEK-293T or ß2M$^{-/-}$, CD47^{high} HEK-293T cell lines were cultivated horizontally in T175 flasks in 20 – 30 mL DMEM complete medium and kept at confluence between 20% – 90%. For splitting, HEK-293T or ß2M$^{-/-}$, CD47^{high} HEK-293T cells were washed once with 10 mL PBS and detached by incubation in 3 mL trypsin solution for 3 – 5 min at RT and gentle shaking. Trypsinization process was stopped by addition of 7 mL DMEM complete and cell suspension was further diluted in medium and seeded at the respective cell density.

4.3.3 Lentiviral vector production

For lentiviral vector production 2.2 – 2.5 x10^7 HEK-293T cells or ß2M$^{-/-}$, CD47^{high} HEK-293T cells were seeded into T175 flask or 15cm dishes in 18 – 20 mL DMEM complete and co-transfected with vector production plasmids via polyethyleneimine (PEI). On day of plasmid transfection, medium of the cells were replaced by 10 mL DMEM complete supplemented with additional 5% FBS. Transfection plasmids were mixed in 2.3 mL DMEM without additive and added subsequently to 2.2 mL DMEM without additive containing 140 µL PEI. Plasmid-PEI mixture was mixed thoroughly, incubated for 10 min at RT and added to the producer cells. For T cell targeted vector production HEK cells were co-transfected with 14.4 µg of packaging plasmid pCMVdR8.9, 15.1 µg of transfer plasmid (pSEW-mycCD19.CAR(28z) or pSEW-mycCD19.CAR(BBz) or pSEW-mycCD19.CAR(28,BBz)) and 0.93 µg pHnseDARPin.CD4.29.2, 4.63 µg pCG-Fnse-Δ30 as envelope plasmids for CD4-LVs, or 0.9 µg of pCAGGS-NiV-GΔ34mut4x-L3scFvCD8Vh1, 4.49 µg pCAGGS-NiV-FΔ22 as envelope plasmids for CD8-LVs into 2.5 x 10^7 HEK-293T cells or in ß2M$^{-/-}$, CD47^{high} HEK-293T cells. For the production of VSV-G-LV, 17.5 µg of packaging plasmid pCMVdR8.9, 11.4 µg of transfer plasmid (pSEW-mycCD19.CAR(28z) or pSEW-mycCD19.CAR(BBz) or pSEW-mycCD19.CAR(28,BBz)) and 6.1 µg of envelope plasmid pMDG-2 were used for co-transfection. 6 – 16 h later the transfection mix was replaced by 20 mL DMEM complete and cells were cultivated until 48 h. On day two after transfection the cell supernatant, containing released viral vector particles, was harvested, filtered through a 0.45 µm filter and concentrated by centrifugation at 4500 rpm, 4°C for 24 h through a 20% sucrose cushion. Afterwards, the supernatant was discarded and the pellet

resuspended in 60 µL PBS, resulting in an approximately 300 fold concentrated vector stock. The vector stock was then frozen at -80°C until further use.

Conventional LVs were produced in HEK-293T cells. Phagocytosis shielded LVs (LV^{sh}) were generated in ß2M$^{-/-}$, CD47^{high} HEK-293T cells, which are not expressing MHC-I but overexpressing human CD47. These modified cells were kindly provided by Michela Milani and Alessio Cantore (San Raffaele Telethon Institute for Gene Therapy, IRCCS San Raffaele Scientific Institute, Italy) and are described by (149).

4.3.4 PBMC isolation

PBMC were isolated from buffy coats from anonymous healthy donors purchased from the German Red Cross blood donation center (DRK-Blutspendedienst Hessen, Frankfurt). Blood was diluted 1:1 in PBS to 100mL and 25mL of the pre-mixed blood was layered slowly on top of 15 mL Histopaque®-1077 inside of 50 mL tubes and centrifuged in a swinging bucket rotor at 1800 rpm for 30 min without brake. Afterwards, the PBMC containing layer between the Histopaque® 1077 and the plasma layer of each tube was harvested, pooled and washed once at 300 x g for 10 min. To remove platelets, PBMC were centrifuged at 200 x g for 10 min. Subsequently, remaining erythrocytes were lysed by incubating the cells in 10 mL of 0.86% ammonium chloride solution at 37°C for 10 min. Afterwards, PBMC were washed twice with PBS at 300 x g for 10 min, counted and were used for subsequent experiments or cryopreserved.

4.3.5 PAN T cell isolation

For the isolation of pure human T cells out of freshly isolated or frozen PBMC, the human Pan T Cell Isolation Kit (Miltenyi Biotec) was used. Isolation was performed according to manufactures protocol and isolation purity was afterwards confirmed by anti-human CD3 staining and flow cytometry analysis. Isolated T cells were directly used for further experiments or cryopreserved.

4.3.6 Monocyte isolation

Primary monocytes were isolated from human PBMC by positive selection of CD14 positive cells using an APC conjugated anti- human CD14 antibody in combination with an anti-APC MicroBeads kit (Miltenyi Biotec). PBMC were washed once with MACS buffer before 1 x 10^7 PBMC were labeled with 10 µL of the primary antibody and manufactures protocol was followed. Purity of isolated monocytes was determined by anti-human CD14 staining and flow cytometry analysis. Isolated monocytes were then

directly used for macrophage polarization or supplementation in CAR T cell killing assay.

4.3.7 *In vitro* Macrophage polarization

For Macrophage polarization, 3 – 4 x10^6 isolated monocytes were seeded in a 6-well cell culture plate with 2.5 mL TCM supplemented with 50 ng/mL GM-CSF (Sanofi-Aventis) for 5 – 6 days and a GM-CSF supplemented medium addition of 1mL on day 3. Polarized macrophages were harvested by 10 minutes incubation on ice and subsequent careful scrapping using a cell scrapper.

4.3.8 Primary cells

Primary cells were all cultivated in medium containing 0.5% penicillin and streptomycin. Human PBMC or purified human T cells were cultivated either in TCM or in 4Nutri supplemented with human 50 U/mL IL-2 (Miltenyi Biotec) or 25 U/mL IL-7 (Miltenyi Biotec) and 50 U/mL IL-15 (Miltenyi Biotec).

4.3.9 T cell activation

24-well or 6-well cell culture plates were coated with 0.5 mL or 1 mL per well of 1 µg/mL activating anti-human CD3 antibody (Miltenyi Biotec) in PBS overnight at 4°C or for 2h at 37°C. Plates were subsequently blocked for at least 30 minutes at 37°C with 2% BSA in PBS and washed twice with 1 – 2 mL PBS before. Unless otherwise stated, 2 x 10^6 or 1 x 10^7 of PBMC or T cells were cultivated for 3 days in the prepared plate in 2 mL or 6 mL TCM or 4Nutri medium supplemented with 3 µg/mL activating anti-human CD28 antibody (Miltenyi Biotec) and in addition with either human 50 U/mL IL-2 (Miltenyi Biotec) or 25 U/mL IL-7 (Miltenyi Biotec) and 50 U/mL IL-15 (Miltenyi Biotec). Afterwards, activated cells were harvested for subsequent experiments.

4.3.10 Cell line transduction

Transduction of cell lines was performed at a cell density of 4 x10^4 cells in a flat-bottom 96-well plate by addition of the respective vector dosage in 200 µL of the respective medium and subsequent cultivation for 3 days.

4.3.11 T cell transduction

For T cell transduction, 8x10^4 activated PBMC or T cells were seeded in a flat-bottom 96-well plate with the respective vector dosage in 100 µL of cytokine supplemented medium. Vector cell suspension was then centrifuged at 850 xg, 32°C for 90 minutes

with a subsequent addition of cytokine supplemented medium to 200 µL and further cultivation for 3 days.

4.3.12 Short-term CAR T cell generation

PBMC were activated in 4Nutri medium as described in the “T cell activation” section, but for 48h and afterwards seeded in flat-bottom 96-well plates at a density of 8 x10^4 cell per well. Cells were then incubated with 0.5µL of VSV-LV stock in 200 µL IL-7 and IL-15 supplemented 4Nutri medium for 24h.The resulting short-term generated CAR T cells were defined as vector particle positive and CAR positive cells by flow-cytometry and harvested for experiments. As a control activated PBMC were cultivated in absence of vector particles.

4.3.13 Gene transfer activity assessment of lentiviral vector stocks

Gene transfer activity of the vector stocks was determined by serial dilution and transduction of 8 x 10^4 activated PBMC or 4 x 10^4 A301 (CD4+) and J76S8ab (CD8+) cell line as described in chapter 4.3.10 and 4.3.11. Transducing units (t.u.) were calculated based on the linear range of the gene transfer activity after three days in the CD4+ (CD4-LV) or CD8+ (CD8-LV) cell population determined by flow cytometry analysis.

4.3.14 T cell transduction in presence of human myeloid cells

Activated T cells were seeded at 8 x 10^4 cell density together with 8 x 10^4 (50%), 9 x 10^3 (10%), 3.2 x 10^3 (4%) or no (0%) donor matched monocytes or *in vitro* polarized macrophages in 200µL TCM supplemented with human 25 U/mL IL-7 and 50 U/mL IL-15 inside a flat bottom 96-well plate. CD4-LV or CD8-LV were added to the co-culture, centrifuged at 850 x g and 32°C for 90 min and cultivated for 3 days. Experiment comparing different monocyte and macrophage ratios was performed with 2 – 5 µL vector stock, while the comparison experiment of shielded and non-shielded vectors was carried out with identical vector particle numbers in this assay using 2.1 x10^9 – 3.6 x10^9 particles per condition. Transduction efficiency was determined on CD3+ cells normalized to T cell condition transduced in the absence of monocytes or macrophages to account for donor dependent transduction variability.

4.3.15 Continuous Killing Assay

To evaluate long-term cytotoxicity of different CAR co-stimulatory domains continuous killing assay was performed with CAR T cells generated by 3 days transduction with

VSV-LV, CD4-LV or CD8-LV. Killing assay was started with 1 x 10^4 CAR positive T cells co-cultured at a 1:1 (Effector:Target) ratio with 1x10^4 CellTrace® Violet (CTV) labeled CD19+ Nalm6 cells according to manufacturer's protocol. Co-culture was performed in a flat bottom 96-well plate with 200 µL 4Nutri without cytokine supplementation. CAR T cell level prior killing assay was normalized between different CAR construct condition. Due to the higher transduction efficiency of VSV-LV than T cell targeted LV, conditions were normalized within the VSV-LV group only and within CD4-LV and CD8-LV group by addition of not transduced T cells. To determine CAR unrelated killing not transduced T cells were used as negative control. On day 1, 3 and 5 after co-culture start 2-fold increasing CTV labeled Nalm6 cells (2x10^4, 4x10^4, 8x10^4 on the respective day) were added to the culture. To assess killing activity on different time points, killing assay was performed as replica on multiple plates, which were analyzed on the respective day (day 1, 3, 5 and 7) after killing assay start. To ensure robustness of this assay each condition on each plate was performed in technical triplicates. Cytotoxicity was determined as percentage of viable cells within CTV positive cells and CAR T cell level and PD1 expression were assessed within the CTV negative and CD3+ population by flow-cytometry.

4.3.16 Monocyte supplemented cytotoxicity assay

5 x 10^4 short-term CAR T cells positive for either VSV-G or CAR were co-cultured with 1x10^4 CTV labeled CD19+ Nalm6 cells in 200 µL 4Nutri inside a flat bottom 96-well plate. In addition, co-culture was further supplemented with 5 x 10^3 or no freshly isolated autologous monocytes. 24h – 26h later supernatant was taken, centrifuged at 300xg for 5 min, and transferred into a v bottom 96-well plate and stored at -20°C until cytokine measurement. Cytotoxicity was determined as percentage of viable cells within CTV positive cells and CAR T cell level was assessed within the CTV negative and CD3+ population by flow cytometry.

4.3.17 Cytokine assay

Frozen cell culture supernatant or frozen plasma samples were analyzed with a customized multiplex human or mouse cytokine customized LEGENDplex™ multiplex assay kit (BioLegend) according to manufactures protocol. Samples were measured at the MACS Quant Analyzer10 (Miltenyi Biotec) and analyzed with the Legendplex software (v.8.0) (BioLegend).

4.3.18 Flow cytometry staining

Approximately 1– 5 x 10^5 cells were used for flow-cytometry staining. HEK cells were detached by trypsinization as described in chapter 4.3.2. First, cells were transferred into micronic tubes and washed once by addition of about 1 mL FACS wash buffer and subsequent centrifugation at 350 x g, 4°C for 3 min. Supernatant was removed by using a vacuum pump and leaving approximately 100 µL left in the tube. All subsequent wash steps were performed identically. Primary cells were incubated with 1µL of human FcR block and in case of mouse derived samples also with mouse FcR block reagent for 10 – 15 min at RT. Afterwards, samples were washed once before cells were proceeded with antibody staining for 30 – 40 min at 4°C in the presence of the viability dye efluor780. Finally, cells were washed twice and fixed with 100 µL of FACS fix buffer. Stained samples were stored at 4°C and dark until measurement.

For the vector particle staining against the glycoprotein of VSV, samples were incubated with the primary mouse derived anti-VSV-G antibody for 15 min at 4°C and washed thoroughly twice. Afterwards, cells were stained with secondary AF647 labeled goat derived anti-mouse Fc antibody for additional 15 min at 4°C and subsequently washed three times. This protocol was established by Elham Adabi, a colleague from the group (Molecular Biotechnology and Gene Therapy, Paul-Ehrlich-Institut, Langen). Afterwards, normal antibody staining as described above was performed.

4.3.19 Multi-dimensional reduction analysis

For 2-dimensional visualization of multi-factorial flow cytometry data unsupervised non-linear dimensionality reduction was performed on immunophenotyped splenocytes from huSGM3 and Balb/c mice with the t-distributed Stochastic Neighbor Embedding algorithm (193) integrated in FlowJo V10. First, viable single cells from compensated flow cytometry data of different samples (huSGM3 and Balb/c) were concatenated into one object. The murine markers CD3, CD19, CD11b, CD11c, CD8, CD4, Ly-6G and Ly-6C and the human marker CD45 were selected for the analysis. Default setting of the program was used and the parameter for perplexity was set to 60 to allow sufficient cluster separation. Human cells were identified as human CD45+. Within the murine cells, which were identified as human CD45 negative, T cells were gated on CD3+, B cells on CD19+, lymphoid DCs on CD3-, CD11b-, CD11c+, myeloid DCs on CD11b+, CD11c+, neutrophils on CD3-, CD11b-, Ly6G+, monocytes and

macrophages on CD3-, CD11b-, Ly6G+, Ly6C+ and unidentified cells were determined as other cells.

4.3.20 Nanoparticle tracking analysis

LV stocks were analyzed for particle size and particle concentration by nanoparticle tracking analysis (NTA) at the NanoSight™ NS3000 instrument (Malvern Pananalytic). Concentrated stock was diluted in 0.2 µm filtered PBS to obtain a particle concentration range between 1 x 10^7 and 1 x 10^9 particles/mL suitable for NTA measurement. Dilution was loaded into the flow chamber and measured four times for 60 sec at 25°C using a custom stop-flow protocol and analyzed with the NTA3.3 software.

4.4 Animal work

All animal experiments were performed in accordance with the regulations of the German animal protection law and the respective European Union guidelines. CD34+ cord-blood humanized and non-humanized female NSG-SGM3 (NOD.Cg-Prkdcscid Il2rgtm1Wjl Tg(CMV-IL3,CSF2,KITLG)1Eav/MloySzJ, ID:013,062) mice were purchased from Jackson Laboratory. Humanized NSG-SGM3 mice were acquired 15 – 17 weeks after stem cell engraftment and non-humanized mice 5 – 6 weeks after birth and housed in individually ventilated cages with food and water received ad libitum. Animals were always handled under laminar flow hoods.

4.4.1 *In vivo* CAR T cell generation

4.4.1.1 Cytokine administration

Lyophilized human IL-7 (Peprotech) was reconstituted in water to obtain a concentration of 100 µg/mL and directly used for subsequent dilution or stored at -20°C up to 1 week. For injection IL-7 stock was further diluted in PBS to 2 µg/mL. Each humanized NSG-SGM3 mouse received intravenously (*i.v.*) or subcutaneously (*s.c.*) one dose of 100 µ containing 200 ng IL-7 on day four and one before and day one and three after vector injection. For *i.v.* injection mice were put into a restrainer and mouse tail was warmed using an infrared lamp to dilate vein and IL-7 was injected into the lateral tail vein. For *s.c.* injection mice were restrained and IL-7 was injected under the skin in the neck fold.

4.4.1.2 Vector particle administration

Concentrated LV stocks were thawed on ice and kept at RT until *i.v.* injection. Injection was performed as described in chapter 4.4.1.1. Humanized NSG-SGM3 mice in the

experiment in chapter 2.2.1 received conventionally produced vectors with 2.4 x 10^{11} of CD4-LV, 1.2 or 2 x 10^{11} particles of CD8-LV or 1.6 x 10^{11} CD4-LV and 7.6 x 10^{10} CD8-LV particles (MIX). For the experiment in chapter 2.4.1 8.7 x 10^{10} particles of CD4-LV or CD4-LV^{sh}, 1.4 x 10^{11} particles of CD8-LV or CD8-LV^{sh} were injected. Control mice received PBS instead. For the higher dose group (2x) a 2-times higher vector particle amount of LV^{sh} was administered. General health condition of the animals was assessed regularly by visual monitoring and weight measurement. Data of mice, which had to be sacrificed due to strong, donor related weight loss within the first 8 days after experiment start, was excluded.

4.4.2 CRS model

4.4.2.1 Tumor cell engraftment

EBFP and Luciferase expressing Nalm6 tumor cells were washed twice with 20 mL PBS and centrifugated at 300 x g for 5 min. Subsequently tumor cells were resuspended in appropriate volume of PBS to obtain 1 x 10^7 tumor cells/mL and kept at RT. 1 x 10^6 cells were injected *i.v.* into non-humanized NSG-SGM3 mice as described in chapter 4.4.1.1. Tumor cells were engrafted for 10 days and tumor burden was evaluated at least once per week using *in vivo* imaging system (IVIS). One day before short-term CAR T cells administration, tumor burden was assessed and mice were distributed evenly into two groups based on the tumor signals.

4.4.2.2 *In vivo* Bioluminescence imaging

To assess tumor cell engraftment in the mice the IVIS was used. 150 µg D-luciferin, diluted in PBS per gram body weight, was injected into restrained mice intraperitoneally. 5 min later mice were anesthetized for 5 min with 3% isoflurane. and imaged ventrally and dorsally for 1 sec and 30 sec with the IVIS® Imaging System. Images were analyzed and processed with IVIS® imaging system software.

4.4.2.3 Short-term CAR T cell administration

Short-term CAR T cells were counted, washed twice with 50 mL PBS and kept at RT. 1 x 10^7 vector particle positive and CAR positive short-term CAR T cells, corresponding to 1.4 x 10^7 total cells, or 1.4 x 10^7 T cells, cultivated at the same condition, were injected *i.v.* into the mice as described in chapter 4.4.1.1.

4.4.2.4 General health condition scoring

To assess and score general health condition of the animals, weight loss from experiment start, cage activity and visual appearance were each scored separately from 0 to 3 and added together for the total body score. Healthy mice with no weight loss, active cage activity and healthy appearance were scored with 0. Animals with increasing weight loss (>0%; >5%; >10%), decreasing cage activity (less active; moderate active; barely responsive) and ill-being visual appearance (slightly ruffled fur; ruffled fur with hunched back position; ruffled fur with hunched back position and squinted eyes) were scored accordingly (1; 2; 3). Mice were terminated when total body scoring was higher than 4 or with scoring of 4 on more than two consecutive days.

4.4.2.5 Temperature monitoring

Body skin temperature was assessed by an infrared thermometer (Aponorm) at the ano-genital area with a distance of 1.5 cm from the skin. Mean of technical triplicates was used as temperature value. Temperature change is presented as delta temperature, subtracted from the value prior experiment start on day -10. Changes of more than 2°C to initial temperature value were defined as adverse event.

4.4.3 Blood sampling and cell processing

Mice were anesthetized in 3% isoflurane and blood was drawn retroorbitally, using sterilized thin glass capillaries, and collected in a heparin coated microtainer® blood collection tube. For intermediate bleeding 60 – 100 µl and for the final analysis day up to 1 mL blood was taken. Exact amount of blood, which was processed for FACS measurement, was determined to allow calculation of absolute cell count in the blood. For further processing blood cells were separated from plasma by centrifugation at 300 x g for 5 min and second centrifugation of the supernatant at 16000 x g for 5 min to remove residual cell debris. Plasma was stored at -80°C until cytokine analysis. Blood cells were washed once by filling up with 1 mL PBS and centrifugation at 300 x g for 5 min, subsequently incubated for 15 min in BD pharm lysing solution to lyse erythrocytes and washed twice with PBS before FACS staining was performed.

4.4.4 Harvest of bone marrow cells

Mice were anesthetized in 3% isoflurane and sacrificed by cervical dislocation. Hip bones, femur and tibia were removed and stored in RPMI complete until further processing. Bones were cleaned from attached tissue using a scalpel and ends of

bones were opened and centrifugation at 4,600 x g for 3 min in perforated 0.5 mL tubes inside a fresh 1.5 mL tube containing 100µL RPMI complete to acquire bone marrow cells. Cells were resuspended in 1 mL RPMI complete and passed through a 70 µm cell strainer to obtain a single cell suspension. Cells were washed once by filling up with 10 mL PBS and centrifugation at 300 x g for 5 min. Subsequently, cells were incubated for 15 min in BD pharm lysing solution to lyse erythrocytes and washed twice with PBS before cells were processed for FACS staining, freezing and qPCR.

4.4.5 Harvest of splenocytes

Mice were anesthetized in 3% isoflurane and sacrificed by cervical dislocation and spleen was removed and stored in RPMI complete until further processing. Spleen was minced through a 70 µm cell strainer to obtain a single cell suspension, washed once by filling up with 10 mL PBS and centrifugation at 300 x g for 5 min. Subsequently, cells were incubated for 15 min in BD pharm lysing solution to lyse erythrocytes and washed twice with PBS before cells were processed for FACS staining, freezing, expansion assay. For qPCR processing bulk splenocytes were used or human T cells were isolated via CD3-FTIC staining (clone BW264/56, Miltenyi Biotec) and combination with an anti-FITC MicroBeads kit (Miltenyi Biotec) following manufacture's protocol.

4.4.6 Harvest of liver cells

Mice were anesthetized in 3% isoflurane and sacrificed by cervical dislocation and liver without the gallbladder was removed and stored in RPMI complete until further processing. Liver cells were isolated using the mouse liver dissociation kit (Miltenyi Biotec) according to the manufacturer's protocol. To obtain a single cell suspension cells were passed through a 70 µm cell strainer, washed once by filling up with 20 mL PBS and centrifugation at 300 x g for 10 min. Subsequently, cells were incubated for 15 min in BD pharm lysing solution to lyse erythrocytes and washed twice with PBS before cells were processed for FACS staining and freezing.

4.4.7 Harvest of lung cells

Mice were anesthetized in 3% isoflurane and sacrificed by cervical dislocation and lung was removed and stored in RPMI complete until further processing. Lung cells were isolated using the mouse lung dissociation kit (Miltenyi Biotec) according to the manufacturer's protocol. To obtain a single cell suspension cells were passed through a 70 µm cell strainer, washed once by filling up with 20 mL PBS and centrifugation at

300 x g for 10 min. Subsequently, cells were incubated for 15 min in BD pharm lysing solution to lyse erythrocytes and washed twice with PBS before cells were processed for FACS staining and freezing.

4.4.8 Expansion Assay

Expansion assay was performed with 1 x 10^5 fresh isolated splenocytes and CD19+ irradiated Raji or Nalm6 cells at an effector:target ratio of 1:1 in RPMI complete supplemented with 50 U/mL human IL-2 or 25 U/mL human IL-7) with 50 U/mL human IL-15 and a medium change two times a week.

4.5 Statistical analysis

Statistical analysis was carried out with GraphPad Prism 8. Statistical testing was performed as described in the figure legends. Differences were considered statistically significant at $p < 0.05$.

5 References

1. Murphy KM, Travers P, Walport M. Janeway Immunologie. 7., Auflage, korrigierter Nachdruck 2014. Berlin, Heidelberg: Springer Spektrum; 2014.

2. Moretta A, Bottino C, Vitale M, Pende D, Cantoni C, Mingari MC et al. Activating receptors and coreceptors involved in human natural killer cell-mediated cytolysis. Annu Rev Immunol 2001; 19:197–223.

3. Lanier LL. NK cell recognition. Annu Rev Immunol 2005; 23:225–74.

4. Prager I, Watzl C. Mechanisms of natural killer cell-mediated cellular cytotoxicity. J Leukoc Biol 2019; 105(6):1319–29.

5. Guermonprez P, Valladeau J, Zitvogel L, Théry C, Amigorena S. Antigen presentation and T cell stimulation by dendritic cells. Annu Rev Immunol 2002; 20:621–67.

6. Neefjes J, Jongsma MLM, Paul P, Bakke O. Towards a systems understanding of MHC class I and MHC class II antigen presentation. Nat Rev Immunol 2011; 11(12):823–36.

7. Alt FW, Blackwell TK, DePinho RA, Reth MG, Yancopoulos GD. Regulation of genome rearrangement events during lymphocyte differentiation. Immunol Rev 1986; 89:5–30.

8. McHeyzer-Williams LJ, Malherbe LP, McHeyzer-Williams MG. Helper T cell-regulated B cell immunity. Curr Top Microbiol Immunol 2006; 311:59–83.

9. Germain RN. T-cell development and the CD4-CD8 lineage decision. Nat Rev Immunol 2002; 2(5):309–22.

10. Smith-Garvin JE, Koretzky GA, Jordan MS. T cell activation. Annu Rev Immunol 2009; 27:591–619.

11. Pagès F, Ragueneau M, Rottapel R, Truneh A, Nunes J, Imbert J et al. Binding of phosphatidylinositol-3-OH kinase to CD28 is required for T-cell signalling. Nature 1994; 369(6478):327–9.

12. Chen L, Flies DB. Molecular mechanisms of T cell co-stimulation and co-inhibition. Nat Rev Immunol 2013; 13(4):227–42.

13. Schwartz RH. A cell culture model for T lymphocyte clonal anergy. Science 1990; 248(4961):1349–56.

14. Brocker T, Karjalainen K. Signals through T cell receptor-zeta chain alone are insufficient to prime resting T lymphocytes. J Exp Med 1995; 181(5):1653–9.

15. Schwartz RH. T cell anergy. Annu Rev Immunol 2003; 21:305–34.

16. Li T, Wu B, Yang T, Zhang L, Jin K. The outstanding antitumor capacity of CD4+ T helper lymphocytes. Biochim Biophys Acta Rev Cancer 2020; 1874(2):188439.

17. Agarwal S, Hanauer JDS, Frank AM, Riechert V, Thalheimer FB, Buchholz CJ. In Vivo Generation of CAR T Cells Selectively in Human CD4+ Lymphocytes. Mol Ther 2020; 28(8):1783–94.

18. Barry M, Bleackley RC. Cytotoxic T lymphocytes: all roads lead to death. Nat Rev Immunol 2002; 2(6):401–9.

19. Golubovskaya V, Wu L. Different Subsets of T Cells, Memory, Effector Functions, and CAR-T Immunotherapy. Cancers (Basel) 2016; 8(3).

20. Hunter CA, Jones SA. IL-6 as a keystone cytokine in health and disease. Nat Immunol 2015; 16(5):448–57.

21. Brehm MA, Daniels KA, Welsh RM. Rapid production of TNF-alpha following TCR engagement of naive CD8 T cells. J Immunol 2005; 175(8):5043–9.

22. Bradley JR. TNF-mediated inflammatory disease. J Pathol 2008; 214(2):149–60.

23. Burdon D, Tiedje T, Pfeffer K, Vollmer E, Zabel P. The role of tumor necrosis factor in the development of multiple organ failure in a murine model. Crit Care Med 2000; 28(6):1962–7.

24. Dellinger RP. Inflammation and coagulation: implications for the septic patient. Clin Infect Dis 2003; 36(10):1259–65.

25. McNab F, Mayer-Barber K, Sher A, Wack A, O'Garra A. Type I interferons in infectious disease. Nat Rev Immunol 2015; 15(2):87–103.

26. Zhang J-M, An J. Cytokines, inflammation, and pain. Int Anesthesiol Clin 2007; 45(2):27–37.

27. Italiani P, Boraschi D. From Monocytes to M1/M2 Macrophages: Phenotypical vs. Functional Differentiation. Front Immunol 2014; 5:514.

28. Jakubzick CV, Randolph GJ, Henson PM. Monocyte differentiation and antigen-presenting functions. Nat Rev Immunol 2017; 17(6):349–62.

29. Verreck FAW, Boer T de, Langenberg DML, van der Zanden L, Ottenhoff THM. Phenotypic and functional profiling of human proinflammatory type-1 and anti-inflammatory type-2 macrophages in response to microbial antigens and IFN-gamma- and CD40L-mediated costimulation. J Leukoc Biol 2006; 79(2):285–93.

30. Sallusto F, Lanzavecchia A. Efficient presentation of soluble antigen by cultured human dendritic cells is maintained by granulocyte/macrophage colony-stimulating factor plus interleukin 4 and downregulated by tumor necrosis factor alpha. J Exp Med 1994; 179(4):1109–18.

31. Pinho S, Frenette PS. Haematopoietic stem cell activity and interactions with the niche. Nat Rev Mol Cell Biol 2019; 20(5):303–20.

32. Pardoll DM. The blockade of immune checkpoints in cancer immunotherapy. Nat Rev Cancer 2012; 12(4):252–64.

33. Hodi FS, O'Day SJ, McDermott DF, Weber RW, Sosman JA, Haanen JB et al. Improved survival with ipilimumab in patients with metastatic melanoma. N Engl J Med 2010; 363(8):711–23.

34. Larkin J, Chiarion-Sileni V, Gonzalez R, Grob JJ, Cowey CL, Lao CD et al. Combined Nivolumab and Ipilimumab or Monotherapy in Untreated Melanoma. N Engl J Med 2015; 373(1):23–34.

35. Rosenberg SA, Packard BS, Aebersold PM, Solomon D, Topalian SL, Toy ST et al. Use of tumor-infiltrating lymphocytes and interleukin-2 in the immunotherapy of patients with metastatic melanoma. A preliminary report. N Engl J Med 1988; 319(25):1676–80.

36. Rosenberg SA, Yang JC, Sherry RM, Kammula US, Hughes MS, Phan GQ et al. Durable complete responses in heavily pretreated patients with metastatic melanoma using T-cell transfer immunotherapy. Clin Cancer Res 2011; 17(13):4550–7.

37. Ahmadzadeh M, Johnson LA, Heemskerk B, Wunderlich JR, Dudley ME, White DE et al. Tumor antigen-specific CD8 T cells infiltrating the tumor express high levels of PD-1 and are functionally impaired. Blood 2009; 114(8):1537–44.

38. Baitsch L, Baumgaertner P, Devêvre E, Raghav SK, Legat A, Barba L et al. Exhaustion of tumor-specific $CD8^+$ T cells in metastases from melanoma patients. J Clin Invest 2011; 121(6):2350–60.

39. Robbins PF, Kassim SH, Tran TLN, Crystal JS, Morgan RA, Feldman SA et al. A pilot trial using lymphocytes genetically engineered with an NY-ESO-1-reactive T-cell receptor: long-term follow-up and correlates with response. Clin Cancer Res 2015; 21(5):1019–27.

40. Sterner RC, Sterner RM. CAR-T cell therapy: current limitations and potential strategies. Blood Cancer J 2021; 11(4):69.

41. Shah NN, Johnson BD, Schneider D, Zhu F, Szabo A, Keever-Taylor CA et al. Bispecific anti-CD20, anti-CD19 CAR T cells for relapsed B cell malignancies: a phase 1 dose escalation and expansion trial. Nat Med 2020; 26(10):1569–75.

42. Baird JH, Frank MJ, Craig J, Patel S, Spiegel JY, Sahaf B et al. CD22-directed CAR T-cell therapy induces complete remissions in CD19-directed CAR-refractory large B-cell lymphoma. Blood 2021; 137(17):2321–5.

43. Tambaro FP, Singh H, Jones E, Rytting M, Mahadeo KM, Thompson P et al. Autologous CD33-CAR-T cells for treatment of relapsed/refractory acute myelogenous leukemia. Leukemia 2021; 35(11):3282–6.

44. Prommersberger S, Reiser M, Beckmann J, Danhof S, Amberger M, Quade-Lyssy P et al. CARAMBA: a first-in-human clinical trial with SLAMF7 CAR-T cells prepared by virus-free Sleeping Beauty gene transfer to treat multiple myeloma. Gene Ther 2021; 28(9):560–71.

45. Siegler E, Li S, Kim YJ, Wang P. Designed Ankyrin Repeat Proteins as Her2 Targeting Domains in Chimeric Antigen Receptor-Engineered T Cells. Hum Gene Ther 2017; 28(9):726–36.

46. Balakrishnan A, Rajan A, Salter AI, Kosasih PL, Wu Q, Voutsinas J et al. Multispecific Targeting with Synthetic Ankyrin Repeat Motif Chimeric Antigen Receptors. Clin Cancer Res 2019; 25(24):7506–16.

47. Munter S de, Ingels J, Goetgeluk G, Bonte S, Pille M, Weening K et al. Nanobody Based Dual Specific CARs. Int J Mol Sci 2018; 19(2).

48. Guest RD, Hawkins RE, Kirillova N, Cheadle EJ, Arnold J, O'Neill A et al. The role of extracellular spacer regions in the optimal design of chimeric immune receptors: evaluation of four different scFvs and antigens. J Immunother 2005; 28(3):203–11.

49. Hudecek M, Lupo-Stanghellini M-T, Kosasih PL, Sommermeyer D, Jensen MC, Rader C et al. Receptor affinity and extracellular domain modifications affect tumor recognition by ROR1-specific chimeric antigen receptor T cells. Clin Cancer Res 2013; 19(12):3153–64.

50. Hudecek M, Sommermeyer D, Kosasih PL, Silva-Benedict A, Liu L, Rader C et al. The nonsignaling extracellular spacer domain of chimeric antigen receptors is decisive for in vivo antitumor activity. Cancer Immunol Res 2015; 3(2):125–35.

51. Alabanza L, Pegues M, Geldres C, Shi V, Wiltzius JJW, Sievers SA et al. Function of Novel Anti-CD19 Chimeric Antigen Receptors with Human Variable Regions Is Affected by Hinge and Transmembrane Domains. Mol Ther 2017; 25(11):2452–65.

52. Ying Z, Huang XF, Xiang X, Liu Y, Kang X, Song Y et al. A safe and potent anti-CD19 CAR T cell therapy. Nat Med 2019; 25(6):947–53.

53. Eshhar Z, Waks T, Gross G, Schindler DG. Specific activation and targeting of cytotoxic lymphocytes through chimeric single chains consisting of antibody-binding domains and the gamma or zeta subunits of the immunoglobulin and T-cell receptors. Proc Natl Acad Sci U S A 1993; 90(2):720–4.

54. Hwu P, Shafer GE, Treisman J, Schindler DG, Gross G, Cowherd R et al. Lysis of ovarian cancer cells by human lymphocytes redirected with a chimeric gene composed of an antibody variable region and the Fc receptor gamma chain. J Exp Med 1993; 178(1):361–6.

55. Hwu P, Yang JC, Cowherd R, Treisman J, Shafer GE, Eshhar Z et al. In vivo antitumor activity of T cells redirected with chimeric antibody/T-cell receptor genes. Cancer Res 1995; 55(15):3369–73.

56. Krause A, Guo HF, Latouche JB, Tan C, Cheung NK, Sadelain M. Antigen-dependent CD28 signaling selectively enhances survival and proliferation in genetically modified activated human primary T lymphocytes. J Exp Med 1998; 188(4):619–26.

57. Maher J, Brentjens RJ, Gunset G, Rivière I, Sadelain M. Human T-lymphocyte cytotoxicity and proliferation directed by a single chimeric TCRzeta /CD28 receptor. Nat Biotechnol 2002; 20(1):70–5.

58. Imai C, Mihara K, Andreansky M, Nicholson IC, Pui C-H, Geiger TL et al. Chimeric receptors with 4-1BB signaling capacity provoke potent cytotoxicity against acute lymphoblastic leukemia. Leukemia 2004; 18(4):676–84.

59. Carpenito C, Milone MC, Hassan R, Simonet JC, Lakhal M, Suhoski MM et al. Control of large, established tumor xenografts with genetically retargeted human T cells containing CD28 and CD137 domains. Proc Natl Acad Sci U S A 2009; 106(9):3360–5.

60. Zhong X-S, Matsushita M, Plotkin J, Riviere I, Sadelain M. Chimeric antigen receptors combining 4-1BB and CD28 signaling domains augment PI3kinase/AKT/Bcl-XL activation and CD8+ T cell-mediated tumor eradication. Mol Ther 2010; 18(2):413–20.

61. Morgan RA, Yang JC, Kitano M, Dudley ME, Laurencot CM, Rosenberg SA. Case report of a serious adverse event following the administration of T cells transduced with a chimeric antigen receptor recognizing ERBB2. Mol Ther 2010; 18(4):843–51.

62. Till BG, Jensen MC, Wang J, Qian X, Gopal AK, Maloney DG et al. CD20-specific adoptive immunotherapy for lymphoma using a chimeric antigen receptor with both CD28 and 4-1BB domains: pilot clinical trial results. Blood 2012; 119(17):3940–50.

63. Enblad G, Karlsson H, Gammelgård G, Wenthe J, Lövgren T, Amini RM et al. A Phase I/IIa Trial Using CD19-Targeted Third-Generation CAR T Cells for Lymphoma and Leukemia. Clin Cancer Res 2018; 24(24):6185–94.

64. Levine BL. Performance-enhancing drugs: design and production of redirected chimeric antigen receptor (CAR) T cells. Cancer Gene Ther 2015; 22(2):79–84.

65. Wang X, Rivière I. Clinical manufacturing of CAR T cells: foundation of a promising therapy. Mol Ther Oncolytics 2016; 3:16015.

66. Levine BL, Miskin J, Wonnacott K, Keir C. Global Manufacturing of CAR T Cell Therapy. Mol Ther Methods Clin Dev 2017; 4:92–101.

67. Vormittag P, Gunn R, Ghorashian S, Veraitch FS. A guide to manufacturing CAR T cell therapies. Curr Opin Biotechnol 2018; 53:164–81.

68. Riddell SR, Sommermeyer D, Berger C, Liu LS, Balakrishnan A, Salter A et al. Adoptive therapy with chimeric antigen receptor-modified T cells of defined subset composition. Cancer J 2014; 20(2):141–4.

69. Turtle CJ, Hanafi L-A, Berger C, Gooley TA, Cherian S, Hudecek M et al. CD19 CAR-T cells of defined CD4+:CD8+ composition in adult B cell ALL patients. J Clin Invest 2016; 126(6):2123–38.

70. Gardner RA, Finney O, Annesley C, Brakke H, Summers C, Leger K et al. Intent-to-treat leukemia remission by CD19 CAR T cells of defined formulation and dose in children and young adults. Blood 2017; 129(25):3322–31.

71. Sereti I, Dunham RM, Spritzler J, Aga E, Proschan MA, Medvik K et al. IL-7 administration drives T cell-cycle entry and expansion in HIV-1 infection. Blood 2009; 113(25):6304–14.

72. Cavalieri S, Cazzaniga S, Geuna M, Magnani Z, Bordignon C, Naldini L et al. Human T lymphocytes transduced by lentiviral vectors in the absence of TCR activation maintain an intact immune competence. Blood 2003; 102(2):497–505.

73. Frank AM, Braun AH, Scheib L, Agarwal S, Schneider IC, Fusil F et al. Combining T-cell-specific activation and in vivo gene delivery through CD3-targeted lentiviral vectors. Blood Adv 2020; 4(22):5702–15.

74. Abou-El-Enein M, Elsallab M, Feldman SA, Fesnak AD, Heslop HE, Marks P et al. Scalable Manufacturing of CAR T cells for Cancer Immunotherapy. Blood Cancer Discov 2021; 2(5):408–22.

75. Donnadieu E, Luu M, Alb M, Anliker B, Arcangeli S, Bonini C et al. Time to evolve: predicting engineered T cell-associated toxicity with next-generation models. J Immunother Cancer 2022; 10(5).

76. Hollyman D, Stefanski J, Przybylowski M, Bartido S, Borquez-Ojeda O, Taylor C et al. Manufacturing validation of biologically functional T cells targeted to CD19 antigen for autologous adoptive cell therapy. J Immunother 2009; 32(2):169–80.

77. Maude SL, Frey N, Shaw PA, Aplenc R, Barrett DM, Bunin NJ et al. Chimeric antigen receptor T cells for sustained remissions in leukemia. N Engl J Med 2014; 371(16):1507–17.

78. Davila ML, Riviere I, Wang X, Bartido S, Park J, Curran K et al. Efficacy and toxicity management of 19-28z CAR T cell therapy in B cell acute lymphoblastic leukemia. Sci Transl Med 2014; 6(224):224ra25.

79. Teachey DT, Lacey SF, Shaw PA, Melenhorst JJ, Maude SL, Frey N et al. Identification of Predictive Biomarkers for Cytokine Release Syndrome after Chimeric Antigen Receptor T-cell Therapy for Acute Lymphoblastic Leukemia. Cancer Discov 2016; 6(6):664–79.

80. Hay KA, Hanafi L-A, Li D, Gust J, Liles WC, Wurfel MM et al. Kinetics and biomarkers of severe cytokine release syndrome after CD19 chimeric antigen receptor-modified T-cell therapy. Blood 2017; 130(21):2295–306.

81. Lee DW, Santomasso BD, Locke FL, Ghobadi A, Turtle CJ, Brudno JN et al. ASTCT Consensus Grading for Cytokine Release Syndrome and Neurologic Toxicity Associated with Immune Effector Cells. Biol Blood Marrow Transplant 2019; 25(4):625–38.

82. Lee DW, Gardner R, Porter DL, Louis CU, Ahmed N, Jensen M et al. Current concepts in the diagnosis and management of cytokine release syndrome. Blood 2014; 124(2):188–95.

83. Brudno JN, Kochenderfer JN. Toxicities of chimeric antigen receptor T cells: recognition and management. Blood 2016; 127(26):3321–30.

84. Strati P, Ahmed S, Furqan F, Fayad LE, Lee HJ, Iyer SP et al. Prognostic impact of corticosteroids on efficacy of chimeric antigen receptor T-cell therapy in large B-cell lymphoma. Blood 2021; 137(23):3272–6.

85. Giavridis T, van der Stegen SJC, Eyquem J, Hamieh M, Piersigilli A, Sadelain M. CAR T cell-induced cytokine release syndrome is mediated by macrophages and abated by IL-1 blockade. Nat Med 2018; 24(6):731–8.

86. Norelli M, Camisa B, Barbiera G, Falcone L, Purevdorj A, Genua M et al. Monocyte-derived IL-1 and IL-6 are differentially required for cytokine-release syndrome and neurotoxicity due to CAR T cells. Nat Med 2018; 24(6):739–48.

87. Barrett DM, Singh N, Hofmann TJ, Gershenson Z, Grupp SA. Interleukin 6 Is Not Made By Chimeric Antigen Receptor T Cells and Does Not Impact Their Function. Blood 2016; 128(22):654.

88. Singh N, Hofmann TJ, Gershenson Z, Levine BL, Grupp SA, Teachey DT et al. Monocyte lineage-derived IL-6 does not affect chimeric antigen receptor T-cell function. Cytotherapy 2017; 19(7):867–80.

89. Sachdeva M, Duchateau P, Depil S, Poirot L, Valton J. Granulocyte-macrophage colony-stimulating factor inactivation in CAR T-cells prevents monocyte-dependent release of key cytokine release syndrome mediators. J Biol Chem 2019; 294(14):5430–7.

90. Arcangeli S, Bove C, Mezzanotte C, Camisa B, Falcone L, Manfredi F et al. CAR T cell manufacturing from naive/stem memory T lymphocytes enhances antitumor responses while curtailing cytokine release syndrome. J Clin Invest 2022; 132(12).

91. Morris EC, Neelapu SS, Giavridis T, Sadelain M. Cytokine release syndrome and associated neurotoxicity in cancer immunotherapy. Nat Rev Immunol 2022; 22(2):85–96.

92. Gust J, Hay KA, Hanafi L-A, Li D, Myerson D, Gonzalez-Cuyar LF et al. Endothelial Activation and Blood-Brain Barrier Disruption in Neurotoxicity after Adoptive Immunotherapy with CD19 CAR-T Cells. Cancer Discov 2017; 7(12):1404–19.

93. Santomasso B, Bachier C, Westin J, Rezvani K, Shpall EJ. The Other Side of CAR T-Cell Therapy: Cytokine Release Syndrome, Neurologic Toxicity, and Financial Burden. Am Soc Clin Oncol Educ Book 2019; 39:433–44.

94. Parker KR, Migliorini D, Perkey E, Yost KE, Bhaduri A, Bagga P et al. Single-Cell Analyses Identify Brain Mural Cells Expressing CD19 as Potential Off-Tumor Targets for CAR-T Immunotherapies. Cell 2020; 183(1):126-142.e17.

95. Sheth VS, Gauthier J. Taming the beast: CRS and ICANS after CAR T-cell therapy for ALL. Bone Marrow Transplant 2021; 56(3):552–66.

96. Bonifant CL, Jackson HJ, Brentjens RJ, Curran KJ. Toxicity and management in CAR T-cell therapy. Mol Ther Oncolytics 2016; 3:16011.

97. Xu Y, Zhang M, Ramos CA, Durett A, Liu E, Dakhova O et al. Closely related T-memory stem cells correlate with in vivo expansion of CAR.CD19-T cells and are preserved by IL-7 and IL-15. Blood 2014; 123(24):3750–9.

98. Fraietta JA, Lacey SF, Orlando EJ, Pruteanu-Malinici I, Gohil M, Lundh S et al. Determinants of response and resistance to CD19 chimeric antigen receptor (CAR) T cell therapy of chronic lymphocytic leukemia. Nat Med 2018; 24(5):563–71.

99. Arcangeli S, Falcone L, Camisa B, Girardi F de, Biondi M, Giglio F et al. Next-Generation Manufacturing Protocols Enriching TSCM CAR T Cells Can Overcome Disease-Specific T Cell Defects in Cancer Patients. Front Immunol 2020; 11:1217.

100. Ghassemi S, Nunez-Cruz S, O'Connor RS, Fraietta JA, Patel PR, Scholler J et al. Reducing Ex Vivo Culture Improves the Antileukemic Activity of Chimeric Antigen Receptor (CAR) T Cells. Cancer Immunol Res 2018; 6(9):1100–9.

101. Eyquem J, Mansilla-Soto J, Giavridis T, van der Stegen SJC, Hamieh M, Cunanan KM et al. Targeting a CAR to the TRAC locus with CRISPR/Cas9 enhances tumour rejection. Nature 2017; 543(7643):113–7.

102. MacLeod DT, Antony J, Martin AJ, Moser RJ, Hekele A, Wetzel KJ et al. Integration of a CD19 CAR into the TCR Alpha Chain Locus Streamlines Production of Allogeneic Gene-Edited CAR T Cells. Mol Ther 2017; 25(4):949–61.

103. Sheridan C. Off-the-shelf, gene-edited CAR-T cells forge ahead, despite safety scare. Nat Biotechnol 2022; 40(1):5–8.

104. Michels A, Ho N, Buchholz CJ. Precision medicine: In vivo CAR therapy as a showcase for receptor-targeted vector platforms. Mol Ther 2022; 30(7):2401–15.

105. Smith TT, Stephan SB, Moffett HF, McKnight LE, Ji W, Reiman D et al. In situ programming of leukaemia-specific T cells using synthetic DNA nanocarriers. Nat Nanotechnol 2017; 12(8):813–20.

106. Parayath NN, Stephan SB, Koehne AL, Nelson PS, Stephan MT. In vitro-transcribed antigen receptor mRNA nanocarriers for transient expression in circulating T cells in vivo. Nat Commun 2020; 11(1):6080.

107. Rurik JG, Tombácz I, Yadegari A, Méndez Fernández PO, Shewale SV, Li L et al. CAR T cells produced in vivo to treat cardiac injury. Science 2022; 375(6576):91–6.

108. Pfeiffer A, Thalheimer FB, Hartmann S, Frank AM, Bender RR, Danisch S et al. In vivo generation of human CD19-CAR T cells results in B-cell depletion and signs of cytokine release syndrome. EMBO Mol Med 2018; 10(11).

109. Agarwal S, Weidner T, Thalheimer FB, Buchholz CJ. In vivo generated human CAR T cells eradicate tumor cells. Oncoimmunology 2019; 8(12):e1671761.

110. Huckaby JT, Landoni E, Jacobs TM, Savoldo B, Dotti G, Lai SK. Bispecific binder redirected lentiviral vector enables in vivo engineering of CAR-T cells. J Immunother Cancer 2021; 9(9).

111. Naldini L, Trono D, Verma IM. Lentiviral vectors, two decades later. Science 2016; 353(6304):1101–2.

112. Kustikova OS, Wahlers A, Kuhlcke K, Stahle B, Zander AR, Baum C et al. Dose finding with retroviral vectors: correlation of retroviral vector copy numbers in single cells with gene transfer efficiency in a cell population. Blood 2003; 102(12):3934–7.

113. Hacein-Bey-Abina S, Kalle C von, Schmidt M, McCormack MP, Wulffraat N, Leboulch P et al. LMO2-associated clonal T cell proliferation in two patients after gene therapy for SCID-X1. Science 2003; 302(5644):415–9.

114. Hacein-Bey-Abina S, Garrigue A, Wang GP, Soulier J, Lim A, Morillon E et al. Insertional oncogenesis in 4 patients after retrovirus-mediated gene therapy of SCID-X1. J Clin Invest 2008; 118(9):3132–42.

115. Sakuma T, Barry MA, Ikeda Y. Lentiviral vectors: basic to translational. Biochem J 2012; 443(3):603–18.

116. Naldini L, Blömer U, Gallay P, Ory D, Mulligan R, Gage FH et al. In vivo gene delivery and stable transduction of nondividing cells by a lentiviral vector. Science 1996; 272(5259):263–7.

117. Finkelshtein D, Werman A, Novick D, Barak S, Rubinstein M. LDL receptor and its family members serve as the cellular receptors for vesicular stomatitis virus. Proc Natl Acad Sci U S A 2013; 110(18):7306–11.

118. Amirache F, Lévy C, Costa C, Mangeot P-E, Torbett BE, Wang CX et al. Mystery solved: VSV-G-LVs do not allow efficient gene transfer into unstimulated T cells, B cells, and HSCs because they lack the LDL receptor. Blood 2014; 123(9):1422–4.

119. Mochizuki H, Schwartz JP, Tanaka K, Brady RO, Reiser J. High-titer human immunodeficiency virus type 1-based vector systems for gene delivery into nondividing cells. J Virol 1998; 72(11):8873–83.

120. Ruella M, Xu J, Barrett DM, Fraietta JA, Reich TJ, Ambrose DE et al. Induction of resistance to chimeric antigen receptor T cell therapy by transduction of a single leukemic B cell. Nat Med 2018; 24(10):1499–503.

121. Funke S, Maisner A, Mühlebach MD, Koehl U, Grez M, Cattaneo R et al. Targeted cell entry of lentiviral vectors. Mol Ther 2008; 16(8):1427–36.

122. Bender RR, Muth A, Schneider IC, Friedel T, Hartmann J, Plückthun A et al. Receptor-Targeted Nipah Virus Glycoproteins Improve Cell-Type Selective Gene Delivery and Reveal a Preference for Membrane-Proximal Cell Attachment. PLoS Pathog 2016; 12(6):e1005641.

123. Yang L, Bailey L, Baltimore D, Wang P. Targeting lentiviral vectors to specific cell types in vivo. Proc Natl Acad Sci U S A 2006; 103(31):11479–84.

124. Yang H, Joo K-I, Ziegler L, Wang P. Cell type-specific targeting with surface-engineered lentiviral vectors co-displaying OKT3 antibody and fusogenic molecule. Pharm Res 2009; 26(6):1432–45.

125. Liang M, Morizono K, Pariente N, Kamata M, Lee B, Chen ISY. Targeted transduction via CD4 by a lentiviral vector uses a clathrin-mediated entry pathway. J Virol 2009; 83(24):13026–31.

126. Frank AM, Buchholz CJ. Surface-Engineered Lentiviral Vectors for Selective Gene Transfer into Subtypes of Lymphocytes. Mol Ther Methods Clin Dev 2019; 12:19–31.

127. Plückthun A. Designed ankyrin repeat proteins (DARPins): binding proteins for research, diagnostics, and therapy. Annu Rev Pharmacol Toxicol 2015; 55:489–511.

128. Anliker B, Abel T, Kneissl S, Hlavaty J, Caputi A, Brynza J et al. Specific gene transfer to neurons, endothelial cells and hematopoietic progenitors with lentiviral vectors. Nat Methods 2010; 7(11):929–35.

129. Zhou Q, Schneider IC, Gallet M, Kneissl S, Buchholz CJ. Resting lymphocyte transduction with measles virus glycoprotein pseudotyped lentiviral vectors relies on CD46 and SLAM. Virology 2011; 413(2):149–52.

130. Zhou Q, Uhlig KM, Muth A, Kimpel J, Lévy C, Münch RC et al. Exclusive Transduction of Human CD4+ T Cells upon Systemic Delivery of CD4-Targeted Lentiviral Vectors. J Immunol 2015; 195(5):2493–501.

131. Frank AM, Weidner T, Brynza J, Uckert W, Buchholz CJ, Hartmann J. CD8-Specific Designed Ankyrin Repeat Proteins Improve Selective Gene Delivery into Human and Primate T Lymphocytes. Hum Gene Ther 2020; 31(11-12):679–91.

132. Charitidis FT, Adabi E, Thalheimer FB, Clarke C, Buchholz CJ. Monitoring CAR T cell generation with a CD8-targeted lentiviral vector by single-cell transcriptomics. Mol Ther Methods Clin Dev 2021; 23:359–69.

133. Shultz LD, Lyons BL, Burzenski LM, Gott B, Chen X, Chaleff S et al. Human lymphoid and myeloid cell development in NOD/LtSz-scid IL2R gamma null mice engrafted with mobilized human hemopoietic stem cells. J Immunol 2005; 174(10):6477–89.

134. Ito M, Hiramatsu H, Kobayashi K, Suzue K, Kawahata M, Hioki K et al. NOD/SCID/gamma(c)(null) mouse: an excellent recipient mouse model for engraftment of human cells. Blood 2002; 100(9):3175–82.

135. Pearson T, Shultz LD, Miller D, King M, Laning J, Fodor W et al. Non-obese diabetic-recombination activating gene-1 (NOD-Rag1 null) interleukin (IL)-2 receptor common gamma chain (IL2r gamma null) null mice: a radioresistant model for human lymphohaematopoietic engraftment. Clin Exp Immunol 2008; 154(2):270–84.

136. Shultz LD, Keck J, Burzenski L, Jangalwe S, Vaidya S, Greiner DL et al. Humanized mouse models of immunological diseases and precision medicine. Mamm Genome 2019; 30(5-6):123–42.

137. King MA, Covassin L, Brehm MA, Racki W, Pearson T, Leif J et al. Human peripheral blood leucocyte non-obese diabetic-severe combined immunodeficiency interleukin-2 receptor gamma chain gene mouse model of xenogeneic graft-versus-host-like disease and the role of host major histocompatibility complex. Clin Exp Immunol 2009; 157(1):104–18.

138. Ito R, Katano I, Kawai K, Hirata H, Ogura T, Kamisako T et al. Highly sensitive model for xenogenic GVHD using severe immunodeficient NOG mice. Transplantation 2009; 87(11):1654–8.

139. Brehm MA, Kenney LL, Wiles MV, Low BE, Tisch RM, Burzenski L et al. Lack of acute xenogeneic graft- versus-host disease, but retention of T-cell function following engraftment of human peripheral blood mononuclear cells in NSG mice deficient in MHC class I and II expression. FASEB J 2019; 33(3):3137–51.

140. Stripecke R, Münz C, Schuringa JJ, Bissig K-D, Soper B, Meeham T et al. Innovations, challenges, and minimal information for standardization of humanized mice. EMBO Mol Med 2020; 12(7):e8662.

141. Dougan M, Dranoff G, Dougan SK. GM-CSF, IL-3, and IL-5 Family of Cytokines: Regulators of Inflammation. Immunity 2019; 50(4):796–811.

142. Broudy VC. Stem Cell Factor and Hematopoiesis. Blood 1997; 90(4):1345–64.

143. Ito R, Takahashi T, Katano I, Kawai K, Kamisako T, Ogura T et al. Establishment of a human allergy model using human IL-3/GM-CSF-transgenic NOG mice. J Immunol 2013; 191(6):2890–9.

144. Rongvaux A, Willinger T, Martinek J, Strowig T, Gearty SV, Teichmann LL et al. Development and function of human innate immune cells in a humanized mouse model. Nat Biotechnol 2014; 32(4):364–72.

145. Wunderlich M, Chou F-S, Link KA, Mizukawa B, Perry RL, Carroll M et al. AML xenograft efficiency is significantly improved in NOD/SCID-IL2RG mice constitutively expressing human SCF, GM-CSF and IL-3. Leukemia 2010; 24(10):1785–8.

146. Billerbeck E, Barry WT, Mu K, Dorner M, Rice CM, Ploss A. Development of human CD4+FoxP3+ regulatory T cells in human stem cell factor-, granulocyte-macrophage colony-stimulating factor-, and interleukin-3-expressing NOD-SCID IL2Rγ(null) humanized mice. Blood 2011; 117(11):3076–86.

147. Ho N, Agarwal S, Milani M, Cantore A, Buchholz CJ, Thalheimer FB. In vivo generation of CAR T cells in the presence of human myeloid cells. Mol Ther Methods Clin Dev 2022; 26:144–56.

148. Schulz D, Severin Y, Zanotelli VRT, Bodenmiller B. In-Depth Characterization of Monocyte-Derived Macrophages using a Mass Cytometry-Based Phagocytosis Assay. Sci Rep 2019; 9(1):1925.

149. Milani M, Annoni A, Moalli F, Liu T, Cesana D, Calabria A et al. Phagocytosis-shielded lentiviral vectors improve liver gene therapy in nonhuman primates. Sci Transl Med 2019; 11(493).

150. Kapitza L. T cell-targeted gene delivery: Rapid CAR T cell generation without full activation. UNSPECIFIED; 2022.

151. Mei J, Riedel N, Grittner U, Endres M, Banneke S, Emmrich JV. Body temperature measurement in mice during acute illness: implantable temperature transponder versus surface infrared thermometry. Sci Rep 2018; 8(1):3526.

152. Ye C, Yang H, Cheng M, Shultz LD, Greiner DL, Brehm MA et al. A rapid, sensitive, and reproducible in vivo PBMC humanized murine model for determining therapeutic-related cytokine release syndrome. FASEB J 2020; 34(9):12963–75.

153. Mosier DE, Stell KL, Gulizia RJ, Torbett BE, Gilmore GL. Homozygous scid/scid;beige/beige mice have low levels of spontaneous or neonatal T cell-induced B cell generation. J Exp Med 1993; 177(1):191–4.

154. Shultz LD, Schweitzer PA, Christianson SW, Gott B, Schweitzer IB, Tennent B et al. Multiple defects in innate and adaptive immunologic function in NOD/LtSz-scid mice. J Immunol 1995; 154(1):180–91.

155. Roder J, Duwe A. The beige mutation in the mouse selectively impairs natural killer cell function. Nature 1979; 278(5703):451–3.

156. Serreze DV, Gaskins HR, Leiter EH. Defects in the differentiation and function of antigen presenting cells in NOD/Lt mice. J Immunol 1993; 150(6):2534–43.

157. Ghassemi S, Durgin JS, Nunez-Cruz S, Patel J, Leferovich J, Pinzone M et al. Rapid manufacturing of non-activated potent CAR T cells. Nat Biomed Eng 2022; 6(2):118–28.

158. Jamali A, Kapitza L, Schaser T, Johnston ICD, Buchholz CJ, Hartmann J. Highly Efficient and Selective CAR-Gene Transfer Using CD4- and CD8-Targeted Lentiviral Vectors. Mol Ther Methods Clin Dev 2019; 13:371–9.

159. Cordes N, Kolbe C, Lock D, Holzer T, Althoff D, Schäfer D et al. Anti-CD19 CARs displayed at the surface of lentiviral vector particles promote transduction of target-expressing cells. Mol Ther Methods Clin Dev 2021; 21:42–53.

160. Yang J, He J, Zhang X, Li J, Wang Z, Zhang Y et al. Next-day manufacture of a novel anti-CD19 CAR-T therapy for B-cell acute lymphoblastic leukemia: first-in-human clinical study. Blood Cancer J 2022; 12(7):104.

161. Zhang C, He J, Liu L, Wang J, Wang S, Liu L et al. Novel CD19 chimeric antigen receptor T cells manufactured next-day for acute lymphoblastic leukemia. Blood Cancer J 2022; 12(6):96.

162. Ullman-Culleré MH, Foltz CJ. Body condition scoring: a rapid and accurate method for assessing health status in mice. Lab Anim Sci 1999; 49(3):319–23.

163. Weißmüller S, Kronhart S, Kreuz D, Schnierle B, Kalinke U, Kirberg J et al. TGN1412 Induces Lymphopenia and Human Cytokine Release in a Humanized Mouse Model. PLoS One 2016; 11(3):e0149093.

164. Matas-Céspedes A, Brown L, Mahbubani KT, Bareham B, Higgins J, Curran M et al. Use of human splenocytes in an innovative humanised mouse model for prediction of immunotherapy-induced cytokine release syndrome. Clin Transl Immunology 2020; 9(11):e1202.

165. Demetri GD, Griffin JD. Granulocyte colony-stimulating factor and its receptor. Blood 1991; 78(11):2791–808.

166. Deshmane SL, Kremlev S, Amini S, Sawaya BE. Monocyte chemoattractant protein-1 (MCP-1): an overview. J Interferon Cytokine Res 2009; 29(6):313–26.

167. Jamali A, Hadjati J, Madjd Z, Mirzaei HR, Thalheimer FB, Agarwal S et al. Highly Efficient Generation of Transgenically Augmented CAR NK Cells Overexpressing CXCR4. Front Immunol 2020; 11:2028.

168. Ng YY, Du Z, Zhang X, Chng WJ, Wang S. CXCR4 and anti-BCMA CAR co-modified natural killer cells suppress multiple myeloma progression in a xenograft mouse model. Cancer Gene Ther 2022; 29(5):475–83.

169. Neelapu SS, Locke FL, Bartlett NL, Lekakis LJ, Miklos DB, Jacobson CA et al. Axicabtagene Ciloleucel CAR T-Cell Therapy in Refractory Large B-Cell Lymphoma. N Engl J Med 2017; 377(26):2531–44.

170. Li W, Qiu S, Chen J, Jiang S, Chen W, Jiang J et al. Chimeric Antigen Receptor Designed to Prevent Ubiquitination and Downregulation Showed Durable Antitumor Efficacy. Immunity 2020; 53(2):456-470.e6.

171. Saito Y, Kametani Y, Hozumi K, Mochida N, Ando K, Ito M et al. The in vivo development of human T cells from CD34(+) cells in the murine thymic environment. Int Immunol 2002; 14(10):1113–24.

172. Gordon S, Plüddemann A. Tissue macrophages: heterogeneity and functions. BMC Biol 2017; 15(1):53.

173. Rodriguez PL, Harada T, Christian DA, Pantano DA, Tsai RK, Discher DE. Minimal "Self" peptides that inhibit phagocytic clearance and enhance delivery of nanoparticles. Science 2013; 339(6122):971–5.

174. Sosale NG, Ivanovska II, Tsai RK, Swift J, Hsu JW, Alvey CM et al. "Marker of Self" CD47 on lentiviral vectors decreases macrophage-mediated clearance and increases delivery to SIRPA-expressing lung carcinoma tumors. Mol Ther Methods Clin Dev 2016; 3:16080.

175. Oldenborg PA, Zheleznyak A, Fang YF, Lagenaur CF, Gresham HD, Lindberg FP. Role of CD47 as a marker of self on red blood cells. Science 2000; 288(5473):2051–4.

176. Chao MP, Jaiswal S, Weissman-Tsukamoto R, Alizadeh AA, Gentles AJ, Volkmer J et al. Calreticulin is the dominant pro-phagocytic signal on multiple human cancers and is counterbalanced by CD47. Sci Transl Med 2010; 2(63):63ra94.

177. Stewart SJ, Fujimoto J, Levy R. Human T lymphocytes and monocytes bear the same Leu-3(T4) antigen. J Immunol 1986; 136(10):3773–8.

178. Zhen A, Krutzik SR, Levin BR, Kasparian S, Zack JA, Kitchen SG. CD4 ligation on human blood monocytes triggers macrophage differentiation and enhances HIV infection. J Virol 2014; 88(17):9934–46.

179. Lund JM, Alexopoulou L, Sato A, Karow M, Adams NC, Gale NW et al. Recognition of single-stranded RNA viruses by Toll-like receptor 7. Proc Natl Acad Sci U S A 2004; 101(15):5598–603.

180. Mühlebach MD, Wolfrum N, Schüle S, Tschulena U, Sanzenbacher R, Flory E et al. Stable transduction of primary human monocytes by simian lentiviral vector PBj. Mol Ther 2005; 12(6):1206–16.

181. Schüle S, Kloke B-P, Kaiser JK, Heidmeier S, Panitz S, Wolfrum N et al. Restriction of HIV-1 replication in monocytes is abolished by Vpx of SIVsmmPBj. PLoS One 2009; 4(9):e7098.

182. Satoh T, Manel N. Gene transduction in human monocyte-derived dendritic cells using lentiviral vectors. Methods Mol Biol 2013; 960:401–9.

183. Hrecka K, Hao C, Gierszewska M, Swanson SK, Kesik-Brodacka M, Srivastava S et al. Vpx relieves inhibition of HIV-1 infection of macrophages mediated by the SAMHD1 protein. Nature 2011; 474(7353):658–61.

184. Bobadilla S, Sunseri N, Landau NR. Efficient transduction of myeloid cells by an HIV-1-derived lentiviral vector that packages the Vpx accessory protein. Gene Ther 2013; 20(5):514–20.

185. Neil S, Martin F, Ikeda Y, Collins M. Postentry restriction to human immunodeficiency virus-based vector transduction in human monocytes. J Virol 2001; 75(12):5448–56.

186. Rouas R, Uch R, Cleuter Y, Jordier F, Bagnis C, Mannoni P et al. Lentiviral-mediated gene delivery in human monocyte-derived dendritic cells: optimized design and procedures for highly efficient transduction compatible with clinical constraints. Cancer Gene Ther 2002; 9(9):715–24.

187. Bose S, Jardetzky TS, Lamb RA. Timing is everything: Fine-tuned molecular machines orchestrate paramyxovirus entry. Virology 2015; 479-480:518–31.

188. Müller U, Steinhoff U, Reis LF, Hemmi S, Pavlovic J, Zinkernagel RM et al. Functional role of type I and type II interferons in antiviral defense. Science 1994; 264(5167):1918–21.

189. Brown BD, Sitia G, Annoni A, Hauben E, Sergi LS, Zingale A et al. In vivo administration of lentiviral vectors triggers a type I interferon response that restricts hepatocyte gene transfer and promotes vector clearance. Blood 2007; 109(7):2797–805.

190. Maser I-P, Hoves S, Bayer C, Heidkamp G, Nimmerjahn F, Eckmann J et al. The Tumor Milieu Promotes Functional Human Tumor-Resident Plasmacytoid Dendritic Cells in Humanized Mouse Models. Front Immunol 2020; 11.

191. Zufferey R, Dull T, Mandel RJ, Bukovsky A, Quiroz D, Naldini L et al. Self-inactivating lentivirus vector for safe and efficient in vivo gene delivery. J Virol 1998; 72(12):9873–80.

192. Oelsner S, Friede ME, Zhang C, Wagner J, Badura S, Bader P et al. Continuously expanding CAR NK-92 cells display selective cytotoxicity against B-cell leukemia and lymphoma. Cytotherapy 2017; 19(2):235–49.

193. Laurens van der Maaten, Geoffrey Hinton. Visualizing Data using t-SNE. Journal of Machine Learning Research 2008; 9(86):2579–605. Available from: URL: http://jmlr.org/papers/v9/vandermaaten08a.html.

6 Abbreviations

Abbreviation	Definition
B cells	B lymphocytes
B-ALL	B cell acute lymphoblastic leukemia
BBB	blood-brain-barrier
BSA	Bovine serum albumin
CAR	Chimeric antigen receptor
CD	Cluster of differentiation
CD4-LV	CD4 receptor-targeted lentiviral vector
CD8-LV	CD8 receptor-targeted lentiviral vector
CRS	Cytokine release syndrome
CTV	CellTrace® Violet
DARPin	Designed ankyrin repeat protein
DC	Dendritic cell
DMEM	Dulbecco’s Modified Eagle Medium
DMSO	Dimethyl sulfoxide
DNA	Desoxyribonucelic acid
E. coli	Escherichia coli
EDTA	Ethylenediaminetetraacetic acid
FBS	Fetal bovine serum
FcR	Fc receptor
GM-CSF	Granulocyte-macrophage colony-stimulating factor
GvHD	Graft-versus host disease
HEK	Human embryonic kidney
HEPES	N-2-hydroxyethylpiperazine-N'-2-ethanesulfonic acid
HIV-1	Human immunodeficiency virus-1
HSC	Hematopoietic stem cell
huSGM3	CD34+ stem cell humanized NSG-SGM3
i.v.	Intravenous
ICANS	immune effector cell-associated neurotoxicity syndrome
IFN-γ	Interferon γ
IVIS	In vivo imaging system
LTR	Long terminal repeat
LVs	Lentiviral vector

LV^{sh}	Phagocytosis shielded lentiviral vector
MFI	Mean fluorescence intensity
MHC	Major histocompatibility complex
MIX	Mixture of CD4 and CD8 targeted lentiviral vector suspension
MV	Measles virus
NaN_3	Sodium azide
NEB	New England Biolabs
NiV	Nipah virus
NK	Natural killer
NOG	NODShi.Cg-$Prkdc^{scid}Il2rg^{tm1Sug}$
NRG	NOD.Cg-$Rag1^{tm1Mom}IL2rg^{tm1Wjl}$
NSG	NOD.Cg-$Prkdc^{scid}Il2rg^{tm1Wjl}$
NTA	Nanoparticle tracking analysis
PBMC	Pperipheral blood mononuclear cells
PCR	Polymerase chain reaction
PD-1	Programmed cell death
PEI	Polyethyleneimine
PRR	Pattern recognition receptors
qPCR	Quantitative polymerase chain reaction
RNA	Ribonucelic acid
s.c.	Subcutaneous
SCF	Stem cell factor
scFv	Single chain variable fragment
SIN	Self-inactivating
SIRPα	CD172a
ssRNA	Single stranded ribonucleic acid
T cells	T lmyphocyte
T.u.	Transducing units
TCR	T cell receptor
TLR	Toll-like receptor
TMD	Transmembrane domain
TNF-α	Tumor necrosis factor α
TRAC	T cell receptor alpha constant

tSNE	t-distributed Stochastic Neighbor Embedding
VCN	Vector copy number
VSV-G	Vesicular stomatitis virus glycoprotein
VSV-LV	Lentiviral vector pseudotyped with vesicular stomatitis virus glycoprotein
WPRE	Woodchuck hepatitis posttranscriptional element
β2M	β2 microglobulin

7 List of Publications

7.1 Original research

Ho N., Agarwal S., Milani M., Cantore A., Buchholz CJ. and Thalheimer FB. *In vivo* generation of CAR T cells in the presence of human myeloid cells. Mol Ther Methods Clin Dev (2022) doi: 10.1016/j.omtm.2022.06.004.

7.2 Review articles

Michels A., **Ho N.**, Buchholz CJ. Precision medicine: *In vivo* CAR therapy as a showcase for receptor-targeted vector platforms. Mol Ther (2022) doi: 10.1016/j.ymthe.2022.05.018.

7.3 Conference presentations

In vivo CAR T cell generation in humanized mouse models

Naphang Ho and Christian J. Buchholz

Jackson Laboratory symposium *In vivo* tools for immunotherapy for immunotherapy drug development: predicting PK, efficacy, and toxicity of drug candidates using humanized models in Heidelberg, Germany, 17th June 2022

In vivo CAR T cell generation in humanized NSG-SGM3 mice

Naphang Ho, Shiwani Agarwal, Christian J. Buchholz and Frederic B. Thalheimer

Virtual DG-GT Morning Symposium (virtual) 19th October 2021

Investigation of acute side effects by CAR T cells in humanized mouse models

Naphang Ho, Shiwani Agarwal, Laura Kapitza, Annika M. Frank, Alexander Michels, Frederic B. Thalheimer, Christian J. Buchholz

EMBO Practical Course. Humanized mice in biomedicine: Challenges and innovations. In Heidelberg, Germany, 3rd – 8th November 2019

7.4 Conference poster presentations

In vivo CAR T cell generation in presence of human myeloid cells

Naphang Ho, Shiwani Agarwal, Michela Milani, Alessio Cantore, Christian J. Buchholz and Frederic B. Thalheimer

10th Universitäres Centrum für Tumorerkrankungen (UCT) Science Day in Frankfurt am Main, Germany, 29th June 2022

In vivo CAR T cell generation in presence of human myeloid cells

Naphang Ho, Shiwani Agarwal, Michela Milani, Alessio Cantore, Christian J. Buchholz and Frederic B. Thalheimer

25th American Society of Gene and Cell Therapy (ASGCT) Annual Meeting conference in Washington DC, US, 16th – 19th May 2022

In vivo CAR T cell generation in humanized NSG-SGM3 mice

Naphang Ho, Shiwani Agarwal, Christian J. Buchholz and Frederic B. Thalheimer

European Society of Gene and Cell Therapy (ESGCT) Annual Meeting conference (virtual) 19th – 22nd October 2021

Investigation of acute side effects by CAR T cells in humanized mouse models

Naphang Ho, Shiwani Agarwal, Laura Kapitza, Annika M. Frank, Alexander Michels, Frederic B. Thalheimer, Christian J. Buchholz

Annual Paul-Ehrlich-Institut Retreat 2020 in Ronneburg, Germany, 29th – 31st January 2020

8 *Curriculum Vitae*

Personal information

Name: Naphang Ho

Education

Since December 2018	PhD study at the TU-Darmstadt. Performed in the research group of Prof. Dr. Christian Buchholz at the Paul-Ehrlich Institut. Title: Human myeloid enhanced model systems: Tools for advanced evaluation of short-term CAR T cells and *in vivo* CAR T cell generation
Sept. 2016 – Oct. 2018	Master of Science in Technische Biologie at the TU-Darmstadt Master thesis performed in the research group of Prof. Dr. Ger van Zandbergen at the Paul-Ehrlich Institut with the title: Modulating impact of apoptotic Leishmania major parasites on the cytokine response in primary human cells upon infection.
Sept. 2013 – Aug. 2016	Bachelor of Science in Biowissenschaften at the Goethe-University Frankfurt am Main.
Okt. 2005 – Aug. 2013	Abitur (higher education entrance qualification) at the Albert-Einstein-Gymnasium in Maintal.

Work experience

Sept. 2018 – Nov. 2018	Research scientist in the research group of Prof. Dr. Ger van Zandbergen at the Paul-Ehrlich Institut.

9 Acknowledgement

An erster Stelle möchte ich mich sehr herzlich bei Prof. Dr. Christian Buchholz für die Möglichkeit bedanken in seiner Arbeitsgruppe meine Dissertation durchführen zu können und an solch hochinteressanten Projekten arbeiten zu dürfen. Seine Ratschläge und die gemeinsamen Diskussionen zum Thema haben maßgeblich zur Weiterentwicklung meiner wissenschaftlichen Fähigkeiten und zur Erstellung der Arbeit beigetragen.

Bei Prof. Dr. Prof. Dr. Alexander Löwer möchte ich mich für die unkomplizierte Betreuung seitens der TU-Darmstadt bedanken. Aber auch für das Einbringen in den Thesis-Komitee-Meetings bin ich ihm, Prof. Dr. Cristina Cardoso und Prof. Dr. Zoe Waibler dankbar.

Ein besonderer Dank gilt Frederic. Danke für deine zahlreichen Diskussionen, die das Projekt vorangetrieben haben und deine großartige Betreuung bei den Mausarbeiten.

Ein großer Dank gilt vor allem auch der gesamten Arbeitsgruppe für die tolle Arbeitsatmosphäre und die vielen hilfreichen Diskussionen zu meinen Projekten. Insbesondere auch eure Unterstützung während der vielen finalen Analysetagen. Vielen Dank Alex, Annika, Laura, Angela, Samuel, Tati, Gundi, Julia, Manu, Shiwani, Frederic, Elham, Burak, Doro, Luca, Mar, Filip, Arezoo, Lea S., Lea K., Nora, Mehryad, Fabian, Vanessa, Jessi, Iris. Ich werde die schöne Zeit mit unseren regelmäßigen kulturellen und kulinarischen Ausflügen in guter Erinnerung behalten.

Bei meiner gesamten Familie möchte ich mich für ihre großartige Unterstützung bedanken. Meine Mutter, die nie den Glauben an mich verliert. Mein Bruder, Napyin, und mein Vater für ihren bedingungslosen Beistand.

Am allermeisten möchte ich mich bei meiner Frau, Yelim bedanken. Vielen Dank für deine seelische Unterstützung während der gesamten Zeit und dafür, dass du einfach da bist für mich. Ohne dich wäre ich nicht dort, wo ich jetzt bin.

10 Ehrenwörtliche Erklärung

Ich erkläre hiermit, dass ich die vorliegende Arbeit entsprechend den Regeln guter wissenschaftlicher Praxis selbstständig und ohne unzulässige Hilfe Dritter angefertigt habe.

Sämtliche aus fremden Quellen direkt oder indirekt übernommenen Gedanken sowie sämtliche von Anderen direkt oder indirekt übernommenen Daten, Techniken und Materialien sind als solche kenntlich gemacht. Die Arbeit wurde bisher bei keiner anderen Hochschule zu Prüfungszwecken eingereicht. Die eingereichte elektronische Version stimmt mit der schriftlichen Version überein.

Darmstadt, den

_____